Matrix Assisted Laser Desorption Ionization Time-of-Flight Mass Spectrometry: Velocity Measurements Using Orthogonal and Axial Injection and Applications to Characterization of Wheat Proteins

By

Ragnar G. Dworschak

A Thesis Submitted to the Faculty of Graduate Studies in Partial Fulfillment of the requirements for the Degree of

Doctor of Philosophy

Department of Physics and Astronomy
University of Manitoba
Winnipeg Manitoba Canada

THE UNIVERSITY OF MANITOBA

FACULTY OF GRADUATE STUDIES

*****

COPYRIGHT PERMISSION

Matrix Assisted Laser Desorption Ionization Time-of-Flight Mass Spectrometry: Velocity Measurements Using Orthogonal and Axial Injection and Applications to Characterization of Wheat Proteins

BY

Ragnar G. Dworschak

A Thesis/Practicum submitted to the Faculty of Graduate Studies of The University of Manitoba in partial fulfillment of the requirement of the degree

Of

DOCTOR OF PHILOSOPHY

Acknowledgements

This thesis is dedicated to my mother, Diana Elizabeth Warren. She would have taken great pleasure in this accomplishment, even though reading it would further clarify for her that science was closer to my heart than the art of the English language. Of course my family provided support for this endeavor: My Aunt Cynthia, whose countless BFE's with turnip puff helped me stave off hunger... Cathy offering to have her grade 8 gifted students help me in my experiments, Caroline providing waffles and a warm Christmas environment, offering to call up this Werner chap and "encouraging" him to finish looking at my chapter 4, Dave and Joy for simply being Dave and Joy and ALWAYS being there for me, continually providing all intellectual and physiological dietary requirements so that I neither physically nor spiritually sublimated away under the burden of THE THESIS, and it was good. My father Hermann, who I would have liked to show around Winnipeg at least once and to show him how EXPERIMENTALISTS play in the lab.

I want to thank Werner Ens and Ken Standing for allowing me the time in the TOF group to do this work. It was always very fascinating to listen to stories from Dr. S. about the early days of MS and TOF. Since I'm at liberty here to say whatever I want, since this is the only page in my thesis not falling under anyone's scrutiny...I need to say that Werner was a great supervisor because he is very low stress, unflappable and calm but utterly incapable of finishing anything without a DEADline. This is ok; he certainly makes up for this in other ways. A couple of things stand out about Werner: his tremendous grasp of concepts and the ease with which he imparts this knowledge to a grad student and the fact that everytime I had to have him step into the lab and help troubleshoot an experimental problem on which I was getting exactly nowhere, it was as if the instrument saw Werner coming and said "OK I give up, I'll work fine now...". His troubleshooting methodology was always creative, effective and therefore impressive...If only Werner could see his way to spend more time in the lab with students and impart some of this ability to them, that would be great. As an aside, it's been shown through some recreational genealogy and simple observation that Werner is a direct descendent of Inspector Gadget.

Vic Spicer. Where does one start? I learned more from Vic than I would have, had he been someone else from whom I learned less. See what I mean? Vic defines eclectic taste, generosity, curiosity, recreational antelope paste, and other things I'm not comfortable trying to spell. Vic is famous in my own mind for his frequent "vignettes" that graced my office walls over the years. An example is at the end of these acknowledgements. Be content; be very content if you don't understand it, really. I look forward to the privilege of hosting Vic in Ottawa during a holiday he owes himself, if he can escape the deep potential well that is his Winnipeg. It's OK Vic; Ottawa has squirrels, come east, man!

RELAX! [1]

I'd like to offer at least a little insight into why it was a 10 year odyssey rather than a conventional 4-5 year trip. Principally, it was 2 activities about which I am still passionate that frequently "diluted" my efforts towards my PhD. These were tutoring and traveling. I was fortunate to become the physics / chemistry / calculus / math tutor and food taster at St. Johns Ravenscourt High School. I had the problem that I could simply NOT say no to tutoring a student. I have to admit the renumeration was appreciated and facilitated the passion for traveling. In fact the joy and tremendous satisfaction of tutoring has never left me and is embodied in the process of tutoring a student and witnessing the "light" coming on. The traveling for me was necessary as I have always been strongly driven to see what and who's out there. Climbing up a volcano in Nicaragua or having one explode behind you while

dining on pickled sea bass in Costa Rica only added to my TOF education...The Holy Grail would be of course to dine at the Restaurant at the End of the Universe, but Vic says without a *Fresh* pocket octopus, the serving staff tends to ignore you. The biggest "delay" in my PhD was joining Nortel Networks in May 2000 and working in the metallic thin films group, finally becoming team leader. As the purchase of our Optoelectronics group by Bookham Inc. drew nearer it was my colleagues that kept me happy going into "work" each day. The day after being laid off from Nortel, I started at Ionalytics, also in Ottawa, as a field scientist with the promise to them that I would finish my PhD finally. This job brings me happily back into the mass spectrometry conformation and allows me to TRAVEL! which I really enjoy.

Music always played a big role in my life and my PhD years were no exception. I would like to thank and apologize to the various late night students in the Allen building for "listening" to me practice my trombone in the stairwells. With no mute and a Bach 42B tenor trombone, they really had no choice But to listen, wherever they were in the building. The Winnipeg Folk Festival will always be a part of me. I started as a Daytime Stage Crew member in 1995, becoming Family Stage manager in 1998 and finally Stage 1 manager in 2000. What a great experience and I'm looking forward to coming back to it for years to come.

What's next? Probably a shower and a shave and then to enjoy life, finally learning how to play the trombone properly, music composition, more traveling and maybe even a family. But I wouldn't be able to continue on nor have done what I did these past 10 years without the family I've described here. Thanks.

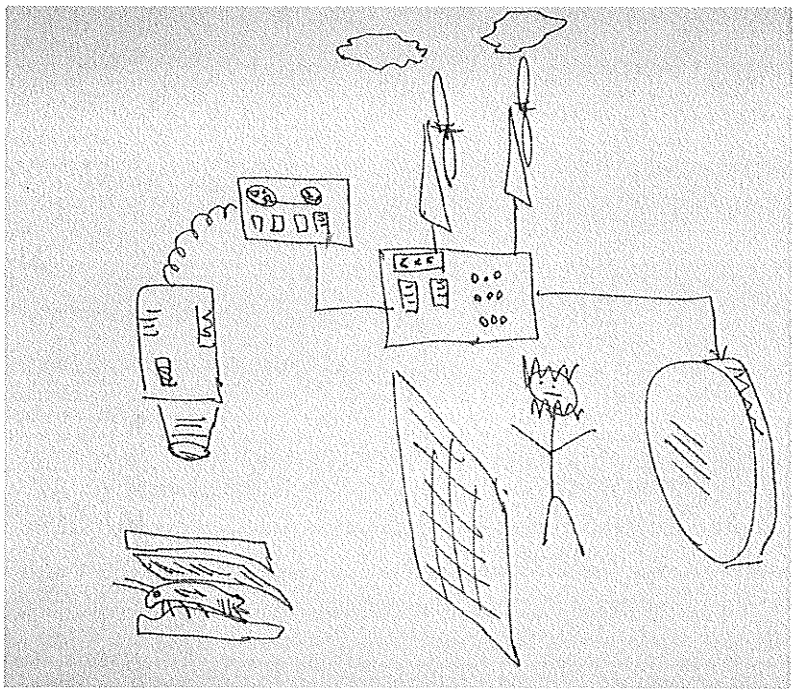

through the interesting use of a rotting shrimp and brie sandwich as time base and wind farm as the power supply, ragnar personally experiences delayed extraction
Vic Spicer 2004

1. Gilles Roy, TOF lab, 2:17 pm, 11 June 1996

Abstract

Orthogonal-injection was introduced to allow continuous ion sources to be coupled to time-of-flight mass spectrometers, but also demonstrated promising features for pulsed sources such as MALDI. We tested the feasibility of using a simple implementation orthogonal injection TOF with a MALDI source without collisional cooling. The experiment demonstrated that high resolution is achievable in principle in such an instrument, but only with impractical sacrifices in intensity. Subsequent work in this laboratory has demonstrated that the addition of collisional cooling makes orthogonal MALDI not only feasible, but advantageous in several respects.

The instrument used for the above feasibility test was well-suited for measurements of initial velocity distributions in MALDI, avoiding problems of field penetration and questions of time-scale of the plume expansion that seemed to produce rather conflicting results in axial TOF measurements. Average initial velocities of peptides and proteins above about 1000 daltons were found to be largely mass independent around 800 m/s, plus or minus about 15% depending on the matrix used. This result is slightly higher, but still quite consistent with earlier measurements using axial TOF with the field-free method (~750 m/s), but a factor of two higher than the first reports using the delayed-extraction method. The experiments also showed that in contrast to the average velocity, the *width* of the velocity distribution increases significantly with increasing mass. The matrix velocity measurements confirm earlier experiments that show the benzoic acid derivatives have generally higher velocities than the cinnamic acid derivatives. Measurements of the velocity component in the direction back toward the laser with different sample orientations suggest that the surface orientation is the main determiner of the plume direction. On the other hand, preliminary measurements using the field-free method in the axial TOF geometry show higher velocities of matrix and analyte ions for more normal laser incidence, and for single crystals parallel to the sample surface compared to polycrystalline surfaces, suggesting the orientation of the crystal face with respect to the incident laser direction plays a role in the desorption process.

Matrix-assisted laser desorption/ionization mass spectrometry (MALDI/MS) was used to analyse the protein composition in several common and durum wheat varieties. Mass spectra were obtained directly from crude and partially purified wheat gliadin and reduced glutenin subunit fractions. Mass spectra of the gliadins and the low molecular weight glutenin subunits show a complex pattern of proteins in the 30 - 40 kDa range. The observed gliadin patterns showed some promise for variety identification. The mass spectra of the high molecular weight glutenin subunits are much simpler and the complete high molecular weight subunit profile can be determined directly from a single mass spectrum. This may prove particularly useful in wheat breeding programs for rapid identification of lines containing subunits associated with superior quality.

Table of Contents

1 Introduction

1.1 Background to the Field of Biological Mass Spectrometry

Analytical chemists and biochemists have long sought accurate, sensitive methods for determining the molecular masses of biopolymers such as proteins and carbohydrates. The continuing objective in the development of biological mass spectrometry is to increase the measurable mass range, resolution, accuracy and the sensitivity of the measurement. Traditional methods of mass spectrometry, which proved so useful for measuring compounds with low molecular masses, were of little use for measuring underivatized compounds with high molecular masses. Mass spectrometry requires that the sample molecules, which may be present in the condensed phase, be converted into intact, ionized molecules in the gas phase. This soft ionization requirement is difficult to achieve for biopolymers because they are polar and massive and therefore extremely nonvolatile and thermolabile. Over the last three decades, several volatilization and ionization techniques have been developed to softly ionize these larger molecules.

We now survey two areas of soft ionization: From the condensed state, the desorption and ionization of large, nonvolatile, thermolabile organic molecules in a single step is comprised of three principal approaches: particle or photon bombardment and field desorption. Secondly, ionization directly from the liquid phase with a strong electric field, in particular electrospray ionization (ESI).

The first application of particle induced desorption and ionization to produce large molecular ions from a solid, nonvolatile, thermolabile organic material was reported by Macfarlane and Torgerson in 1976 [1] who used high energy fission fragments of mass ~100 Da and energy of ~100MeV from the spontaneous

nuclear fission of ^{252}Cf. This technique became known as plasma desorption mass spectrometry (PDMS), where the plasma component of the name comes from the plasma induced by the fission fragment as it interacts with matter. PDMS was one of the earliest and widely applied techniques for biomolecular mass analysis [2,3,4,5]. Following the initial success of this technique, biomolecular ions of close to 2 kDa were successfully desorbed and analysed [6]. By 1984, molecular ions of mass greater than 20 kDa were observed with a conducting target foil as backing [7], and by 1989 Jonsson et al. substantially improved the measurable mass range of biomolecules by absorbing the sample onto a nitrocellulose substrate after which the sample could be washed [8]. Subsequently, intact molecular ions have been desorbed up to a mass of about 34.6 kDa [9] and beyond to 45 kDa [10]. However, one drawback with PDMS in the high mass range is that the technique always requires a considerable time in the range tens of minutes to hours for the accumulation of a complete spectrum [11].

After the successful application of PDMS to biomolecular analysis, the technique caused renewed interest in time-of-flight mass spectrometry (TOF-MS) analysis. PDMS couples naturally with TOF-MS while avoiding some of the problems previously associated with the limited resolution of TOF-MS. Firstly, from the fission process of PDMS, one of the recoiling fragments may be used to give a well defined start time for the TOF spectrum. Secondly, the acceleration field of the TOF-MS instrument is maintained at a high, stable DC potential, rather than employing a pulsed extraction. Finally, the ions are ejected from a solid equipotential surface; thus the energy and spatial spread is much smaller than for traditional gaseous ion sources. Since the introduction of the TOF principle for mass separation of a pulsed ion packet in 1946 [12], the use of TOF-MS has been limited by relatively poor resolution in comparison to other types of mass spectrometer analyser systems such as the magnetic sector instruments. In 1955 Wiley and McLaren [13] published a design for a TOF-MS system with a description of the focusing conditions required for their gaseous ionization

source. TOF mass spectrometers were used with pulsed lasers in the 1960s for rapid vapourization and analysis of coals, elemental analysis, isotope ratio measurements, and pyrolysis [14]. The laser microprobe was developed in 1975 [15]. Resonance ionization mass spectrometers have been used in a number of laboratories for isotopic analysis, and TOF mass spectrometers have been used to study multiphoton ionization (MPI) processes of organic molecules. For the most part, these instruments have been used to record ions of relatively low mass.

Soon after the discovery of PDMS, another application as a variation of secondary ion mass spectrometry (SIMS) emerged. In the late 1970's, Benninghoven and Sichtermann reported the intense emission of pseudomolecular and diagnostic fragment ions resulting from the bombardment of amino acids by small atomic ions in the low keV energy range [16,17]. This technique was referred to as static SIMS where the sample surface doesn't physically change significantly from the bombardment with the very low atomic ion current of ~nA/cm^2. This technique was regarded as an unexpected development of SIMS. The low primary ion currents, in turn, produced low secondary ion currents, which decreases even further for increasing sizes of molecular ions. Therefore, this technique was limited in mass range to a few hundred Da when scanning instruments were used because of the losses due to scanning the mass spectrum using a sector-field instrument. Numerous authors have since demonstrated the utility of static SIMS to measure the distribution of specific organic compounds in biological samples [18,19].

The mass range and sensitivity of the static SIMS technique was improved by coupling this ionization source to a TOF analyzer. A low-energy pulsed ion gun with 5 keV Cs+ ions was reported by Chait and Standing in 1981 [20] and demonstrated induced desorption of molecular ions of mass around 1300 Da [21]. Etched silver targets were typically used as a substrate in SIMS for smaller

molecules [22]. For larger biomolecules with nitrocellulose as a substrate, the sample could be washed, removing the soluble contamination. The largest biomolecule observed with this technique is about 14 kDa [23].

The SIMS technique, coupled to a scanning analyser, saw an increase in the observable mass range by using samples dissolved in glycerol and employing primary particle fluxes typical of dynamic SIMS [24]. This current is typically greater than 10^{-5} A/cm^2 and orders of magnitude larger than static SIMS. This method was introduced using a neutral particle beam and was therefore named Fast Atom Bombardment (FAB) [25,26]. With the neutral particle beam and the continual supply of secondary ions from the renewal of the liquid matrix, FAB lends itself to coupling easily with sector and quadrupole instruments. FAB analysis is typically used up to a mass-range of a few thousand Da [27,28]. In the higher mass range for FAB, results for proteins in the 10 – 20 kDa range suffer from a low signal-to-noise ratio even for sample amounts in the 10 μg range [29].

Since the early 1960s, a variety of lasers with vastly different wavelengths ranging from the far-UV to the far-IR and pulse widths ranging from picoseconds to CW irradiation have been used to generate ions of organic molecules for mass analysis [30]. With such a breadth of variation possible in experimental conditions, it is not surprising that different combinations of lasers and spectrometers have evolved for different applications such as trace analysis in inorganic and organic samples, microanalysis with submicron spatial resolution, and molecular spectroscopy by laser postionization of neutrals in the gas phase [31]. The different kinds of lasers used for desorption complicate the intercomparison of laser desorption ionization (LDI) results and it has so far proven impossible to provide a universal description of the dynamics of energy deposition and ion formation [32]. Early work on LDI-MS was reviewed in detail by Conzemius and Capellen in 1980 [14] and further by Hillenkamp in 1983 and 1985 [32,33,34]

In 1976, the use of a nanosecond pulsed laser, together with TOF-MS, was first used to study biological material [35] followed by further systematic attempts to generate ions of organic molecules with lasers [36,37]. As observed by Hillenkamp, after more than three decades of systematic observations, two general principles have evolved [31]:

First, efficient and controllable energy transfer to the sample requires resonant absorption of the molecule at the laser wavelength. Consequently, lasers emitting in the far-UV, which can couple to electronic states, or in the far-IR, which can excite rovibrational states, give the best results.

Second, to avoid thermal decomposition of the thermally labile molecules, the energy must be transferred within a very short time on the order of ns. With these short pulse durations and the fact that laser beams can easily be focused to spot sizes that are small compared to the other dimensions of the ion source, the ions are generated essentially at a point source in space and time. This feature makes them ideally suited for use with TOF-MS.

In the LDI technique, the illumination of a solid sample with a short intense light pulse produces molecular ions from thermally labile molecules. Sensitivities in the picomole range have been reported [36,38,39]. The efficiency of the LDI mechanism is a complex function of many variables, including the wavelength and power density of the laser radiation, the incident angle of the radiation, the optical absorption characteristics of the sample, the thickness of the sample layer, and the nature of the substrate surface [40,41,42,43]. Although exceptions exist [39,43], LDI appears to be most efficient [44] when the laser wavelength matches an intense absorption band of the sample, but direct absorption of radiation by the analyte can lead to fragmentation and failure to obtain molecular mass information. With early experiments in LDI, the problem emerged that the

mass range of ions was limited that could be desorbed intact. Experimental observations showed that this limit was on the order of ~1 kDa for biopolymers and up to 9 kDa for synthetic polymers, depending on experimental conditions and molecular structure, otherwise severe fragmentation occurred [45].

Towards the end of the 1980's, two methods of soft ionization were discovered that revolutionized the world of biological mass spectrometry. The measurable mass range increased by at least two orders of magnitude, the amount of sample required went down by at least 3 orders of magnitude and the analysis time decreased by at least two orders of magnitude. These techniques are ESI and Matrix Assisted Laser Desorption / Ionization (MALDI) and both were recognized for their immense contribution to mass spectrometry by receiving the 2002 Nobel Prize. The following is a brief description of ESI and the rest of the thesis focuses on MALDI.

In 1988, Fenn reported the successful use of ESI-MS in which a very diluted analyte solution was sprayed from a needle, at atmospheric pressure, held at a few kV with respect to ground, forming highly charged droplets [46,47]. The ions are introduced to the mass spectrometer through a small orifice or a capillary separated from vacuum by a few stages of differential pumping. This system was able to softly ionize large biological molecules without causing them to fragment [48]. In the ESI process, multiprotonated molecules $(M+nH)^{n+}$ can form with an average of one positive charge per kDa for denatured proteins and when mass analysed, result in a sequence of consecutive peaks at $(M+nH)/n$ along the m/z scale. A simple quadrupole mass spectrometer, well suited to a continuous ion source, with a limited mass range of up to $m/z \sim 2000$ can therefore measure molecular weights up to orders of magnitude larger. The unknown charge state of the ion can be derived from any two adjacent peaks because they are all derived from a single molecular mass [49]. A deconvolution algorithm is used to

mathematically transform a spectrum with several peaks of multiply charged ions into one peak corresponding to a singly charged ion [50].

In the case of LDI, the main breakthrough allowing the intact desorption of the higher masses came with the idea of dispersing the sample in a radiation-absorbing matrix in order to limit radiation damage to the analyte. Karas et al. realized that the use of a solid organic matrix could circumvent this problem of the analyte species breaking up due to these resonant and non-resonant mechanisms and were able to obtain spectra of mellitin and other peptides of molecular mass up to 3 kDa [44]. This was followed by results from Karas and Hillenkamp showing the MALDI process with molecular masses exceeding 10 kDa with the use of post acceleration [51]. The addition of the organic matrix resulted in the mainstream use of the name for this process called Matrix-Assisted Laser Desorption / Ionization or MALDI. The name matrix assisted laser desorption was originally used in 1985 by Karas et al. to describe the absorbing matrix effect of tryptophan (Trp) when mixed with alanine (Ala), since without Trp, Ala required about ten times more laser fluence for desorption [52]. Independent work at about the same time by Tanaka et al. showed a similar effect with a liquid matrix in which a fine metal powder of 30 nm particle size was suspended [53]. Results showed the intact desorption and ionization of the molecular ion chymotrypsinogen with a mass of 25717 Da and molecular clusters of other species up to 100 kDa. Up to the present time, the MALDI method has rapidly grown with the discovery of new matrices [54,55], extending the method to other classes of samples such as glycopeptides, carbohydrates and nucleotides, with masses up around 300 kDa [56] routinely being analysed. The history of how this remarkable early achievement provided a key impetus to further development of MALDI, has been described by Beavis [57]. With the advances in MALDI and ESI in combination with the availability of genomic databases, the analysis of proteins has been revolutionized. These mass spectrometry techniques are now routinely used to identify proteins by comparing the peptide mass maps with protein

databases, and for protein finger-printing and biomarker discovery by examining the pattern of intact proteins in simplified mixtures.

1.2 Thesis Outline

This chapter is the first of two to examine the background of MALDI-TOF-MS. In this chapter we looked at the background of biological mass spectrometry leading to the discovery of MALDI. In Chapter 2, we look at the way MALDI is implemented in the laboratory then present a brief overview of the principal desorption and ionization models.

The third chapter describes the original orthogonal MALDI system (OMALDI) built and the modeling results which showed the potential for tremendous resolution and then experimental results which showed its insufficient sensitivity for a practical mass spectrometer instrument.

Although the OMALDI instrument had limited use as a mass spectrometer, it was particularly suited to measure ion desorption velocity distributions in a novel way. The fourth chapter presents some of these velocity distributions obtained with the OMALDI instrument. Other results presented here include some interesting pictures showing the morphological changes in the monolithic crystalline sample under laser irradiation and ablation providing some insight into desorption and subsequent velocity measurement results.

The fifth chapter presents preliminary results of velocity measurements from polycrystalline and monolithic crystalline samples of DHB and insulin plus DHB at two different laser incidence angles. The experimental configurations used here include the field free and delayed extraction techniques.

The sixth and final chapter contains results from studying wheat proteins with the axial MALDI technique. The wheat gliadins along with the low and high molecular weight glutenins are examined. The MALDI application to the analysis of wheat gliadins has lead to work in using MALDI as a variety identification tool. The use of MALDI to examine the high molecular weight glutenin proteins has revealed the presence of some proteins that had not been detected through the standard HPLC approach.

1.3 References

1. R. D. Macfarlane, R. P. Skowronski and D. F. Torgerson, *Biochem. Biophys. Res. Commun.* **60** (1974) 616
2. R. D. Macfarlane, J. C. Hill, D. L. Jacobs and R. G. Phelps in: Mass Spectrometry in the Analysis of Large Molecules, John Wiley, Chichester 1986, pp. 1- 12
3. B. Sundqvist, A. Hedin, P. Hakansson, I. Kamensky, M. Salehpour and G. Swe, *Int. J. Mass Spectrom. Ion Proc.* **65** (1985) 69
4. I. Kamensky and A. G. Craig, *Anal Instrum.* **16** (1987) 71
5. B. T. Chait and F. H. Field, *Int. J. Mass Spectrom. Ion Proc.* **65** (1985) 169
6. R. D. Macfarlane and D. F. Torgerson, *Int. J. Mass Spectrom. Ion Processes* **21** (1976) 81
7. B.U.R. Sundqvist, P. Roepstorff, J. Fohlman, A. Hedin, P. Håkansson, I. Kamensky, M. Lindberg, M. Salephour and G. Säve, *Science* **226** (1984) 696
8. G. P. Jonsson, A. B. Hedin, P. L. Hakansson, B. U. R. Sundqvist, B. G. S. Swe, P. F. Nielsen, P. Roepsdorff, K. E. Johansson, I. Kamensky and M. S. L. Lindberg, *Anal. Chem.* **58** (1986) 1084
9. A. G. Craig, A. Engstrom, H. Bennich and I. Kamensky, *Proceedings of the 35th ASMS Conference on Mass Spectrometry and Allied Topics*, Denver CO (1987)
10. G. P. Jonsson, A. B. Hedin, P. L. Hakansson and B.U.R. Sundqvist, *Rapid Commun. Mass Spectrom.* **3** (1989) 190
11. I. Jardine, G. F. Scanlan and A. Tsarbopoulos, *Anal. Chem.* **60** (1988) 1087
12. W.E. Stephens, *Phys. Rev.* **69** (1946) 691
13. W. C. Wiley and I. H. McLaren, *Rev. Sci. Instr.* **26** (1955) 1150
14. R. J. Conzemius and J. M. Capellen, *Int. J. Mass Spectrom. Ion Physics* **34** (1980) 197
15. F. Hillenkamp, R. Kaufmann, R. Nitsche and E. Unsold, *Appl. Phys.* **8** (1975) 341

16. A. Benninghoven, and W. K. Sichtermann, *Anal. Chem.* **50** (1978) 1180
17. A. Benninghoven, D. Jaspers and W. Sichtermann, *Appl. Phys.* **11** (1976) 35
18. A. Benninghoven, B. Hagenhoff and E. Niehuis, *Anal. Chem.* **65** (1993) 630A
19. P.J. Todd, J. M. McMahon, R. T. Short and C. A. McCandlish, *Anal. Chem.* **69** (1997) 529A
20. B. T. Chait, K. G. Standing, *Int. J. Mass Spectrom. Ion Phys.* **40** (1981) 185
21. W. Ens, K.G. Standing, B.T. Chait, and F.H. Field, *Anal. Chem.* **53** (1981) 1241
22. A. Benninghoven, E. Hiehues, D. Greifendorf, D. van Leyen and W. Lange in: SIMS V. A. Benninghoven et al. (Eds.), Springer Series in Chemical Physics Vol. 44, Springer, Berlin (1986), p.497
23. W. Ens, P. Hakansson, B.U.R. Sundqvist, Secondary Ion Mass Spectrometry SIMS VI, Ed. A.M. Buber, A Benninghoven, H.W. Werner and G. Soldzian (Wiley, Chichester 1988) 623
24. M. Barber, S. Bordoli, G. J. Elliot, R. D. Sedgwick and A. N. Taylor, *Anal. Chem.* **54** (1982) 645A
25. D. J. Surman and J. C. Vickerman, J. Chem. Soc., Chem. Commun., 325 (1981) 342
26. M. Barber, R. S. Bordoli, R. D. Sedgwick, A. N. Taylor, *J. Chem. Soc., Chem. Commun.* **1981** (1981) 325
27. M. Barber, R.S. Bordoli, G.J. Elliot, R.D. Sedgwick, A.N. Tyler and B.N. Green, *J. Chem. Soc. Chem. Commun.* **1982** (1982) 936
28. A. Dell and H.R. Morris, *Biochem. Biophys. Res. Commun.* **106** (1982) 1456
29. M. Barber and B. N. Green, *Rapid Commun. Mass Spectrom.* **1** (1987) 80
30. F. J. Vastola, R. O. Mumma, A. J. Pirone, *Org. Mass Spectrom.* **3** (1970) 101
31. F. Hillenkamp, M. Karas, R. C. Beavis and B. T. Chait, *Anal. Chem.* **63** (1991) 1193A
32. F. Hillenkamp and A. Benninghoven (Ed.), *Proc. Of the 2nd Int. Conf. On Ion Formation from Organic Solids, Springer Series in Chem. Phys.* Vol. 25, Springer Verlag, New York, 1983, pp.190
33. F. Hillenkamp, in Secondary Ion Mass Spectrometry, SIMS V, Ed. by A. Benninghoven, R.J. Colton, D.S. Simmons and H.W. Werner, Springer Series in Chem. Phys. **44** (1986) 471
34. F. Hillenkamp, *Advances in Mass Spectrometry* **11A** (1989) 354
35. E. Unsold, F. Hillenkamp and R. Nitsche, *Analysis* **4** (1976) 115
36. M. A. Posthumus, P. G. Kistemaker, H. L. C. Meuzelaar and M. C. ten Neuver de Brauw, *Anal. Chem.* **50** (1978) 985
37. K-D Kupka, F. Hillenkamp and C. Schiller in *Advances in Mass Spectrometry*; Heyden & Sons: London, 1980, Vol. **8A**; p. 935
38. R. J. Cotter, *Anal. Chem.* **56** (1984) 485A
39. J. Grotemeyer, E. W. Schlag, *Biomed. Environ. Mass Spectrom.* **16** (1988) 143

40. F. P. Novak, K. Balasanmugan, K. Viswanadham, C. D. Parker, Z. A. Wilk, D. Mattern and D. M. Hercules, *Int. J. Mass Spectrom. Ion Phys.* **53** (1983) 135
41. W. B. Emary, O. W. Hand and R. G. Cooks in Lasers and Mass Spectrometry; D. M. Lubman, Ed.; Oxford University Press: New York, 1990
42. J. A. McCloskey In Methods in Enzymology-Mass Spectrometry; J. A. McCloskey, Ed.; Academic Press: San Diego, 1990; Vol. 193, p. 771.
43. J. Grotemeyer, K. Walter, U. Boesl, E. W. Schlag, *Int. J. Mass Spectrom. Ion Processes* **78** (1987) 69
44. M. Karas, D. Bachmann, U. Bahr and F. Hillenkamp, *Int. J. Mass Spectrom. Ion Processes* **78** (1987) 53
45. B. Spengler, M. Karas, U. Bahr and F. Hillenkamp, *J. Phys. Chem.* **91** (1987) 6502
46. J. B. Fenn, M. Mann, C. K. Meng, S. F. Wong and C. M. Whitehouse, *Science* **246** (1989) 64
47. J. B. Fenn, M. Mann, C. K. Meng, S. F. Wong and C. M. Whitehouse, *Mass Spectrom. Rev.* **9** (1990) 37
48. C. K. Meng, M. Mann and J. B. Fenn, *Z. Phys. D* **10** (1988) 361
49. K. Biemann, *Annu. Rev. Biochem.* **61** (1992) 977
50. M. Mann, C. K. Meng and J. B. Fenn, *Anal. Chem.* 61 (1989) 1702
51. M. Karas and F. Hillenkamp, *Anal. Chem.* **60** (1988) 2299
52. M. Karas, D. Bachmann and F. Hillenkamp, *Anal. Chem.* **57** (1985) 2935
53. K. Tanaka, H. Waki, Y. Ido, S. Akita, Y. Yoshida and T. Yoshida, *Rapid Commun. Mass Spectrom.* **2** (1988) 151
54. R. C. Beavis and B. T. Chait, *Rapid Commun. Mass Spectrom.* **3** (1989) 432
55. R. C. Beavis and B. T. Chait, *Rapid Commun. Mass Spectrom.* **3** (1989) 233
56. A. Overberg, M. Karas and F. Hillenkamp, *Rapid Commun. Mass Spectrom.* **5** (1991) 492
57. R. C. Beavis, *Org. Mass Spectrom.* **27** (1992) 653

2. Principles of MALDI-TOF-MS

2.1 Introduction

MALDI has emerged as a major analytical tool in biotechnology, biochemistry and proteomics [1,2,3,4,5,6,7,8]. In the original MALDI technique, the sample protein was mixed into a solution containing a large molar excess of nicotinic acid and this solution was dried on an inert metal substrate to give a microcrystalline solid layer [9,10,11,12]. Under appropriate conditions, the biomolecules of interest are incorporated into the matrix crystals [11,13,14]. MALDI ions were formed when the sample was irradiated with laser pulses from the 266 nm frequency-quadrupled output of a Nd:YAG (Nd:YAG(4)) laser. The nicotinic acid matrix absorbs strongly at this wavelength and therefore preferentially absorbs the laser radiation at this wavelength compared to the matrix embedded protein. A laser pulse with sufficient irradiance causes the mixture of matrix and protein to go into the gas phase in the form of neutrals with a large number of ions with 1^+ and 2^+ charge states dominating [1]. Significant intact ion yield has been observed in the spectra of proteins obtained by this method [15]. Among the advantages of a MALDI system are its high sensitivity in the femtomolar range and the low sensitivity of the method to contaminants. The relative tolerance to these contaminants, such as salts, buffers and detergents, necessitates little effort with regard to sample preparation [16] and therefore there has been great interest in MALDI for the structural analysis of biological molecules [17].

Subsequently, it was discovered that the biomolecules under examination could be generated using other types of matrix materials [10,18,19]. The effect has been observed using a variety of pulsed lasers and laser pulse widths [20,21,22,23] and it has been used in the ion sources of different types of mass spectrometers [24,18,25,26,27].

This chapter will provide an overview of the major components of a MALDI-TOF-MS system. This will include sections covering some common matrices used, sample preparation methodology, an outline of the evolution of the MALDI-TOF-MS extraction configurations and a discussion of the ion detection and data quality. In this thesis, only vacuum MALDI will be addressed, discussions about recent developments in atmospheric pressure MALDI can be found elsewhere [28,29].

2.2 Source Region

2.2.1 Matrix Overview

MALDI causes the nondestructive vaporization and ionization of both large and small biomolecules. In MALDI analysis, the analyte is first co-crystallized, after evaporation of the solvent used for preparation, with a large molar excess of a suitable matrix compound, typically a UV-absorbing weak organic acid [30]. Present in large excess relative to the analyte, the matrix serves as a solvent for analyte molecules, effectively isolating them, thereby limiting analyte aggregation, which would otherwise hinder molecular ion formation [31]. As matrix desorption is usually performed from solid material, the ability of a matrix to form a solid solution of analyte molecules is essential [32]. Laser radiation of this analyte-matrix mixture then results in the vaporization and ionization of the matrix that carries the analyte with it. The matrix therefore plays a key role by strongly absorbing the laser light energy and causing, indirectly, the analyte to vaporize. The matrix also serves as a proton donor and receptor, acting to ionize the analyte in both positive and negative ionization modes, respectively [33,34]. MALDI was initially developed for the UV wavelength range where electronic excitation of aromatic matrix molecules forms the initial excitation step; rovibronic

excitation by wavelengths in the IR region has also later been proven to work [35].

In the original method, the signals produced using 3-pyridinecarboxylic acid or nicotinic acid were characteristically much broader than the instrumental mass resolution of the mass spectrometer used, resulting in a mass resolution – defined as $m/\Delta m$, measured at the full width, half maximum (FWHM) of a peak – of approximately 50 and a mass accuracy of 0.1% [36]. A large component of the peak width was shown to be a photochemically generated adduction of the nicotinic acid matrix molecule to the protein analyte [37]. Several new matrix types have been discovered that can be used to desorb protein molecules, which produce much less intense and more easily resolved photochemically generated adducts [38].

Early work by Beavis and Chait surveyed more than fifty compounds as possible matrices for the laser desorption of proteins with a laser wavelength of λ = 266 nm [37,38]. They then reported the application of pulsed 355 nm laser light from the frequency tripled output of a Nd:YAG laser to the desorption of proteins. This requires the use of a different class of matrix that absorbs strongly at that wavelength. In later work, Beavis studied more than 300 potential matrices, of which only 7 proved acceptable [39]. The three cinnamic acid derivatives in this group all have the following characteristics: (i) a carboxylic acid functional group, and (ii) an aromatic ring that acts as a chromophore for the absorption of UV radiation. From the three matrices; ferulic acid, 3, 4-dihydroxy cinnamic acid (caffeic acid) and sinapinic acid, excellent protein mass spectra were obtained, demonstrating clearly that a nitrogen laser with λ = 337 nm could be used as an alternative to the Nd:YAG system. The use of this longer wavelength also eliminates any possible absorption of the laser light by the analyte biopolymer, possibly leading to their decomposition, as most classes of biopolymers do not absorb light at this wavelength [40,9]. Of the 7 matrices recognized, only sinapinic acid has become a standard matrix in the field.

The rapid development of MALDI as a vital analytical tool can be partially attributed to the identification of a number of effective matrices [41,42,43,44,37,38,40,54]. Matrices of highly similar structures and optical absorption characteristics can yield large differences in MALDI efficiencies for the same compound, while different compound types, such as DNA and proteins, behave very differently in the same matrix under the same conditions [45]. Factors such as morphology of the matrix-sample film and molecular co-crystallization [44,54,46,55] are important for obtaining useful MALDI spectra. The most common matrices are summarized in Table 2-1:

Table 2-1 : Summary of the most common MALDI matrices in use.

Short Name	Full Name	Main Application	Reference
α-cyano	α-cyano-4-hydroxycinnamic acid	Small peptides	12
Sinapinic	3,5-dimethoxy-4-hydroxycinnamic acid	proteins	10
DHB	2,5-dihydroxybenzoic acid	proteins	54
3-HPA	3-hydroxypicolinic acid	DNA, nucleic acids	47

Among the more unusual matrices are a frozen matrix of anthranilic acid for DNA analysis [48], and an ice matrix for work done in IR MALDI [49].

Liquid matrices present some advantages over solid matrices for MALDI, such as the potential for the direct interface with liquid separation techniques using either flow-injection or continuous-flow MALDI [50,51]. The solid phase matrix system performs better than the liquid system in UV-MALDI.

Binary matrix mixtures composed of two or more compounds that have properties adjustable for specific experimental conditions showed promise in forming an effective matrix material. The binary components can be selected to operate at specific laser wavelengths and their constituent ratios can be adjusted

to change the features of the mass spectra generated from the mixture [52]. For example, the Hillenkamp group showed that DHB used in the high mass region above 50 kDa, gave improved signal when the matrix was combined with a structurally similar compound such as 5-methoxysalicylic acid (MSA) [53]. This mixture later became known as sDHB and is used rather infrequently today compared to neat DHB.

2.2.2 Sample Preparation Overview

This section will give an overview of the standard sample preparation techniques used to produce solid, polycrystalline samples. These were the techniques employed in the work presented in this thesis.

The original sample preparation technique is called the dried droplet method. In this method, the matrix compound, depending on its solubility, was dissolved in water, water/ethanol, water/methanol or water/acetonitrile mixtures at a concentration of 5 to 10 g/L. The analyte was typically dissolved in 0.1% trifluoroacetic acid to a concentration of 1 – 10 μM. One part analyte was added to ten parts matrix to form the sample/analyte solution. To a flat, inert metal probe, a small amount of this solution, on the order of 0.5 to 2 μl, is applied. The solvent is removed in a stream of warm air and the microcrystalline sample is then transferred to the vacuum chamber. Thus the typical absolute sample amount used for analysis is in the range of 1 pmol or less. In the case of sinapinic acid, care has to be taken to protect the matrix solution from prolonged exposure to light and to avoid heating in the evaporation step [38,40]. Dried sinapinic acid preparations can be furthermore cleaned from precipitated water soluble contaminants like inorganic salts by immersing the dried sample in cold distilled water [97]. Depending on the matrix and the solvents used, the microscopic structure of the preparations may vary between rather homogenous amorphous layers, a dense packing of tiny crystallites, such as sinapinic acid, or

relatively large crystal needles grown from the rim of the droplet as in DHB. Large, well developed crystals on the order of mm in length can be grown from matrix/protein solutions, which show excellent MALDI spectra with respect to S/N ratio, and reproducibility from shot to shot [54]. Co-crystallization of the matrix and the analyte but not of water soluble contaminants may also explain the capability of some matrices to tolerate high levels of contamination [32].

Using the dried droplet method described above, crystals often form along the perimeter of the sample spot with sparse coverage in the middle [55]. For this reason the signal intensity can vary widely with the position of laser irradiation of the dried droplet [55,56]. Use of etched silver foil substrates has shown better uniformity of ion production with respect to irradiation position on the dried droplet [57]. Subsequent sample preparation improvements which gained popularity are described below.

While MALDI is tolerant of [97] or immune to [58] high concentrations of salts, buffers, and other involatile components commonly present in protein preparations, performance is usually better with clean samples. Also some impurities like urea and glycerol quench the signal because they inhibit crystallization.

Xiang and Beavis [59] developed a method to permit removal of such contaminants from protein samples prepared for MALDI analysis. This sample preparation technique proved superior to the dried droplet method. It consists of applying a droplet of matrix solution to the sample stage and allowing it to dry completely. The non-uniform polycrystalline film formed from the drying is then crushed on the sample surface. Beavis used a microscope slide to crush the matrix, but in our lab, the edge of a small 50 mL beaker resulted in the finest, most uniform crushed polycrystalline film providing multiple, adhered seed or anchor sites. Onto this extremely fine polycrystalline film, a droplet of the usual analyte and matrix mixture is applied to the fine film already present. After adding

the analyte containing liquid sample, a film forms very rapidly (< 15 s) which incorporates proteins in a manner similar to the crystals in the dried-droplet method discussed previously. The droplet is allowed to partially dry, and while it is still moist, the surface is rinsed with cold de-ionized water, either with a stream of water or a large droplet that is allowed to remain on the analyte area for 5-10 seconds, thereby removing water soluble contaminants leading to considerable improvement in performance. The water droplet is then shaken off or the stream of water is terminated and the sample surface is blown dry with air or nitrogen. This sample preparation technique has been named the "crushed matrix" method. A systematic investigation of the effects of different sample drying techniques indicated that vacuum drying is faster and provides better ion yields and resolution in MALDI spectra [60].

Another sample preparation methodology was developed by Vorm et al. which is similar to the crushed matrix method in that it established a very fine polycrystalline layer of matrix on the sample stage prior to the addition of the analyte [61]. Matrix dissolved in a highly volatile solvent, such as acetone, is applied to the sample stage. This matrix solution achieves very fast evaporation of the solvent, which leads to the formation of a dense, flat, and thin polycrystalline film of matrix only. A small volume of analyte solution is then placed on top of the matrix surface, and the liquid is allowed to evapourate slowly. Following the complete evaporation, the sample can then be washed with cold de-ionized water, either with a stream of water or a large droplet that is allowed to sit on the analyte area for 5-10 seconds, thereby removing water soluble contaminants leading to considerable improvement in performance, similar to the crushed matrix technique. The water droplet is then shaken off or the stream of water is terminated and the sample surface is blown dry with air or nitrogen.

2.2.3 Lasers

To avoid thermal decomposition of the thermally labile molecules in the MALDI technique, the energy from the laser must be delivered within a very short time. Typically, lasers with pulse widths in the 1 – 100 ns range, such as Q-switched Nd:YAG, excimer, TEA-CO2, or the 337 nm N_2 laser systems are used. Given these short durations and the fact that laser beams can easily be focused to spot sizes that are small compared to the other dimensions of the ion source, the ions are generated essentially at a point source in space and time. This feature makes these lasers ideally suited for TOF analysers [9]. The lasers can be operated in single shot mode or more typically, in a repetitive mode with 100Hz being the typical maximum rate.

2.3 TOF Analyser

Since a MALDI ion source uses a pulsed laser, it can be conveniently coupled to a TOF-MS, which requires a well-defined start time. Among the advantages of a TOF-MS system compared to other analysers such as a quadrupole system are the absence of a fundamental mass limit, and the ability to record all ions striking the detector without scanning. This can result in higher signal intensity and accuracy in mass determination, since ions of all masses are measured at the same time. This is particularly suited to the study of large biomolecules. In this section, we examine the evolution of the TOF analyser in the MALDI-TOF system. This begins with the original and most basic configuration of DC axial extraction, followed by the same system with an electrostatic mirror. The next major step in the evolution was the development of Delayed Extraction (DE) followed by orthogonal extraction, in common use today.

2.3.1 Linear TOF

Figure 2-1 shows a schematic diagram of the DC axial mode system, the simplest MALDI-TOF instrument configuration. It uses an axial geometry in which a target is placed with its surface perpendicular to the axis of the TOF instrument, with the sample matrix and analyte combination located on the upper target surface. The target plate is maintained at the full DC accelerating potential with grid 1 grounded above it. The MALDI plume is created within a constant electric field, and is extracted along the instrument axis into the field free drift region where the ion flight time is measured over a linear flight path.

To commence a spectrum acquisition, the laser is triggered to fire a single shot, on the order of a few nanoseconds in length. The MALDI plume of ions is produced when a pulse of laser light is absorbed by the matrix-analyte sample on the target plate. These ions are promptly extracted and accelerated by the static electric field between the target plane and grid 1 as shown. The ions then drift through the field-free region and arrive at the detector. There is a photodetector that detects when the laser is fired. This device sends a signal that starts measuring the time between the laser shot and ion detection. Many investigators subsequently used similar designs with a variety of electrode configurations, ion sources, and detectors [62,63,64]. The acceleration voltages are typically +/- 1 – 30 kV, and the analyser drift lengths typically range from 0.1 - 3 m.

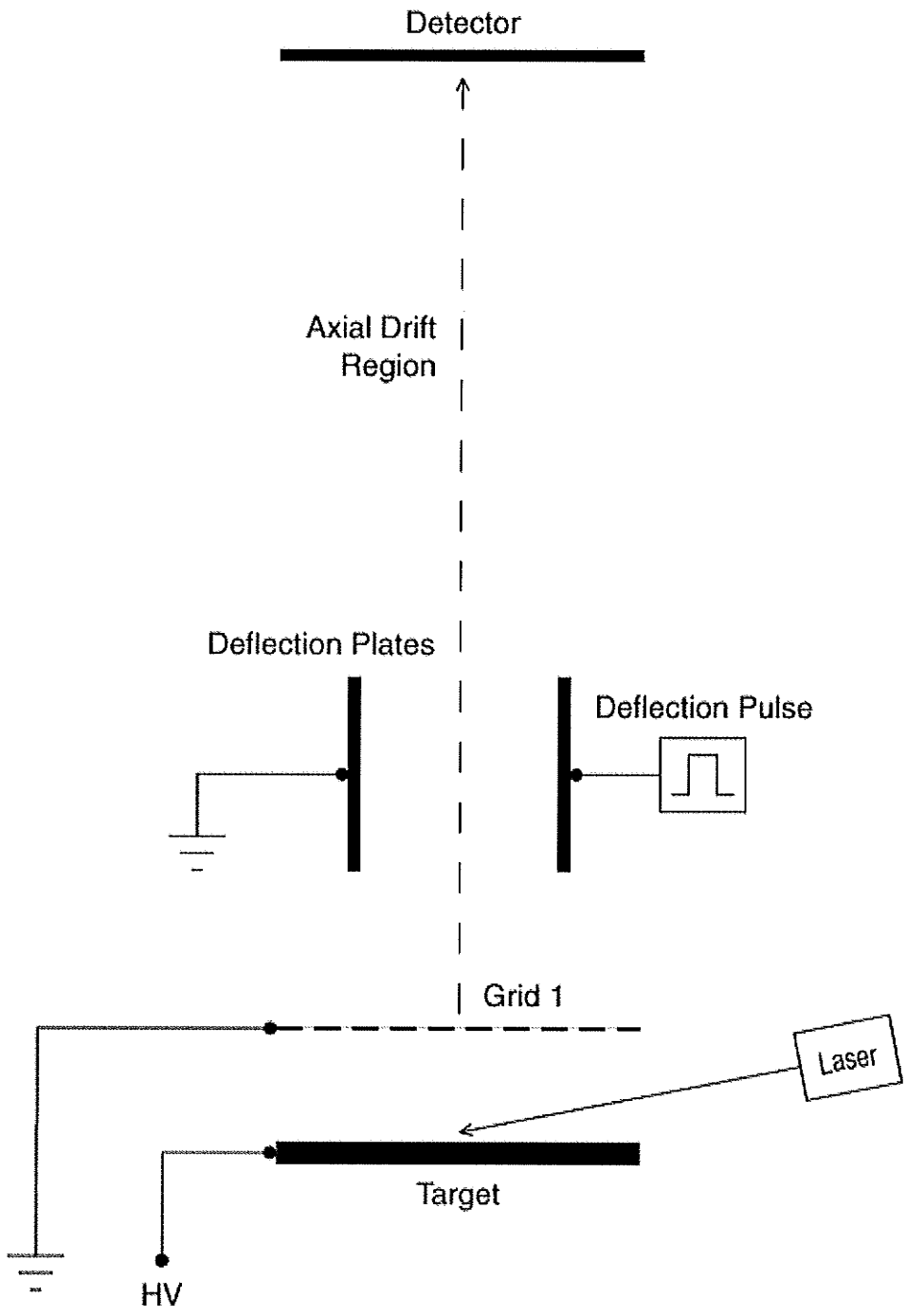

Figure 2-1 : Schematic of the axial mode with prompt extraction including deflector plates for low mass ion suppression.

In the TOF mass spectrometer, ions are formed in a short source region (s) on a target plate held at a potential V. The ions are then accelerated through this

region into a longer, field-free drift region (L) as shown schematically in Figure 2-2. Ideally, all ions enter the drift region with the same kinetic energy:

$$\frac{1}{2}mv_z^2 = qV \qquad (1)$$

where q is the charge on the ion of mass m, in a series of spatially discrete individual ion packets, each traveling with a velocity v_z characteristic of their mass:

$$v_z = \sqrt{\left(\frac{2qV}{m}\right)} \qquad (2)$$

The average velocity of the ion in the source region is half this value. The ion then passes through the grid and travels with constant velocity through a drift region to the plane surface of the detector. Therefore the total time of flight t is the sum of the time spent in the source region and the time spent in the drift region [65]:

$$t = (2s + L)\sqrt{\left(\frac{m}{2qV}\right)} \qquad (3)$$

Measurement of the time of flight determines the mass m, since the other parameters in the equation are known. The time spectrum can be converted directly to a mass to charge spectrum:

$$\frac{m}{q} = \frac{2V}{(2s + L)^2}t^2 \qquad (4)$$

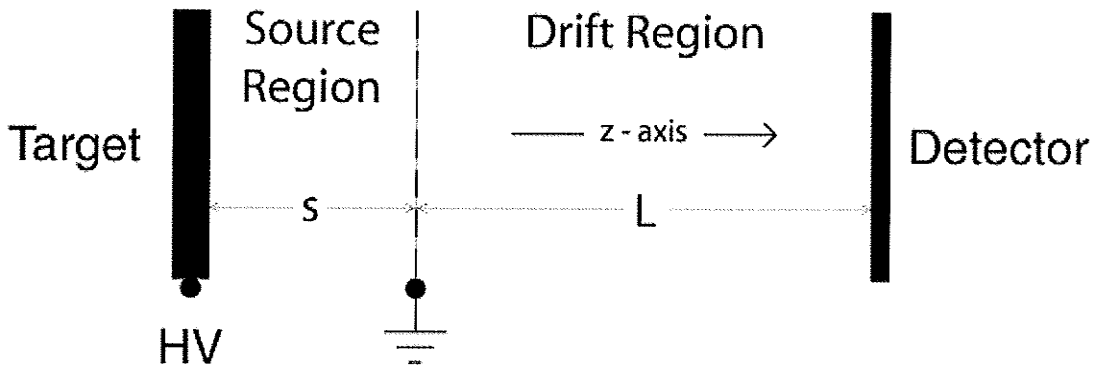

Figure 2-2 : Schematic diagram of the TOF spectrometer regions.

Beavis and Chait and other groups employed pulsed deflector plates to suppress low-mass matrix ions [66,37]. This is done to prevent overloading or saturation of the detector with low mass ions which would render the detector insensitive to subsequent higher mass ions within the same desorption event. To accomplish this, at the time of the laser pulse, a DC potential is applied across the deflection plates until enough time has elapsed such that the unwanted low mass ions have been deflected away from the path leading to the detector. At that point, the potential is switched off, and subsequent ions are not deflected and allowed to drift directly to the detector.

Although this arrangement is simple, severe limitations on resolution are caused because this arrangement does not correct for the initial space and energy spreads of the ions. The MALDI plume is created and ions are ejected from a well-defined surface so the initial spatial spread is small but within the MALDI plume, there are both ions and neutrals, which expand into the vacuum with a substantial energy spread.

2.3.2 Reflecting TOF

A major limitation of early TOF mass analysers has often been relatively poor mass resolution. Earlier studies indicate that the major problem is that the ions

produced by MALDI exhibit a rather broad energy distribution [67,68,69]. Initial velocity of desorbed analyte ions is nearly independent of mass; thus the initial kinetic energy is proportional to the mass of the analyte. In addition, when desorption occurs in a strong electric field, energy is lost presumably by collisions with the neutral plume, and further mass dependent energy dispersion results [86].

In 1973 Mamyrin introduced the ion mirror, as a means for correcting the effects of initial ion velocity or kinetic energy distributions [70]. The reflectron, located at the end of the TOF tube, consists of a series of rings and/or grids with voltages that increase, linearly in the simplest case, up to a value slightly greater than the voltage at the ion source. The ions penetrate the reflectron until they reach zero kinetic energy, turn around, and are accelerated back through the reflectron, exiting with energies identical to their incoming energy but with their z-direction reversed. Ions with larger energies will penetrate the reflectron more deeply and will have longer flight paths. Referring to the reflecting time-of-flight (RTOF) schematic in Figure 2-3, if the total distance the ion travels in a field free region is [65]:

$$L = L_1 + L_2 \qquad (5)$$

then the total time spent in free flight is:

$$t_f = \frac{L}{v_z} \qquad (6)$$

and the total time spent in the mirror is:

$$t_m = \frac{2mv_z}{qE} \qquad (7)$$

where E is the magnitude of the retarding electric field in the mirror. If

$$v_z = v_0 + \delta \qquad (8)$$

then we can expand as a function of $\left(\delta/v_0\right)$ to give a total time of flight of:

$$t = \left(\frac{2mv_0}{qE} + \frac{L}{v_0}\right) + \left(\frac{\delta}{v_0}\right)\left(\frac{2mv_0}{qE} - \frac{L}{v_0}\right) + \cdots \qquad (9)$$

Setting:

$$\frac{2mv_0}{qE} = \frac{L}{v_0} \quad \text{or} \quad E = \frac{2mv_0^2}{qL} \qquad (10)$$

removes the first-order term in $\left(\delta/v_0\right)$. Therefore with the proper choice of geometry and mirror electric fields, the flight times of all ions of a common *m/q* ratio through the drift region and mirror are independent of an initial velocity variation δ to first order for a one stage ion mirror [71]. Under this condition the total time of flight is given by:

$$t = \frac{2L}{v_0} \qquad (11)$$

so the ion spends equal amounts of time in the mirror and in free flight. Higher-order terms can be removed by the use of more complicated electric fields, for example by the two-stage mirror described by Mamyrin [72], but any advantage in doing so is often lost because the resolution may deteriorate because of other effects, particularly in the acceleration region, which must be considered separately.

The source region of the RTOF in Figure 2-3 is similar to the linear mode configuration as shown in Figure 2-1, the mirror is set a small angle with respect to the axis. The exiting ions do not follow the same path as incoming ions and can be recorded by a detector placed adjacent to the source. The reflectron does not diminish the energy spread of the ions; it corrects for the effects of the energy spread on their arrival times at the detector, thereby reducing the time spread of ion arrival Δt. In addition, the reflectron increases the path length and therefore total flight time t. Since the ion mass is proportional to the square of the flight time, mass resolution is related to time resolution by:

$$\frac{m}{\Delta m} = \frac{t}{2\Delta t} \qquad (12)$$

Thus mass resolution is improved both by decreasing Δt and by increasing t.

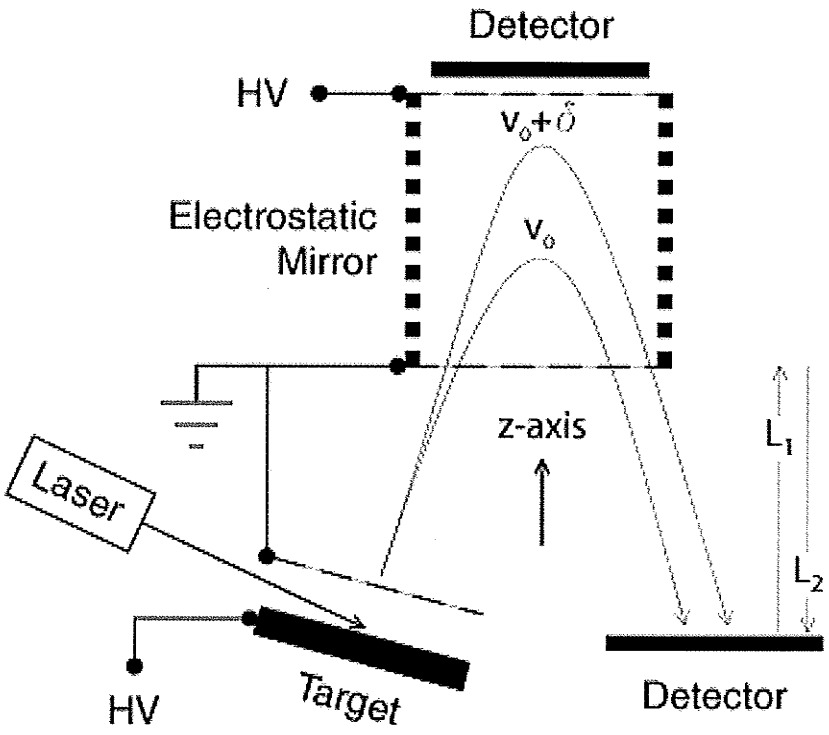

Figure 2-3 : Schematic of a Reflecting TOF analyser configuration with a MALDI source.

2.3.3 Delayed Extraction

As discussed in above, variations in ion kinetic energy can be corrected to a large extent by the use of a reflector. However, effects during ion production or acceleration may give not only a spread in kinetic energy but also a spread in time. The latter effects are not corrected by the mirror.

Wiley and McLaren described a pulsed ion source with two stages of acceleration that provided first order correction for the initial space distribution of ions [73]. These authors also described a technique which they named "time-lag energy focusing" for correcting the effect of initial velocity distributions. In this instrument, the ions are produced in a field-free region, and the accelerating field is turned on by application of a fast pulse at a predetermined, optimized delay time after initial ion formation. Within the delay time, ions will spread out into the extraction gap owing to their initial velocities, thus spreading out in space. On acceleration by the delayed extraction pulse, the faster ions, being closer to the end of the accelerating column, receive a smaller accelerating impulse. The slower ions, being farther from the end of the accelerating column, receive a larger accelerating impulse. If the time delay and the amplitude of the accelerating pulse are adjusted properly, ions of a given mass then arrive at the plane of the detector at the same time.

In the work of Wiley and McLaren, both the initial space and velocity distribution of the ions were present and simultaneous correction for both terms could not be accomplished. In the case of MALDI, the ions start from a well-defined target plane, their subsequent position is correlated to their velocity, in the ideal case. On leaving the MALDI plume, ions have approximately the same velocity distribution independent of mass. The resulting dependence of the energy on mass means that the optimum time focusing conditions have some mass dependence, so resolution can only be optimized for part of the spectrum at a

time. For the same reason, there is a small perturbation in the mass vs. time formula, so high accuracy requires a more complex calibration procedure.

Figure 2-4 shows a schematic diagram of a DE mode system. In this system, the sample matrix and analyte combination is located on the target surface on the upper side. The target plate and grid 2 are maintained at the full accelerating potential with grid 1 grounded above grid 2.

To commence a spectrum acquisition, the laser is triggered to fire a single shot, on the order of a few nanoseconds in length. This causes desorption to take place within the high potential but field free region between the target plate and grid 2. At the same time, a clock starts timing the extraction delay between desorption and pulsed extraction. At the end of this optimized delay time, an extraction pulse of an optimized magnitude is applied to the target plate, forming an acceleration region between the target and grid 2. Then they are accelerated to ground potential at grid 1 where they enter the field-free drift region. The deflection plates can be used to pulse away unwanted low mass ions as in the DC mode. The time of flight of the ions is measured from the time of the extraction pulse to the time when they're detected with a pair of microchannel plate (MCP) detectors after passing through the axial drift region. In this system, the ions are formed in a field free region, extracted at a later time with a fraction of the total accelerating potential and then accelerated through to ground potential in contrast to the prompt extraction system discussed in the previous section where the ions are desorbed and immediately accelerated and extracted through the high field region.

The delayed extraction method is particularly useful for MALDI. The time delay allows the ion plume to expand freely before the extraction field is applied, greatly reducing the number of collisions and the resulting energy spread.

DE can produce remarkably good performance in MALDI even with a linear TOF instrument as discussed earlier [74,75,76]. By itself, the DE focusing method is limited because the narrowest time distributions are achieved for short flight paths, but good mass resolution requires long flight paths to provide time dispersion between ions of different masses. By itself, the reflectron provides energy focusing but does not compensate for time spreads in the source region, so the best results are achieved with DE in combination with a reflectron [77]. In this case the DE parameters are adjusted so that ions of a common *m/z* ratio arrive at a plane near the source at approximately the same time, but with a considerable variation in velocity. The mirror then compensates for the velocity spread. Therefore one has the time lag focusing of DE and velocity focusing of a reflectron to achieve high resolution. Resolutions higher than 20000 have been obtained with this configuration [78].

Several groups have applied similar mass analysers to MALDI, and have shown significantly improved resolution for selected masses as a function of delay time and pulsed field intensity in the ion source [79,80,81,82]. Substantial improvement in mass resolution compared with static ion extraction has been reported. A resolution of 12500 for insulin, with the isotopes resolved nearly to the baseline, has been shown in a 6.4m reflecting mass spectrometer [86,83]. Even in a small linear mass analyzer of 1.2m, a mass resolution of 4000 for peptides can be obtained [86]. For ions up to the 10 kDa range, limitations in mass resolution are determined instead by the time resolution limits of the detector and digitizer systems, especially in small instruments [85].

Larger proteins over approximately 30 kDa exhibit an apparent drop in resolution with delayed extraction compared to lower masses. For cytochrome c (12.36 kDa) a resolution of 2000 [84] and 1025 [82] and for carbonic anhydrase (29.025 kDa) a value of 840 [86] have been reported. Their explanation for the failure of the DE method in the higher-mass range is the peak broadening due to metastable fragmentation as well as adduct ion formation. This fragmentation is

prompt in a linear TOF-MS and can be either prompt or metastable in an RTOF-MS system. Bahr et al. demonstrated that with soft DE conditions, including a weak extraction field and a long delay time, and soft matrices, such as sDHB, considerably better results can be achieved for certain proteins over the whole mass range up to 66 kDa [85].

In addition to improved mass resolution, DE provides other improvements in the quality of MALDI spectra, which are more difficult to quantify. These include a lower level of chemical noise due to reduced prompt fragmentation during acceleration, and significant reduction in the dependence of ion flight times on laser intensity. With DE, peak widths and centroids are much less dependent on the absolute intensity of the ion signal; thus, it is not as necessary to operate near the threshold for ion production to obtain both high resolution and improved mass accuracy [86].

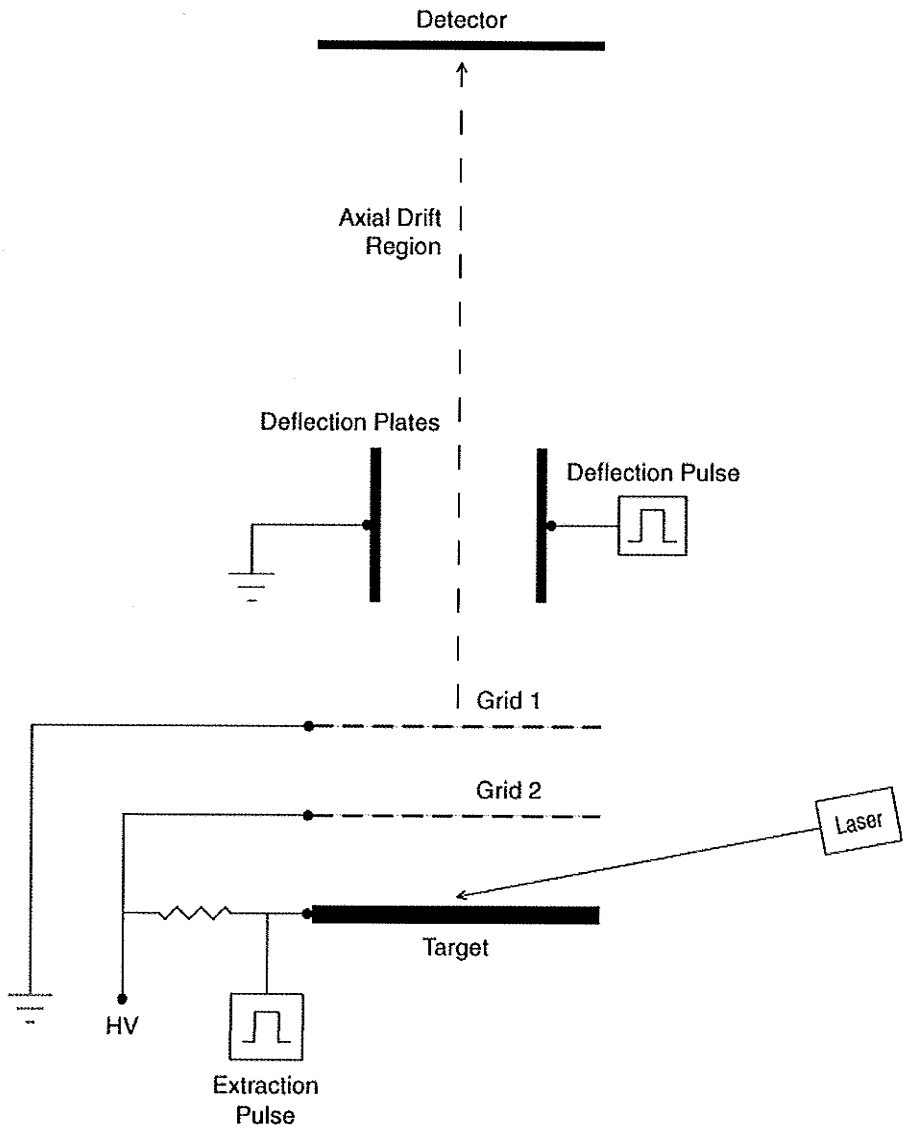

Figure 2-4 : Schematic of the delayed extraction mode including deflector plates for low mass ion suppression.

2.3.4 Orthogonal Extraction

TOF instruments can tolerate a relatively large spatial or velocity spread in a plane perpendicular to the spectrometer axis (z-axis as in Figure 2-2), as witnessed by the large sources typically used in fission fragment desorption. This tolerance has been exploited by injecting electrospray ions into the TOF instrument in a direction perpendicular to the z axis. Orthogonal injection has

also been used with other types of ion sources [87,88,89,90,91,92]. This geometry provides a high efficiency interface for transferring ions from a continuous beam to a pulsed mode. A second advantage is the small velocity spread in the z direction that is usually observed, making high resolution easier to obtain. Verentchikov et al. coupled a reflecting TOF spectrometer with an electrospray ion source using orthogonal ion injection [93].

Modern versions of orthogonal injection configurations typically use some form of collisional cooling prior to the ion extraction. Work done in our lab lead to an orthogonal injection of MALDI ions into a TOF spectrometer through a collisional damping interface [94]. This thesis will focus on earlier work in which an orthogonal injection system was used without collisional cooling. This was a proof of concept prototype that ultimately proved that collisional cooling of the ions is necessary for competitive performance. This work is covered in chapter 3 of this thesis. Chapter 4 will then show results of this early orthogonal spectrometer used to measure initial MALDI ion velocity distributions.

Figure 2-5 shows a schematic diagram of the orthogonal instrument built in our lab from which the OMALDI-MS data presented in this thesis was acquired. The timing concept used here is similar to the DE mode discussed earlier. The laser is triggered to emit a short pulse at which time a delay timer starts. The ions are formed in a MALDI plume that evolves in a direction normal to the surface of the sample into the first acceleration region. After a predetermined delay, the extraction pulse is triggered which sends the ions into the acceleration region where they gain kinetic energy as they fall through the potential to ground at the end of that region. The deflection plates can be used to pulse away unwanted low mass ions. Another use of the deflection plates in the orthogonal configuration is to keep heavier ions on a trajectory so that they will hit the detector. The heavier ions will have a longer flight time through the instrument allowing them more time to drift laterally off the instrument axis because of their initial axial velocity from desorption. The ion flight time is measured from the time

of the extraction pulse to the time when they're detected with a pair of MCP detectors after passing through the axial drift region.

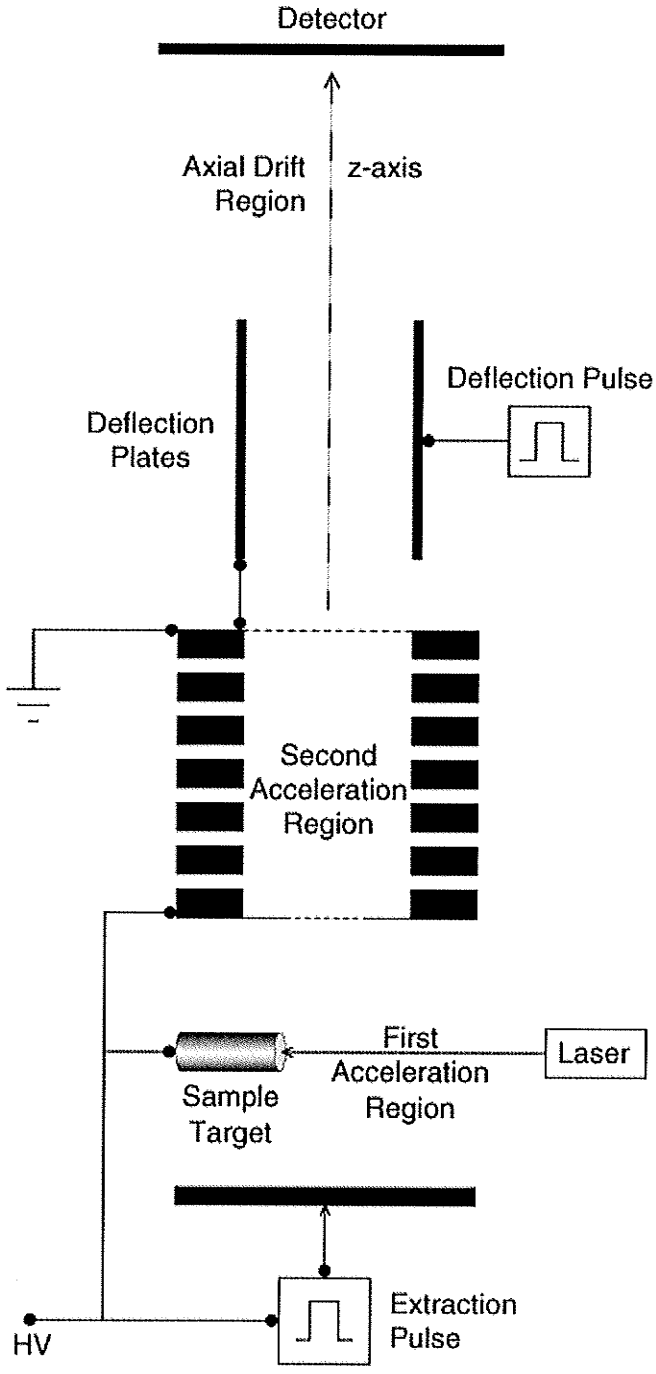

Figure 2-5 : Schematic of the orthogonal extraction mode including deflector plates for low mass ion suppression.

2.4 *Ion Detection and Data Quality*

2.4.1 Ion Detection

Figure 2-6 shows a schematic diagram of the ion detector system. Ions impinge on the CsI coated converter plate at the end of the drift tube and produce an emission of secondary electrons. A converter plate is used as the secondary emission efficiency is greater than that of the microchannel plate system and the plate can be easily pulsed to prevent the detection of low mass ions. Electrons are accelerated away from the converter plate because of the static negative potential applied to the plate. The electrons are forced into a circular path by the magnetic field supplied by several permanent magnets situated around the detector enclosure. These electrons travel through the grounded grid and are accelerated toward the chevron microchannel electron multiplier or microchannel plate (MCP). Two Varian MCPs of 4 cm diameter are separated by a 250 μm stainless steel ring and mounted 1 mm from a stainless steel collector plate. This type of detector is well suited for time-of-flight measurements because of its large active area and good time resolution. A grounded, 90% transmission grid is mounted in front of the detector, used for post acceleration [95].

An MCP consists of an array of continuous dynode electron multipliers (~12 μm diameter) that are oriented at a small angle (~5°) to the plate normal. This angle increases the probability that an incoming electron strikes the channel surface. The plates are mounted with opposing angles to reduce ion feedback. This is the process where positive ions formed by secondary electrons near the channel exits are accelerated back in the channel and initiate a second electron cascade. Typically 1 kV is applied across each plate and 200 V is applied between the second plate and the collector. In this configuration, an electron gain of $\sim 10^7$ is achieved [95].

The cascade of electrons emerging from MCP 2 are incident on a collector plate which is capacitively coupled to a preamplifier. This signal is then introduced into either an oscilloscope, a transient recorder or a time-to-digital converter (TDC) for signal processing.

In axial MALDI systems, a transient recorder is typically used because of the large number of ions that are normally produced in a single shot. It is necessary to match the detector gain carefully to the laser fluence to avoid saturating the transient recorder on intense peaks, and to avoid detector-shadowing problems produced by intense matrix signals. In orthogonal systems, a TDC is typically used where at most a few ions are produced by a given start event [96]. With so few ions per start event, there is sufficient time between ion arrivals at the detector so that the TDC see a maximum of one ion per time channel.

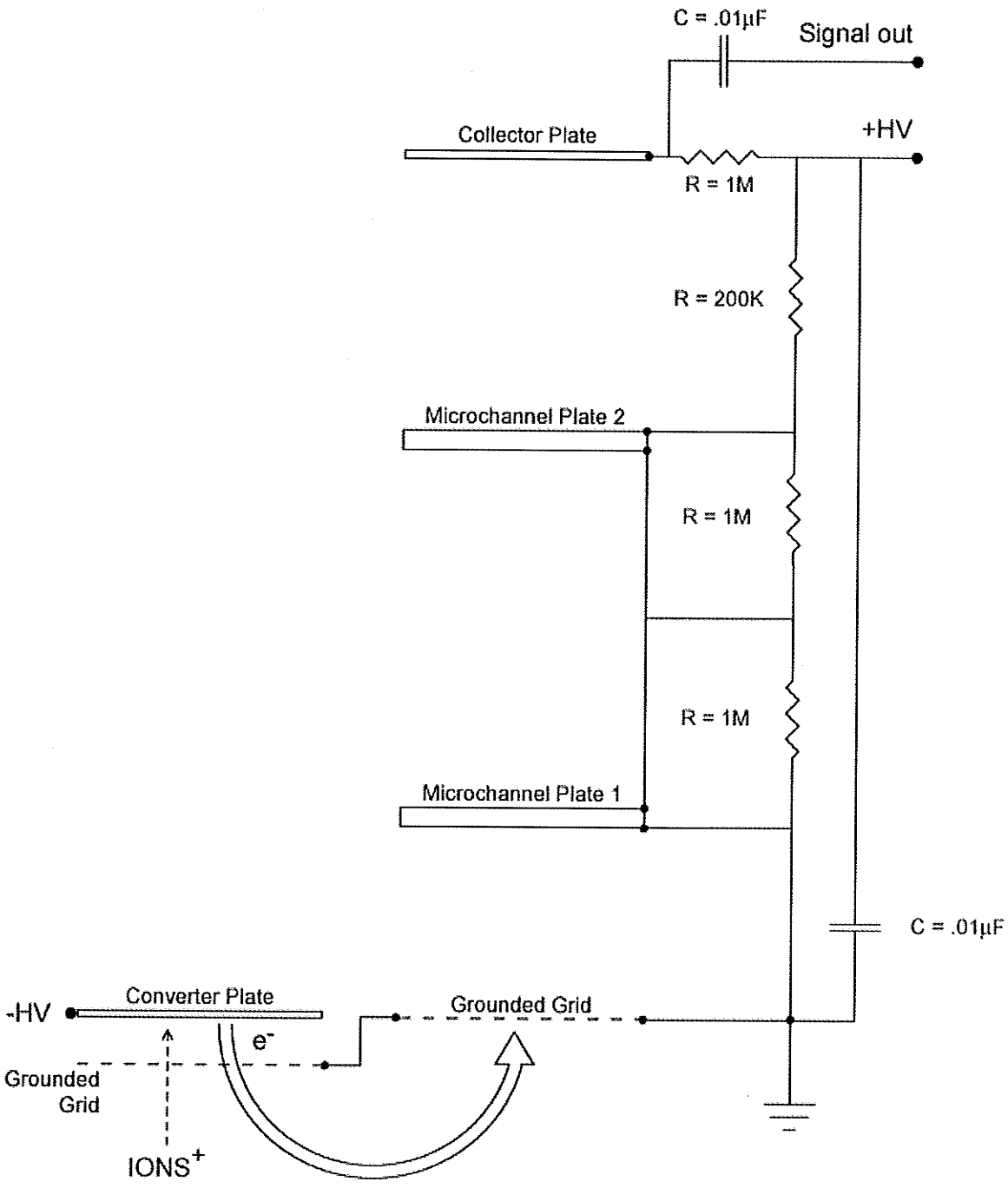

Figure 2-6 : Schematic diagram of the ion detector system.

2.4.2 Mass Calibration

If the accelerating voltage and drift length are known, Equation 4 can be used to determine the *m/z* directly. However, masses generally are obtained from the empirical equation

$$\sqrt{\frac{m}{q}} = at + b \qquad (13)$$

where a and b are calibration constants that depend on the ion accelerations and the ion drift length in the instrument. By knowing the *m/q* ratio of any two ions in a spectrum and by measuring their flight times, it is possible to determine a and b uniquely. Low mass atomic ion peaks are generally well resolved. However, if their peak widths are on the order of only two or three sampling intervals, their time centroids will be inaccurate and will not produce a reliable calibration for extrapolation into the kilodalton and higher mass range.

If a well-characterized species, such as a protein, is added to a sample to be analysed, two ions corresponding to that protein such as $[M+H]^+$ and $[M+2H]^{2+}$, where M represents the intact protein or protein subunit, could be used to calibrate the entire spectrum. This method of adding a single calibrant species is called internal calibration since the calibrant species is added to the unknown sample of interest [97]. In an external mass calibration, a sample containing the calibrant species is analysed in the spectrometer either before or after the sample of interest is analysed. The calibration information from this analysis is then used in subsequent analyses. This technique is used when the spectrometer is known to be very stable and there is no fear of drift in calibration conditions over the time during which the samples of interest are being analysed.

2.4.3 Mass Resolution and Accuracy

After the mass scale is accurately established, mass assignment accuracy is compromised if molecular species like MH^+ and MNa^+ and adduct ions cannot be resolved or if peaks are distorted by metastable fragmentation in the accelerating region. This is why mass resolution and mass accuracy are related. Without good resolution, it is difficult to achieve excellent mass accuracy.

Since isotope peaks are rarely resolved with prompt extraction axial MALDI, mass calibration is performed using some method to centroid a broad, unresolved ion signal. Peak-centroiding methods give reasonably good mass measurement accuracy. Beavis and Chait reported 100 ppm mass accuracy for MALDI-TOF-MS of masses up to ~27 kDa [97]. An obvious limitation of peak-centroiding arises if the peak is skewed due to unresolved ions. For example, many proteins are highly heterogeneous due to phosphorylation, glycosylation, or other types of covalent modifications. In addition, MALDI can produce different ions from the analyte, for example, $[M + H]^+$, $[M + Na]^+$, and $[M + matrix]^+$ adduct ions. These ions may not be resolved in the MALDI-TOF spectrum. The presence of these ions results in a higher measured mass for the analyte. It is also possible that fragmentation of the analyte with the loss of H_2O, CO_2, or other small neutral fragments, reduces the measured mass [98]. Even when artificial peak broadening does not exist, such as when the width of the peak is the same as the isotopic envelope and the individual isotopes are not resolved, there is difficulty achieving 50 ppm accurate mass calibration [99, 83].

Whittal and Li reported 5-70 ppm mass measurement accuracy for peptides via linear MALDI-DE-TOF instruments using internal calibration with an average value of 30-50 ppm [82], similar to the results of Brown and Lennon [100,83].

Edmondson and Russell reported mass measurement accuracy of MALDI-DE-RTOF using external calibration is in the range of 10-15 ppm, and by using

internal calibration the mass measurement accuracy is better than 5 ppm. Although the very best resolution of 10000 – 15000 is obtained by tuning the DE parameters over a narrow mass-to-charge ratio range, good mass measurement accuracy of 5 ppm is obtained by tuning the DE parameters to give good resolution of 6500 over a broad mass-to-charge ratio range of 1-6 kDa. The ability to resolve isotope peaks fully for peptides under 6 kDa greatly improves the mass measurement accuracy of MALDI. An increase in resolution does not necessitate a corresponding increase in mass measurement accuracy. For example, mass resolution of >100000 has been demonstrated for biomolecules by using MALDI-Fourier transform ion cyclotron resonance (FTICR); however, frequency shifts due to imperfect E x B fields complicate mass calibration [101,102]. The MALDI-DE-RTOF internal and external calibration curve functions, as in equation 13 above, are linear over a substantial mass range; they remain accurate even when extrapolated several thousand mass units [103,83]

From equation 12, mass resolution for the TOF mass spectrometer is written as:

$$\frac{m}{\Delta m} = \frac{t}{2\Delta t} \qquad (14)$$

Thus, if the peak width Δt remains constant, mass resolution can be improved by extending the ion flight time t. Reducing the accelerating voltage or increasing the drift tube length can accomplish this. Because high accelerating voltages improve ion transmission, detection efficiency and energy focusing, longer flight lengths of 1-4m have been common. Equally important, however, is the reduction in uncertainties in the time of ion formation, decreasing Δt. In addition, laser jitter or triggering error, bandwidth, detector response, and sampling rate contribute to the overall increase in Δt [104].

The broad and often asymmetric peaks with resolution ranging from 500 down to about 50 for masses above 100 kDa observed with axial MALDI-TOF, are

partially caused by the intrinsic axial velocities of the ejected ions [67,105,106,45]. In addition, unimolecular decay along the TOF flight tube is believed to play a role in determining peak widths [107].

2.5 Desorption Models Overview

Since the MALDI process was discovered, researchers have been trying to understand its fundamental mechanisms. There have been numerous models proposed to explain the desorption and ionization process. Although the details are not well-known, there is a consensus about the broad features of the phenomena. A laser pulse is incident on a binary mixture of analyte usually co-crystallized with a large molar excess of matrix. Energy from the laser is absorbed electronically into the matrix. This causes such an excitation that the matrix undergoes a rapid phase change into the gas phase while expanding into the vacuum carrying with it the analyte molecules. The expanding gas provides collisional cooling for the analyte molecules, so a significant number survive. A fraction of these are ionized, which may reflect their charge state in the solid or the excitation within the matrix causing the ionization of both a portion of the matrix and analyte through the transfer of energy from the excited matrix to the ionization pathways of both compounds.

We begin by looking at two models addressing the transfer of energy from the laser to the matrix. In the first model, Johnson and Sundqvist have applied to MALDI the pressure pulsed sputtering model, which was originally used to describe the sputtering events induced by fast ions in plasma desorption. In this model a pressure gradient is set up perpendicular to the surface by the energy deposited. On exceeding a threshold value, this pressure gradient gives the molecules a net expansion velocity perpendicular to the surface. The ejection of the large molecules is the result of an additive momentum transfer from collisions with fast moving matrix molecules. The large molecules are considered to act as

momentum integrators. Processes such as Coulomb explosion [108], repulsive decays [109] and matrix sublimation [110,111] are possible contributors [112]. Another model by Zhigilei et al. is called the breathing sphere model and was developed for molecular dynamics simulations of laser ablation and desorption of organic solids in which the effect of the internal excitation of matrix molecules by the laser pulse and the relaxation of the excited molecules are described [113]. The model identifies that below threshold, evaporation occurs during which primarily single molecules are desorbed. Above threshold, collective ejection or ablation of large molecular clusters into the gas phase occurs and forms a significant portion of the ejected plume. This is called the collective desorption process [3,114,115], where the laser induced pressure buildup and the phase explosion due to overheating of the irradiated material are the principal processes that determine the dynamics of laser ablation [116].

Next, we look at two models that describe the phase change from solid to gas phase while leaving the analyte molecules intact. Firstly, the homogeneous bottleneck or thermal-spike desorption model developed by Vertes et al. holds that the matrix molecules sublime from the sample surface as a result of local heating. The homogeneous bottleneck model describes the volatilization process as an electronic excitation of the matrix by the UV laser pulse, followed by internal conversion to its vibrational excitation and a competition between energy transfer to the lattice vibrations and to the analyte molecules. This latter transfer is blocked by an energy transfer bottleneck caused by the frequency mismatch between the matrix chemical bonds and the matrix-guest hydrogen bonds and by the scarcity of guest or analyte molecules. In summary, the model describes an inefficient vibrational energy coupling between the laser excited matrix molecules and the analyte. This allows the matrix molecules to become temporarily much hotter than the analyte resulting in homogenous sample heating followed by bulk sample evaporation that can lead to intact, relatively cool analyte molecules. In this model, there is ejection at all laser fluences, but an effective threshold occurs when the fluence is increased to a certain value at which the ejection yield rises

rapidly with the fluence [117,118,119,120]. The second desorption model, proposed by Beavis, is based on the formation of a supersonic jet expansion following laser irradiation of the sample. Similar models have been proposed to describe the laser ablation of polymers [121], the ablation of large molecules in water ice by rapid asymmetric laser heating [122] and MALDI. Beavis explains that there is a rapid phase transition of the matrix molecules from a solid to a high-pressure fluid from a layer of the matrix which is excited by the incident laser light. This fluid is then free to expand adiabatically into the vacuum, forming a supersonic jet, which entrains the analyte molecules within the expanding jet as it changes into the gas phase. The large molecules would be accelerated by the expanding matrix gas, resulting in a uniform velocity distribution for all molecules entrained in the jet.

The final aspect we will look at with two different models is the process of ionization. Knochenmuss et al. looks at the matrix suppression effect in the context of the ionization process. At appropriate matrix to analyte mixing ratios, small to moderate sized analyte ions of 1-20 kDa can fully suppress positively charged matrix ions in MALDI mass spectra. This is true for all matrix species, including radical cations and adducts with protons or alkali-metal ions. The matrix suppression effect is observed regardless of the preferred analyte ion form, be it protonated or an alkali adduct. Initial two-pulse MALDI experiments were performed in which the 337 nm beam from a 3ns pulsed N_2 laser was split, delayed, and recombined on a MALDI sample of valinomycin in DHB matrix. Fixed delays of a few nanoseconds were used to show that nonconcurrent, individually subthreshold pulses could yield excellent MALDI mass spectra. This was a clear indication that energy storage mechanisms are active in UV-MALDI, possibly in the form of excited electronic states [123,124]. From the observation of the matrix suppression effect, a mechanism was proposed for prompt, primary MALDI ionization in which excited matrix molecules are the key species. At least two such excited molecules are believed to be necessary for free ion generation. The model also predicts that the matrix suppression effect will not be observable

with heavy analytes because their large excluded volume precludes desorption at the necessary mixing ratios [125].

The final model of ionization considered here is the "Lucky Survivor" model where "Survivor" refers to the singly charged molecular ions which have a chance of surviving where they have a sufficiently low neutralization cross-section. Proposed by Karas et al., the key feature is the connection between desorption and ionization through cluster-ionization processes as a dominant ionization and charge-separation pathway. They propose that the formation of singly and multiply charged clusters by a deficiency/excess of ions and also by photoionization and subsequent photochemical processes via the matrix, typically occurring in parallel, are the major ionization mechanisms. The model includes the initial formation of more highly charged cluster, and subsequently analyte ions, followed by their charge reduction by electron capture or proton transfer, or both, in the MALDI plume. This accounts for the detection of essentially singly charged ions. The generation of electrons and their partial loss into the surrounding vacuum and solid results in a positively charged ion-neutral plume facilitating a high overall ionization yield. However, these electrons, and also the large excess of protonated matrix ions in the negative ion mode, induce effective ion reneutralization in the plume. These neutralization processes are most effective for the highly charged cluster ions initially formed. One assumption within the model is the statistical charging of clusters by an excess or deficit of ions upon laser ablation This requires precharged analytes and their counterions to be co-crystalized with the host matrix crystals. The concept of preformed ions is well known in other desorption techniques such as SIMS, FAB and LDI, so the existence of cationized as well as preprotonated analytes in solution and in the matrix crystals was suggested for MALDI. Reduction of ionpair interaction by residual solvent facilitates charge separation, which is needed for the production of charged clusters and subsequent ion formation by desolvation [126,127].

2.6 References

1. M. Karas and F. Hillenkamp, *Anal. Chem.* **60** (1988) 2299
2. K. Tanaka, H. Waki, Y. Ido, S. Akita, Y. Yoshida and T. Yoshida, *Rapid Commun. Mass Spectrom.* **2** (1988) 151
3. M. Karas, U. Bahr and F. Hillenkamp, *Int. J. Mass Spectrom. Ion Processes* **92** (1989) 231
4. M. Karas, D. Bachmann, U. Bahr and F. Hillenkamp, *Int. J. Mass Spectrom. Ion Processes* **78** (1987) 53
5. B. T. Chait and S. B. H. Kent, *Science* **257** (1992) 1885
6. F. Hillenkamp, M. Karas, R. C. Beavis and B. T. Chait, *Anal. Chem.* **63** (1991) 1193A
7. B. Musselman and K. Jonscher, *Am. Genomic/Proteomic Tech.* **2** (2002) 22
8. H. Zhu, M. Bilgin and M. Snyder, *Ann. Rev. Biochem.* **72** (2003) 783
9. F. Hillenkamp, M. Karas, R. C. Beavis and B. T. Chait, *Anal. Chem.* **63** (1991) 1193A
10. R. C. Beavis and B. T. Chait, *Rapid Commun. Mass Spectrom.* **3** (1989) 432
11. K. Strupat, M. Karas and F. Hillenkamp, *Int. J. Mass Spectrom. Ion Processes* **111** (1991) 89
12. R. C. Beavis, T. Chaudhary and B. T. Chait, *Org. Mass Spectrom.* **27** (1992) 156
13. R. C. Beavis and J. N. Bridson, *J. Phys. D: Appl. Phys.* **26** (1993) 442
14. S. L. Cohen and B. T. Chait, *Anal. Chem.* **68** (1996) 31
15. R. C. Beavis and B. T. Chait, *Rapid Commun. Mass Spectrom.* **3** (1989) 436
16. M. Karas, U. Bahr, A. Ingendoh, E. Nordhoff, B. Stahl, K. Strupat and F. Hillenkamp, *Anal. Chim. Acta* **241** (1990) 175
17. R. J. Cotter, *Anal. Chem.* **64** (1992) 1027A
18. R. C. Beavis and B. T. Chait, *Rapid Commun. Mass Spectrom.* **3** (1989) 233
19. R. W. Nelson, R. M. Thomas and P. Williams, *Rapid Commun. Mass Spectrom.* **4** (1990) 348
20. M. Salehpour, I. Perera, J. Kjellberg, A. Hedin, M. A. Islamian, P. Hakansson and B. U. R. Sundqvist, *Rapid Commun. Mass Spectrom.* **3** (1989) 259
21. R. C. Beavis and B. T. Chait, *Rapid Commun. Mass Spectrom.* **3** (1989) 436
22. A. Overberg, M. Karas, U. Bahr, R. Kaufmann and F. Hillenkamp, *Rapid Commun. Mass Spectrom.* **4** (1990) 293
23. K. Dreisewerd, M. Schürenberg, M. Karas and F. Hillenkamp, *Int. J. Mass Spectrom. Ion Processes* **154** (1996) 171
24. M. Karas, U. Bahr and F. Hillenkamp, *Int. J. Mass Spectrom. Ion Processes* **92** (1989) 231
25. I. K. Perera, E. Uzcategui, P. Hakansson, G. Brinkmalm, G. Pettersson, G. Johansson and B. U. R. Sundqvist, *Rapid Commun. Mass Spectrom.* **4** (1990) 285

26. B. Spengler and R. J. Cotter, *Anal. Chem.* **62** (1990) 793
27. R. L. Hettich and M.V. Buchanan, *J. Am. Soc. Mass Spectrom.* **2** (1991) 22
28. M. Galicia, A. Vertes and J. H. Callahan, *Anal. Chem.* **74** (2002) 1891
29. J. H. Callahan, M. C. Galicia and A. Vertes, *Appl. Surf. Sci.* **197-198** (2002) 130
30. M. Karas and F. Hillenkamp, *Anal. Chem.* **60** (1988) 2299
31. F. Hillenkamp, M. Karas, A. Ingendoh and B. Stahl In Biological Mass Spectrometry, A. Burlingame and J. A. McCloskey Eds., Elsevier: Amsterdam (1990) 49
32. M. Karas, U. Bahr and U. Giebmann, *Mass Spectrom. Rev.* **10** (1991) 335
33. J. K. Lewis, J. Wei and G. Siuzdak, Encyclopedia of Analytical Chemistry, R. A. Meyers Ed., John Wiley & Sons Ltd, Chichester (2000) pp. 5880 - 5894
34. F. Hillenkamp, M. Karas, D. Holtkamp and P. Klüsener, *Int. J. Mass Spectrom. Ion Processes* **69** (1986) 265
35. A. Overberg, M. Karas, U. Bahr, R. Kaufmann and F. Hillenkamp, *Rapid Commun. Mass Spectrom.* **4** (1990) 293
36. M. Karas, U. Bahr and F. Hillenkamp, *Int. J. Mass Spectrom. Ion Processes* **92** (1989) 231
37. R. C. Beavis and B. T. Chait, *Rapid Commun. Mass Spectrom.* **3** (1989) 233
38. R. C. Beavis and B. T. Chait, *Rapid Commun. Mass Spectrom.* **3** (1989) 432
39. R. C. Beavis, *Org. Mass Spectrom.* **27** (1992) 653
40. R. C. Beavis and B. T. Chait, *Rapid Commun. Mass Spectrom.* **3** (1989) 436
41. S. Zhao, K. V. Somayajula, A. G. Sharkey, D. M. Hercules, F. Hillenkamp, M. Karas and A. Ingendoh, *Anal. Chem.* **63** (1991) 450
42. T-W. D. Chan, A. W. Colburn and P. J. Derrick, *Org. Mass Spectrom.* **27** (1992) 53
43. R. C. Beavis, T. Chaudhary and B. T. Chait, *Org. Mass Spectrom.* **27** (1992) 156
44. F. Hillenkamp, M. Karas, R. C. Beavis and B. T. Chait, *Anal. Chem.* **63** (1991) 1193A
45. A. L. Burlingame, R. K. Boyd and S. J. Gaskell, *Anal. Chem.* **66** (1994) 634R
46. T-W. D. Chan, A. W. Colburn and P. J. Derrick, *Org. Mass Spectrom.* **26** (1991) 342
47. K. J. Wu, A. Steding and C. H. Becker, *Rapid Commun. Mass Spectrom.* **7** (1993) 142
48. D. M. Schieltz, C-W. Chou, C-W. Luo, R. M. Thomas and P. Williams, *Rapid Commun. Mass Spectrom.* **6** (1992) 631
49. S. Berkenkamp, M. Karas and F. Hillenkamp, *Proc. Natl. Acad. Sci. U.S.A.* **93** (1996) 7003
50. T. -W. D Chan, I. Thomas, A. W. Colburn and P. J. Derrick, *Chem. Phys. Lett.* **222** (1994) 579
51. L. Li, A. P. L. Wang and L. D. Coulson, *Anal. Chem.* **65** (1993) 493
52. D. S. Cornett, M. A. Duncan and I. J. Amster, *Anal. Chem.* **65** (1993) 2608

53. M. Karas, H. Ehring, E. Nordhoff, B. Stahl, K. Strupat, F. Hillenkamp, M. Grehl and B. Krebs, *Org. Mass Spectrom.* **28** (1993) 1476
54. K. Strupat, M. Karas and F. Hillenkamp, *Int. J. Mass Spectrom. Ion Processes* **111** (1991) 89
55. S. J. Doktycz, P. J. Savickas and D. A. Krueger, *Rapid Commun. Mass Spectrom.* **5** (1991) 145
56. M. Salehpour, I. Perera, J. Kjellberg, A. Hedin, M. A. Islamian, P. Hakansson and B. U. R. Sundqvist, *Rapid Commun. Mass Spectrom.* **3** (1989) 259
57. W. Ens, Y. Mao, F. Mayer and K. G. Standing, *Rapid Commun. Mass Spectrom.* **5** (1991) 117
58. R. Wang and B. T. Chait, *Curr. Opin. Biotechnol.* **5** (1994) 77
59. F. Xiang and R. C. Beavis, *Rapid Commun. Mass Spectrom.* 8 (1994) 199
60. S. R. Weinberger, K. O. Boernsen, J. W. Finchy, V. Robertson and B. D. Musselman, *Proc. 41st ASMS Conf. Mass Spectrom.*, 1993, 775
61. O. Vorm, P. Roepstorff and M. Mann, *Anal. Chem.* **66** (1994) 3281
62. B. U. R. Sundqvist, I. Kamensky, P.Hakansson, J. Kjellberg, M. Salehpour, S. Widdiyasekera, J. Fohlman, A. P. Peterson and P. Roepstorff, *Biomed. Mass Spectrom.* **11** (1984) 242
63. G. Bolbach, S. Della-Negra, C. Deprun, Y. Le Beyec and K. G. Standing, Rapid Commun. Mass Spectrom. **1** (1987) 22
64. B. T. Chait, K. G. Standing, *Int. J. Mass Spectrom. Ion Phys.* **40** (1981) 185
65. K. G. Standing and W. Ens, "Time-of-flight in mass spectrometers", Encyclopedia of Spectroscopy & Spectrometry, Eds. J. Lindon, G. Tranter and J. Holmes, Academic Press (London, UK) 1999, pp 2360-2365
66. R. C. Beavis and B. T. Chait, *Rapid Commun. Mass Spectrom.* **3** (1989) 233
67. R. C. Beavis, and B. T. Chait, *Chem. Phys. Lett.* **181** (1991) 479
68. J. Zhou, W. Ens, K. G. Standing and A. Verentchikov, *Rapid Commun. Mass Spectrom.* **6** (1992) 671
69. Y. Pan and R. J. Cotter, *Org. Mass Spectrom.* **27** (1992) 3
70. B. A. Mamyrin, V. I. Karataev, D. V. Shmikk and V. A. Zagulin, *Sov. Phys. JETP* **37** (1973) 45
71. X. Tang, R. C. Beavis, W. Ens, F. Lafortune, B. Schueler and K. G. Standing, *Int. J. Mass Spectrom. Ion Processes* **85** (1988) 43
72. V. I. Karataev, B. A. Mamyrin and D. V. Shmikk, *Zh. Tekh. Fiz.* **41** (1971) 1498; *Sov. Phys.-Tech. Phys.* **16** (1972) 1177
73. W. C. Wiley and I. H. McLaren, *Rev. Sci. Instr.* **26** (1955) 1150
74. R. S. Brown and J. Lennon, *Anal. Chem.* **67** (1995) 1998
75. S. M. Colby, T. B. King and J. P. Reilly, *Rapid Commun. Mass Spectrom.* **8** (1994) 865
76. R. M. Whittal and L. Li, *Anal. Chem.* **67** (1995) 1950
77. M. L. Vestal, P. Juhasz and S. A. Martin, *Rapid Commun. Mass Spectrom.* **9** (1995) 1044

78. M. L. Vestal, reported at the *Sanibel Conference on Mass Spectrometry*, Sanibel Island, FL (1998)
79. R. S. Brown, J. J. Lennon and D. Christie, *Desorption '94-Mass Spectrometry of Large Organic Ions by Particle and Photon Induced Desorption*, March 27-31, 1994, Sunriver OR, USA, p. 63.
80. R. S. Brown and J. Lennon, *Anal. Chem.* **67** (1995) 1998
81. S. M. Colby, T. B. King and J. P. Reilly, *Rapid Commun. Mass Spectrom.* **8** (1994) 865
82. R. M. Whittal and L. Li, *Anal. Chem.* **67** (1995) 1950
83. R. D. Edmondson and D. H. Russell, *J. Am. Soc. Mass Spectrom.* **7** (1996) 995
84. D. H. Russell and R. D. Edmondson, *J. Mass Spectrom.* **32** (1997) 263
85. U. Bahr, J. Stahl-Zeng, E. Gleitsmann and M. Karas, *J. Mass Spectrom.* **32** (1997) 1111
86. M. L. Vestal, P. Juhasz and S. A. Martin, *Rapid Commun. Mass Spectrom.* **9** (1995) 1044
87. P. Gerhard, S. Loffler and K. H. Homann, *Chem. Phys. Lett.* **137** (1987) 306
88. J. K. Olthoff, I. A. Lys and R. J. Cotter, *Rapid Commun. Mass Spectrom.* **2** (1988) 171
89. W. B. Emary, I. Lys, R. J. Cotter, R. Simpson and A. Hoffman, *Anal. Chem.* **62** (1990) 1319
90. T. Bergmann, T. P. Martin and H. Schaber, *Rev. Sci. Instrum.* **60** (1989) 792
91. J. H. J. Dawson and M. Guilhaus, *Rapid Commun. Mass Spectrom.* **3** (1989) 155
92. C. H. Sin, E. D. Lee and M. L. Lee, *Anal. Chem.* **63** (1991) 2897
93. A. N. Verentchikov, W. Ens and K. G. Standing, *Anal. Chem.* **66** (1994) 126
94. A. N. Krutchinsky, A. V. Loboda, V. L. Spicer, R. Dworschak, W. Ens and K. G. Standing, Rapid Commun. Mass Spectrom. **12** (1998) 508
95. W. Ens, PhD thesis University of Manitoba, 1984, p 27
96. W. Ens, K. G. Standing and A. Verentchikov, Proceedings of the Int. Conf. on Instrumentation for Time of Flight Mass Spectrometry, G. J. Blanar and R. J. Cotter, Eds., 1992, p. 137
97. R. C. Beavis and B. T. Chait, *Anal. Chem.* **62** (1990) 1836
98. T. Solouki, K. J. Gillig and D. H. Russell, *Rapid Commun. Mass Spectrom.* **8** (1994) 26
99. R. A. Zubarev, P. A. Demirev, P. Hakansson and B. U. R. Sundqvist, *Anal. Chem.* **67** (1995) 3793
100. R. S. Brown and J. Lennon, *Anal. Chem.* **67** (1995) 3990
101. Y. Li, R. T. McIver and R. L. Hunter, *Anal. Chem.* **66** (1994) 2077
102. L. Pasa-Tolic, Y. Huang, S. Guan, H. S. Kim and A. G. Marshall, *J. Mass Spectrom.* **30** (1995) 825
103. R. D. Edmondson and D. H. Russell, *J. Am. Soc. Mass Spectrom.* **7** (1996) 995

104. R. J. Cotter, *Anal. Chem.* **64** (1992) 1027A
105. T. Huth-Fehre and C. H. Becker, *Rapid Commun. Mass Spectrom.* **5** (1991) 378
106. R. C. Beavis and B. T. Chait, In Methods and Mechanisms for Producing Ions from Large Molecules, in the NATO ASI Series B: Physics Vol. 269, ed. By K. G. Standing and W. Ens, p. 227, Plenum Press, New York (1991)
107. B. Spengler, D. Kirsch and R. Kaufmann, *Rapid Commun. Mass Spectrom.* **5** (1991) 198
108. P. K. Haff, *Appl. Phys. Letters* **29** (1976) 473
109. P. Williams and B. U. R. Sundqvist, *Phys. Rev. Letters* **58** (1987) 1031
110. A. Vertes, R. Gijbels and R. D. Levine, *Rapid Commun. Mass Spectrom.* **4** (1990) 228
111. A. Vertes, R. D. Levine, *Chem. Phys. Lett.* **171** (1990) 284
112. R. E. Johnson and B. U. R. Sundqvist, *Rapid Commun. Mass Spectrom.* **5** (1991) 574
113. L. V. Zhigilei, P. B. S. Kodali and B. J. Garrison, *J. Phys. Chem. B* **101** (1997) 2028
114. A. Vertes, R. D. Levine, *Chem. Phys. Lett.* **171** (1990) 284
115. Y. Pan and R. J. Cotter, *Org. Mass Spectrom.* **27** (1992) 3
116. L. V. Zhigilei, P. B. S. Kodali and B. J. Garrison, *Chem. Phys. Lett.* **276** (1997) 269
117. A. Vertes and R. Gijbels, *Scanning Microsc.* **5** (1991) 317
118. A. Vertes, R. Gijbels and R. D. Levine, *Rapid Commun. Mass Spectrom.* **4** (1990) 228
119. A. Vertes, R. D. Levine, *Chem. Phys. Lett.* **171** (1990) 284
120. R. N. Zare and R. D. Levine, *Chem. Phys. Letters* **136** (1987) 593
121. S. G. Hansen, *J. Appl. Phys.* **66** (1989) 3329
122. R. W. Nelson, M. J. Rainbow, D. E. Lohr and P. Williams, *Science* **246** (1989) 1585
123. R. Knochenmuss and A. Vertes, *J. Phys. Chem. B* **104** (2000) 5406
124. R. Knochenmuss, F. Dubois, M. J. Dale and R. Zenobi, *Rapid Commun. Mass Spectrom.* **10** (1996) 871
125. R. Knochenmuss, F. Dubois, M. J. Dale and R. Zenobi, *Rapid Commun. Mass Spectrom.* **10** (1996) 871
126. M. Karas, M. Gluckmann and J. Schafer, *J. Mass Spectrom.* **35** (2000) 1
127. R. Kruger, A. Pfenninger, I. Fournier, M. Gluckmann and M. Karas, *Anal. Chem.* **73** (2001) 5812

3 Orthogonal-injection MALDI time-of-flight mass spectrometry without collisional cooling

3.1 Introduction

In spite of the significant progress made in MALDI time-of-flight mass spectrometry with the introduction of delayed extraction as described in the previous chapter, it has some limitations. On leaving the MALDI plume, ions have approximately the same velocity distribution independent of mass. The resulting dependence of the energy on mass means that the optimum time focusing conditions have some mass dependence, so resolution can only be optimized for part of the spectrum at a time. For the same reason there is a small perturbation in the mass vs. time formula, so high accuracy requires a more complex calibration procedure. Delayed extraction partially decouples the ion production process from the mass measurement, but there is still some dependence of the necessary focusing conditions on the type of matrix, the method of sample preparation, and the laser fluence, although the sensitivity to fluence is smaller than in dc-extraction. Performance in delayed extraction MALDI also remains dependent on a flat equipotential sample surface, so irregular or insulating surfaces present problems. Also, because of the large number of ions that are normally produced in a single shot, they must be measured by a transient recorder. Even so, it is necessary to match the detector gain carefully to the laser fluence to avoid saturating the analog-to-digital converter on intense peaks, and to avoid detector-shadowing problems produced by intense matrix signals.

Finally, delayed extraction has had limited success in improving the resolution for masses above about 30 kDa as discussed earlier.

The deficiencies in delayed extraction suggest that other methods of injecting MALDI ions into time-of-flight instruments should be explored. One such method is orthogonal injection, where ions enter the TOF spectrometer from a direction perpendicular to its axis. Orthogonal injection had already been used by a number of investigators in the early days of MALDI [1] to measure initial velocities or accommodate liquid matrices, however, these were not designed to improve performance and were largely abandoned in favour of axial injection because of problems related to the large velocity, and velocity spread, of the MALDI ion beam and the high local charge density in the ion pulse. Nevertheless, the technique has provided an efficient means of coupling electrospray sources to TOF instruments [2,3], where similar problems are encountered in a less acute form. Figure 3-1 shows a schematic diagram of an orthogonal ESI-MS instrument built in our laboratory [3]. The ions are formed at the electrospray source. Shown as the dotted line, the ions then enter the quadrupole ion guide and are collisionally cooled to form a relatively confined stream of ions with very little velocity in the direction perpendicular to the direction of their flow. The problem with ion velocity spread has thus been largely overcome by this quadrupole ion guide [4,5,6]. Emerging from the guide, they enter the extraction region. The injection pulser provides pulses in the several kHz frequency range to pulse the ions and inject them into the acceleration region. From there, the system is similar to the reflecting instrument discussed earlier. The success with this orthogonal system suggested that similar improvements might be obtained for MALDI ions.

Even without collisional cooling, orthogonal injection of MALDI ions (OMALDI) into a TOF spectrometer [1, 7, 8] has some potential advantages over the usual axial injection geometry. In particular it serves to decouple the ion production process from the mass measurement to a greater extent than is possible even in

delayed-extraction MALDI. Thus there is greater freedom to vary the target conditions without affecting the mass spectrum. The target might be composed of relatively large crystals or it might be placed on an insulating substrate for transmission desorption, but these would not effect the extraction mechanism and hence the focusing capabilities of an OMALDI system. Figure 3-2 shows the relatively larger axial compared to orthogonal component of ion velocity within a MALDI plume. Some natural improvement in resolution might therefore be expected because the largest spread in velocities is along the axis normal to the target, which is perpendicular to the extraction direction or TOF instrument axis.

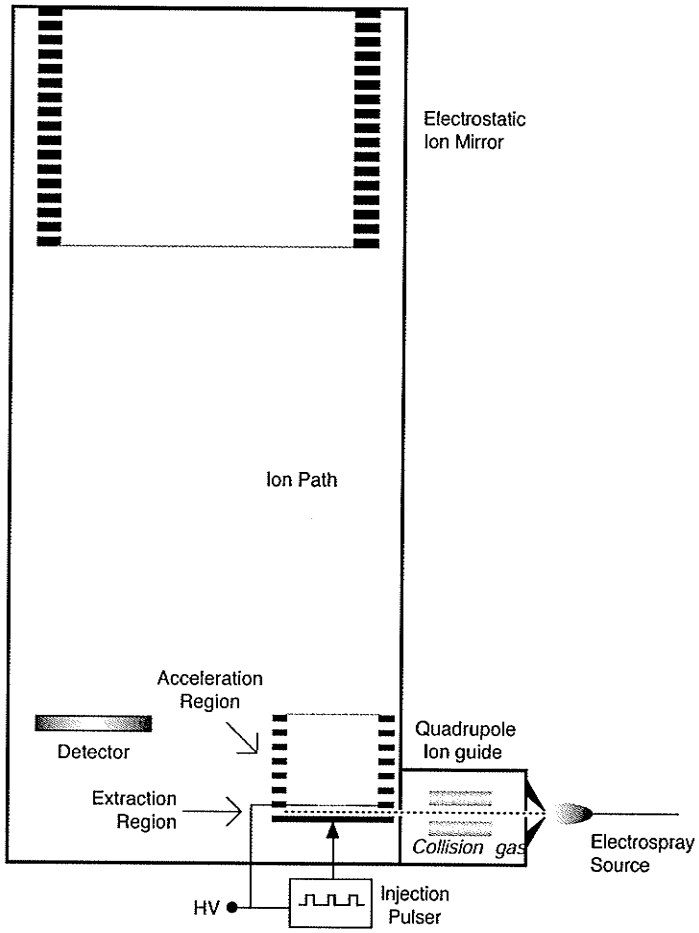

Figure 3-1 : A schematic diagram of Manitoba TOFIII, an ESI-TOF-MS built in our laboratory, from which the idea of OMALDI evolved.

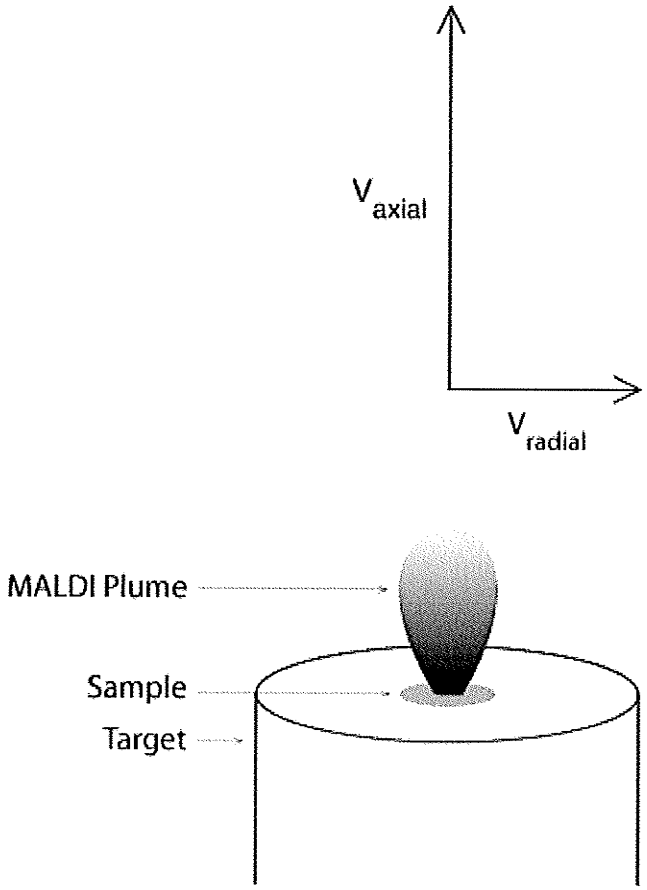

Figure 3-2 : Schematic of the MALDI plume with ion velocity vector components showing the relatively greater axial compared to orthogonal component.

Another aspect to an OMALDI-MS system which must be considered concerns the metastable decay of ions prior to extraction. This concept is illustrated in Figure 3-3. In Figure 3-3 part a), non-reflecting axial MALDI is shown in which the desorption begins with an intact but metastable ion A. The ion undergoes metastable decay by stage B but since the ion center of mass remains the same, all fragments arrive at the detector at essentially the same time and the signal corresponding to a molecular ion is recorded. In Figure 3-3 part b) the desorption results in an intact metastable ion A. The ion undergoes metastable decay by stage B and is then extracted orthogonally along the instrument axis. This is shown at stage D where the individual fragments and the remaining parent ions will each have their own time-of-flight according to the usual calibration. The

time-of-flight spectra shown indicate that for the orthogonal mode (b), the spectrum shows the fragment ions with a much smaller molecular ion peak compared to the time-of-flight spectrum from the non-reflecting linear mode analysis (a) in which there is only a molecular ion peak. Depending on the analysis requirements, this feature may be desirable to help understand molecular structure, but it can also be a disadvantage if one wishes to see a strong molecular ion signal. Axial injection instruments with electrostatic mirrors also separate the decay fragments due to their individual kinetic energies. The flight times in this case are not determined by the usual calibration curve, but the product ion masses can be calculated if the parent ion mass is known [9]. In MALDI, the parent ion is selected by a timed filter before entry to the mirror in a technique called post-source decay (PSD) analysis [10].

Here we report experiments and calculations to test the feasibility of OMALDI-MS without collisional cooling. These experiments were initiated prior to the addition of collisional cooling to the ESI-MS instrument [6], and continued briefly afterward to determine if OMALDI-MS was viable without cooling since it is a simpler geometry, and could possibly be implemented on axial-injection systems with suitable modifications. The results were published as part of a longer paper on orthogonal-injection of MALDI ions in a time-of-flight instrument [12].

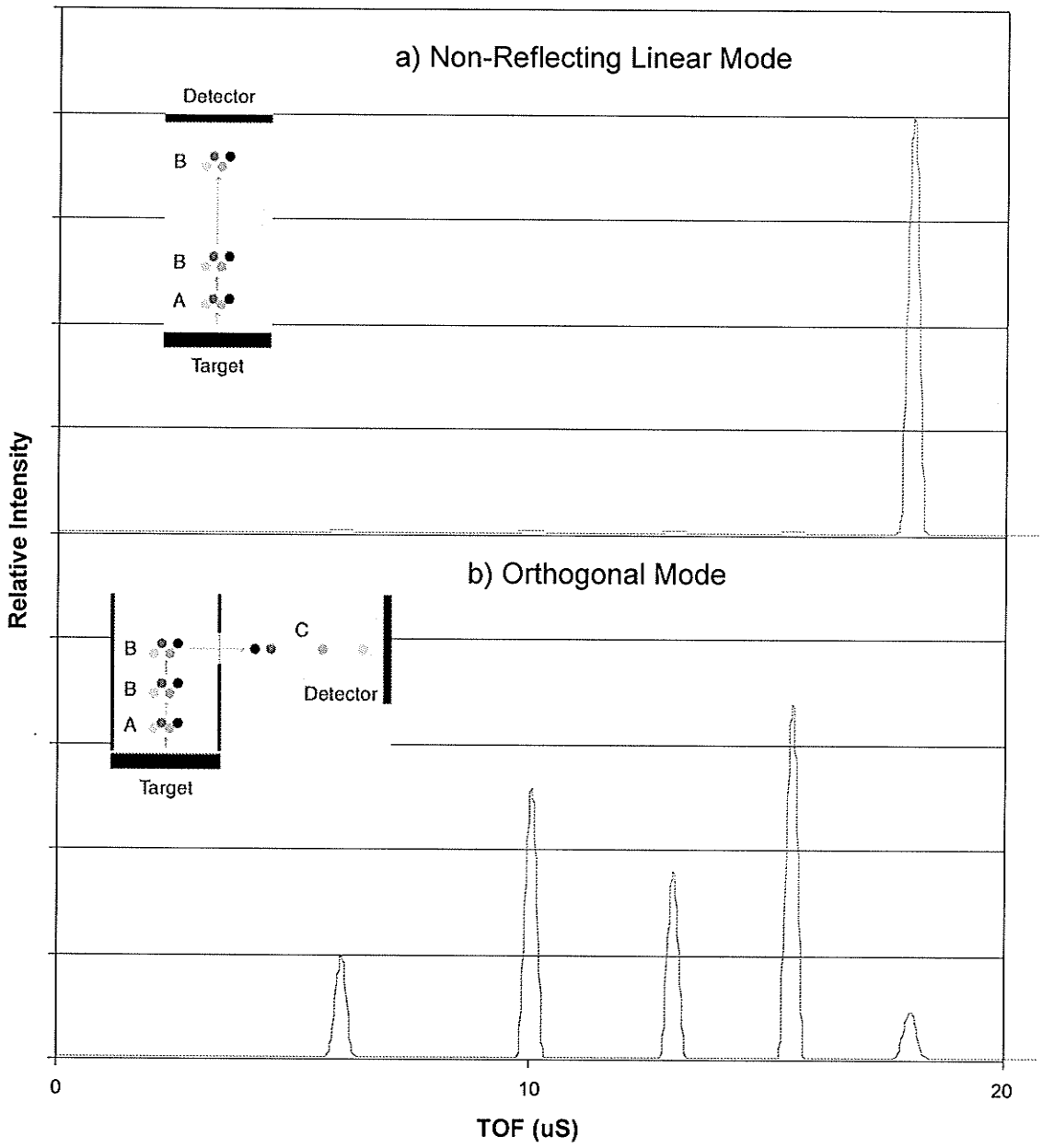

Figure 3-3 : a) Non-reflecting linear MALDI in which the metastable decay fragments arrive at the detector at essentially the same time and b) OMALDI where the metastable decay has occurred prior to extraction, each fragment is analysed separately, reducing the molecular ion signal substantially.

3.2 *Experimental*

3.2.1 OMALDI-MS Instrument Description

Figure 3-4 is a schematic diagram of the OMALDI-MS system designed and built to test the feasibility of OMALDI-MS without collisional cooling. In this instrument, the ion plume is allowed to expand toward the mass spectrometer axis and is then pulsed into the spectrometer. The ions are detected with an MCP detector and recorded with a transient recorder as in usual MALDI experiments. The detector was placed at the spatial focus plane to determine the minimum time width of the injected pulse, and thereby set a limit on the possible resolution for any given length of flight path.

The laser is situated externally to the vacuum chamber and is aimed and focused on the surface of the sample target with an optical lens system. The sample target is held within an initially field free region defined by the backing plate and grid 1 separated by 1.1 cm. This field free region is floated at the accelerating voltage (HV), typically 15 kV. The extraction pulse is applied to the backing plate to inject the ions into the acceleration region and is on the order of 1.5 kV. The acceleration region is 5.5 cm in length and is comprised of a series of flat rings linked by resistors, which provides an electric potential gradient from the HV down to ground at grid 2. The ions then enter a 35-cm axial drift region, and then impact the MCP detector plates, producing a signal which is recorded in the transient recorder. The detector plates are also configured with a pulser which can turn the detector off during the arrival time of intense low-mass ion signals, to avoid detector saturation effects (see section 2.3.1).

Since the axial velocity of the ions in the MALDI plume is largely independent of mass, the corresponding energy $\frac{1}{2}mv^2$ is mass dependent. As a result, the direction of the trajectory in the TOF spectrometer depends on the mass. To

avoid mass discrimination in these experiments, a ramped deflection voltage was applied to the deflection plates shown in Figure 3-4.

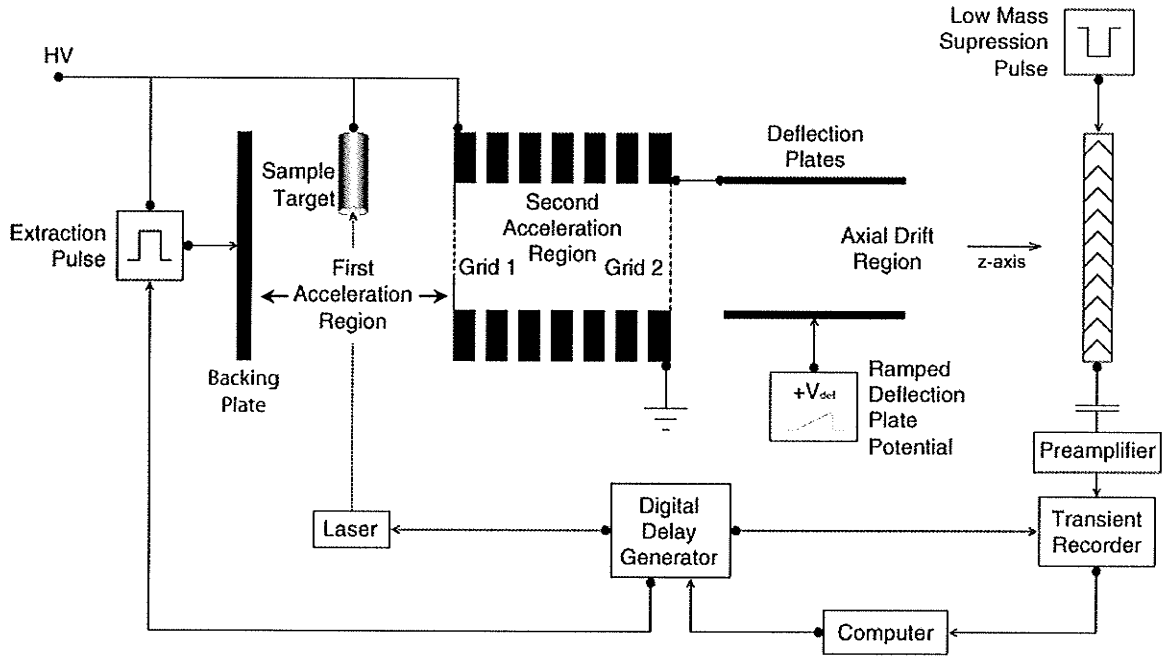

Figure 3-4 : Schematic diagram of the OMALDI-MS system.

3.2.2 Data Acquisition with the OMALDI-MS System

The spectrum acquisition for the OMALDI-MS system, schematically illustrated in Figure 3-4, begins with a trigger pulse from the computer sent to the digital delay generator. The digital delay generator immediately sends a trigger pulse to the laser which fires a ~ 3 nanosecond pulse at the sample target face at a repetition rate up to 20 Hz but typically 10 Hz. The MALDI plume is formed and expands into the first stage, which is initially field-free. The ions have a velocity distribution in both the axial and radial directions as shown in Figure 3-2. After a predetermined time delay τ, the digital delay generator triggers an extraction pulse to the backing plate, and at the same time, triggers the transient recorder to begin recording the signal from the detector. Therefore, the zero time in the TOF spectrum is defined as when the extraction pulse occurs. After the delay

time τ, the ions that have moved into a position accessible to the grid 1 opening are injected into the second acceleration region and on to the detector as described above, and the other ions are lost to the walls of the formerly field free region. Of the lost ions, the faster ions will have gone past the grid 1 opening and the slower ions won't have arrived there before the extraction pulse. The detector current caused by the electron cascade from the impact of the ions produces a voltage pulse which is capacitively coupled to a preamplifier and then recorded as a function of time by the transient recorder with a time resolution of 5 nanoseconds. After the preset time of 100 μs, during which the transient recorder is listening for signal, the computer interrogates the transient recorder and reads in the spectrum data. Another data acquisition cycle begins and subsequent data is automatically summed with the preceding data within the computer and a final spectrum is presented when the desired number of acquisition cycles is reached.

To achieve better time focusing and therefore higher resolution, the sample probe was placed within a tube extending 14 mm beyond the sample face, at the end of which a slit was placed to collimate the ion beam. The sample face is 4 mm in diameter and the slits varied between 4 mm and 1 mm in width. The slit was oriented such that the narrow width was parallel to the z-axis of the instrument. The slit has the effect of eliminating the ions with a larger z-component of velocity. Figure 3-5 (a) shows the MALDI plume with corresponding velocity component orientation. Figure 3-5 (b) through (d) illustrate the maximum angle of acceptance each successively smaller aperture slit will allow through. In Figure 3-5 (b), there is no slit, which corresponds to the largest divergence corresponding to the broadest radial velocity distribution. Finally with the aperture slit shown in (d), the slit is the smallest, allowing the smallest radial velocity distribution and highest resolution.

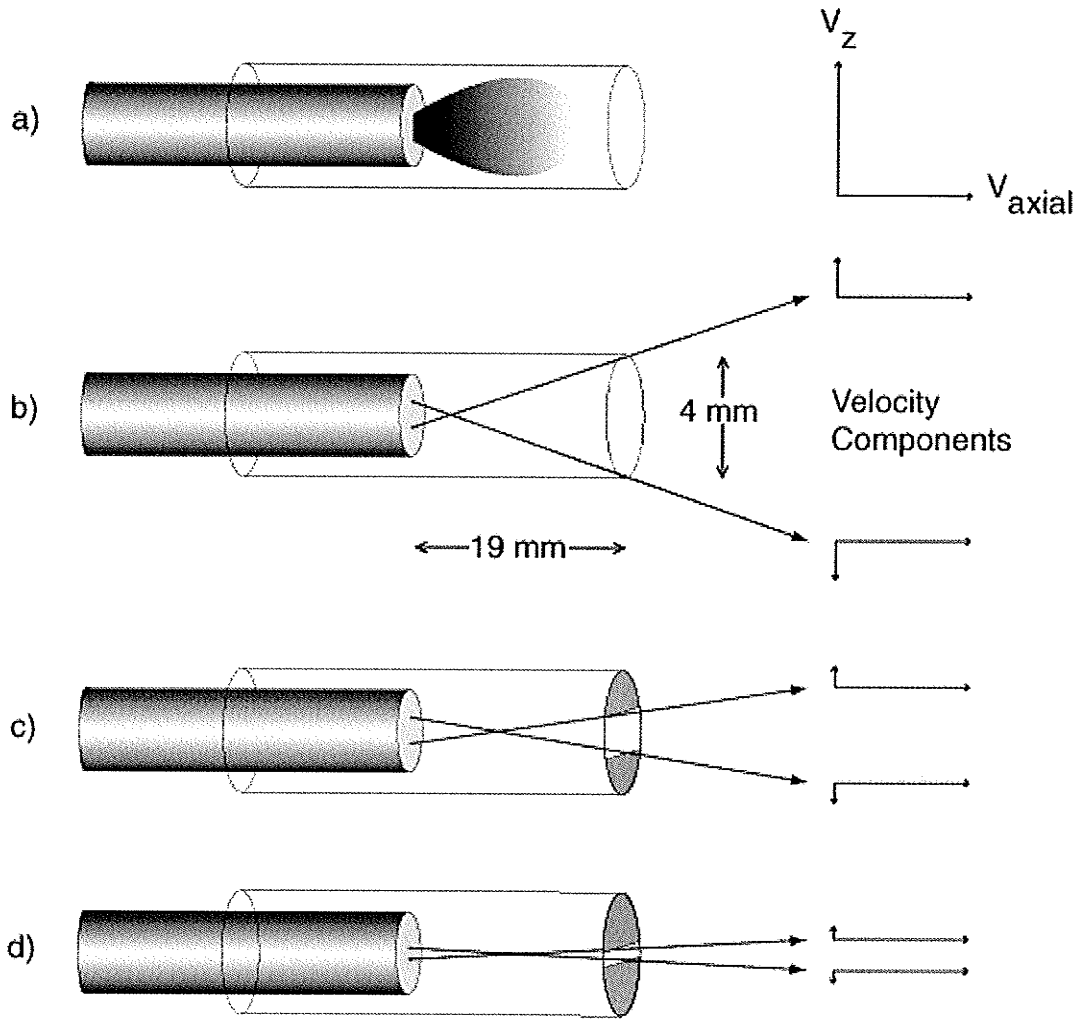

Figure 3-5 : Close-up of sample target tube: a) with no aperture slit and showing orientation of velocity components b), c), d) successively smaller aperture slits for ion beam collimation with relative axial and orthogonal velocity components shown.

3.3 Calculations of Resolution

To evaluate the feasibility of an orthogonal MALDI source without collisional cooling, an estimate was made of the resolution based on the distribution of the flight times calculated directly for five ions distributed along the z-axis as shown in Figure 3-6. Because the ions come from essentially the same point on the target, the z-position is closely correlated to the initial velocity of the ions.

Variation in flight time because of the finite size of the desorption site are expected to be small in comparison.

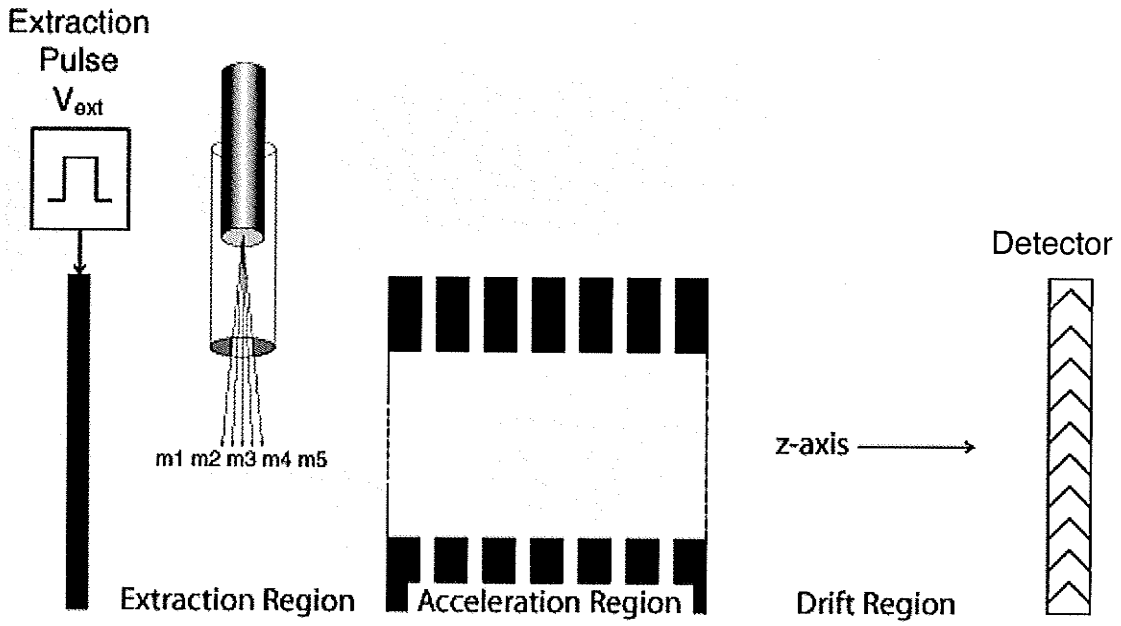

Figure 3-6 : Schematic of the OMALDI-TOF-MS instrument showing the variables used in the calculations.

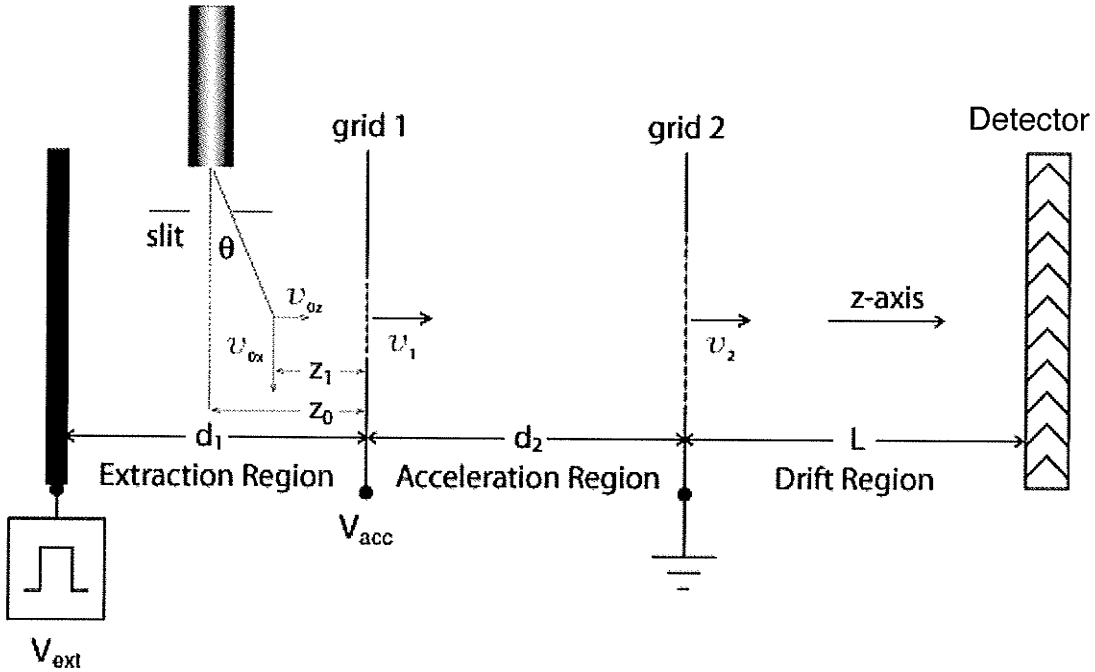

Figure 3-7 : Schematic illustration showing variables used in the resolution calculations.

In the following calculations, the initial axial velocity of the myoglobin ions (MW 16951 Da) was set at 770 m/s from the velocity measurement of bovine superoxide dismutase of a similar mass (MW 15590 Da) determined by Beavis and Chait [11]. Also the delay time τ between the laser shot and time and extraction pulse was fixed at 40 μs. The combination of these fixed values for initial axial velocity and delay time put the ions at the instrument axis prior to extraction, a distance of about 3 cm from the target face. The flight time for an ion desorbed at an angle θ as shown in Figure 3-7 can be expressed as the sum of three components:

$$t = t_1 + t_2 + t_3 \qquad (1)$$

where t_i represents the flight time in the:

t_1 : extraction region

t_2 : acceleration region

t_3 : drift region

From simple kinematics,

$$t_1 = \frac{\left(-v_{0z} + \sqrt{v_{0z}^2 + 2a_1 z_1}\right)}{a_1} \qquad (2)$$

where

$$a_1 = \frac{qV_{ext}}{md_1} \qquad (3)$$

is the acceleration of the ion in the extraction region on application of the extraction potential V_{ext}, where q is the charge of the ion, m is the mass of the ion in and d_1 is the length of the extraction region.

The component of the initial velocity along the instrument axis (z-axis) is:

$$v_{0z} = v_0 \sin\theta \qquad (4)$$

where v_0 is the initial velocity of the ion (770 m/s) after interactions in the plume and θ is the angle to the target normal. The calculation was performed for

$$\theta = 0, \pm \theta_0/2, \pm \theta_0$$

and

$$z_1 = z_0 - v_{0z}\tau \qquad (5)$$

where θ_0 is the maximum acceptance angle defined by the slit width, z_0 is the distance from the target face center to the first grid and τ is the time between desorption and the extraction pulse (40μs).

Calculating t_2 we get:

$$t_2 = \frac{\left(-v_1 + \sqrt{v_1^2 + 2a_2 d_2}\right)}{a_2} \qquad (6)$$

where

$$a_2 = \frac{qV_{acc}}{md_2} \qquad (7)$$

is the acceleration of the ion in the acceleration region of length d_2, across which there is a static potential of V_{acc} and

$$v_1 = v_{0z} + a_1 t_1 \qquad (8)$$

is the final ion velocity in the extraction region and the initial ion velocity in the acceleration region.

Calculating t_3 we get:

$$t_3 = \frac{L}{v_2} \qquad (9)$$

where L is the drift region length and

$$v_2 = v_1 + a_2 t_2 \qquad (10)$$

is the final ion velocity in the acceleration region and the initial ion velocity in the drift region.

The standard deviation Δt of the flight times for the ions desorbed at the five angles is then calculated. The mass resolution can then be calculated from:

$$R = \frac{t}{2\Delta t} \qquad (11)$$

These calculations do not take account of the distribution of velocities that are accepted due to the finite size of the aperture in the plane of the first grid, admitting ions into the spectrometer. A finite aperture must however be assumed, because the time-of-flight is calculated for all five ions with the same υ_0 and τ, so they do not lie along a line. On the other hand, the resolution may be underestimated because the two ions at the greatest angle ($\pm\theta$), which are less probable, especially for the wider slits, are given equal weight in the calculation of the standard deviation. Even so, the calculations are expected to give a reasonable estimate of the resolution, and indicate trends relative to various experimental parameters.

As mentioned above, this experiment was designed to evaluate the orthogonal extraction source geometry to determine the limits of time and mass resolution of a reflecting time-of-flight instrument with such a source. If the plane of the detector is set up to coincide with the object plane for an electrostatic mirror, then the measured time spread will not be increased appreciably, but the flight time will increase in proportion to the effective flight path. Thus, the limiting resolution is higher by the ratio of the effective flight paths. For a typical geometry with a 2.5 m effective flight path, the limiting resolution should be approximately 7 times higher. Of course, effects not considered in these calculations would be expected to dominate at or below about 10,000 resolution, and since this is a competitive resolution for TOF instruments, the goal in these experiments is to realize a resolution of 1500 or higher in this short linear instrument.

To study the focusing capability of this system, we look at the effect on resolution of the extraction pulse height V_{ext}, the acceleration voltage V_{acc}, and the slit width which defines the maximum desorption angle θ_0, for different mass ranges. Since one goal in this experiment was to improve the mass resolution in the higher mass range, many of the following calculations are made for myoglobin (MW 16951 Da). Subsequently, most of the performance gains in time-of-flight

instruments have been made in the lower mass range, but the trends and limits indicated by these calculations remain valid.

The first relationship we look at is the dependence of resolution on the extraction pulse height for a number of slit widths to determine the optimum V_{ext} value for a particular mass and to see how sensitive the resolution is to the slit width. Figure 3-8 is a plot of resolution vs. V_{ext} for myoglobin with mass = 16951 Da with 5 different aperture widths used. The curves show that the resolution peaks for an optimum value of the extraction voltage, and that for sufficiently small slit width, a resolution greater than 1500 is possible. However, as might be expected, the resolution decreases as the slit is opened, and for a slit width of 2 mm or more, the resolution is below 1500.

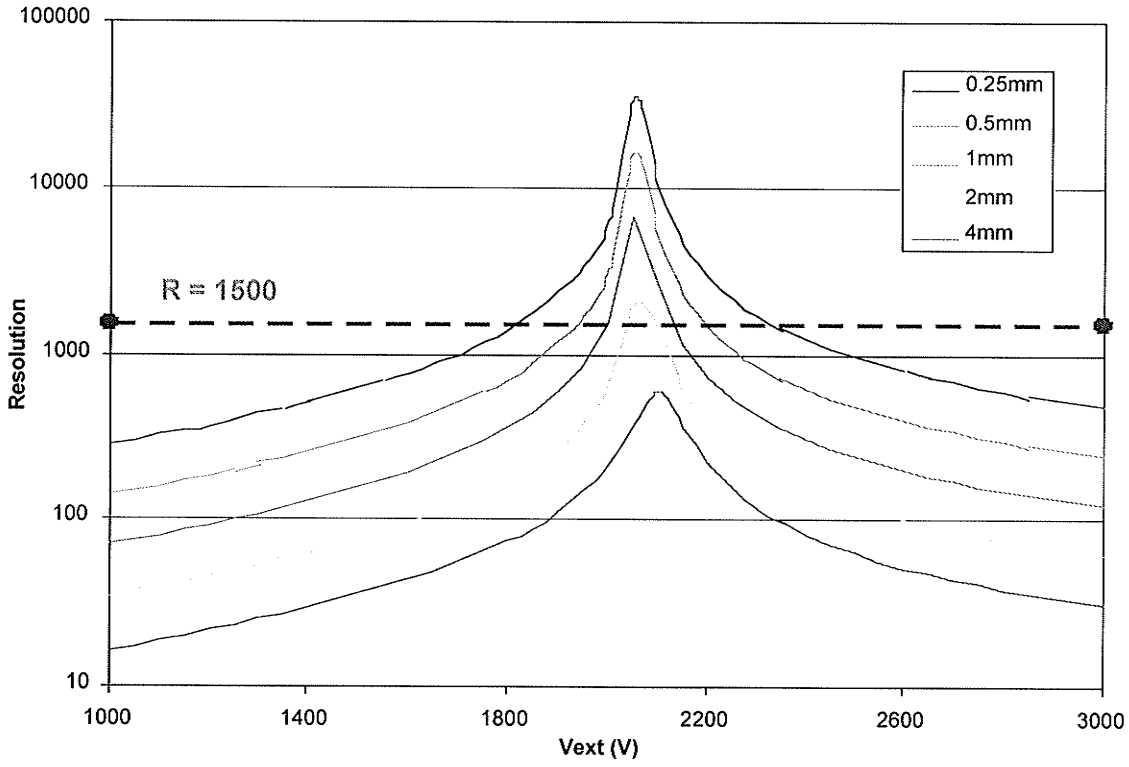

Figure 3-8 : The smaller the aperture, the greater the resolution is for a particular mass but the faster the resolution decreases as Vext varies away from the optimum value for the selected mass.

The effect of the slit width is shown directly in Figure 3-9, where the optimum resolution for myoglobin is plotted as a function of slit width along with the opening area, which should be closely related to the ion acceptance, if not perfectly linear. Note that the intensity of the ion flux through the aperture would not be linear with area as the aperture increases since the ion density has an angular distribution within the plume in the form of $\cos^n \theta$ where n is dependent on the desorption parameters and θ is measured from the target surface normal. The critical aspect of this plot is that as the aperture opens up the resolution drops dramatically. The feasibility of the source therefore depends on the minimum slit width required that provides practical signal intensity.

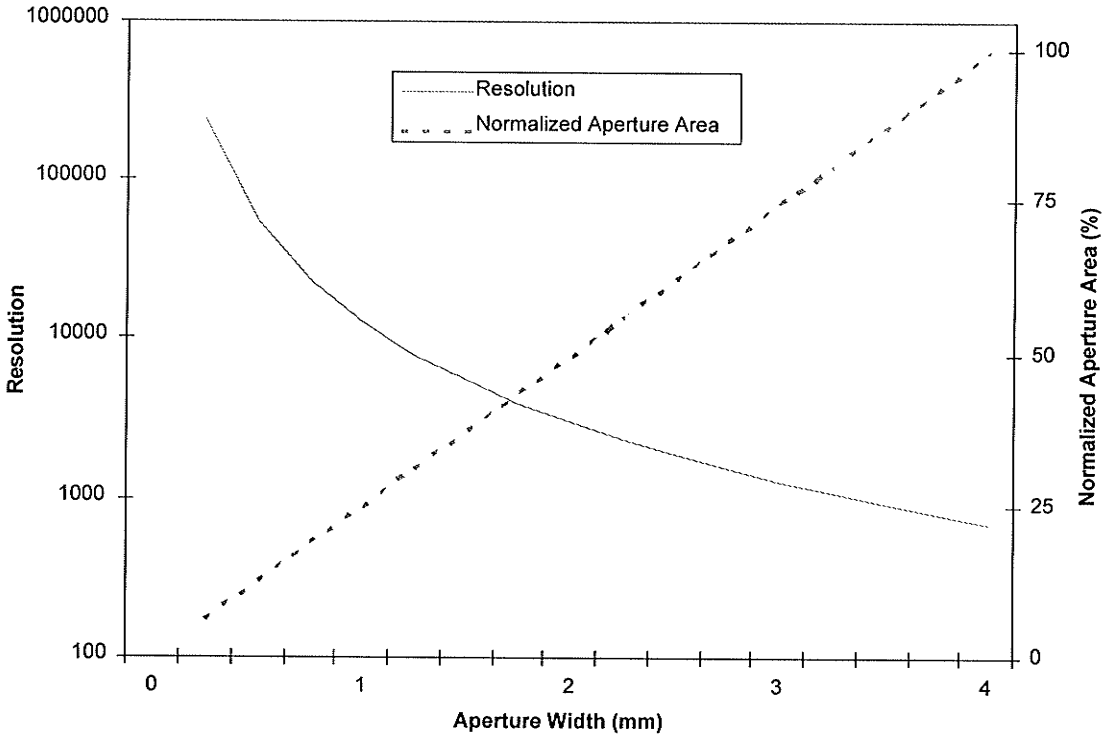

Figure 3-9 : The effect of the slit width on the resolution of myoglobin (MW 16951 Da).

If the source proved feasible, the mass dependence of the resolution is clearly important. This dependence is shown for myoglobin for several slit widths in Figure 3-10. Clearly, even for the narrow slits, where the best resolution is

acceptable, the range of acceptability is quite small. Figure 3-11 shows the mass dependence for optimizations at three separate masses (α-CHCA MW 379 Da, insulin MW 5734 Da, myoglobin MW 16951 Da) and for two slit widths. For the narrowest slit width, acceptable resolution is possible with these three optimizations up to about *m/z* 20,000 . However, for the widest slit width, the resolution is below 1000 over the entire mass range.

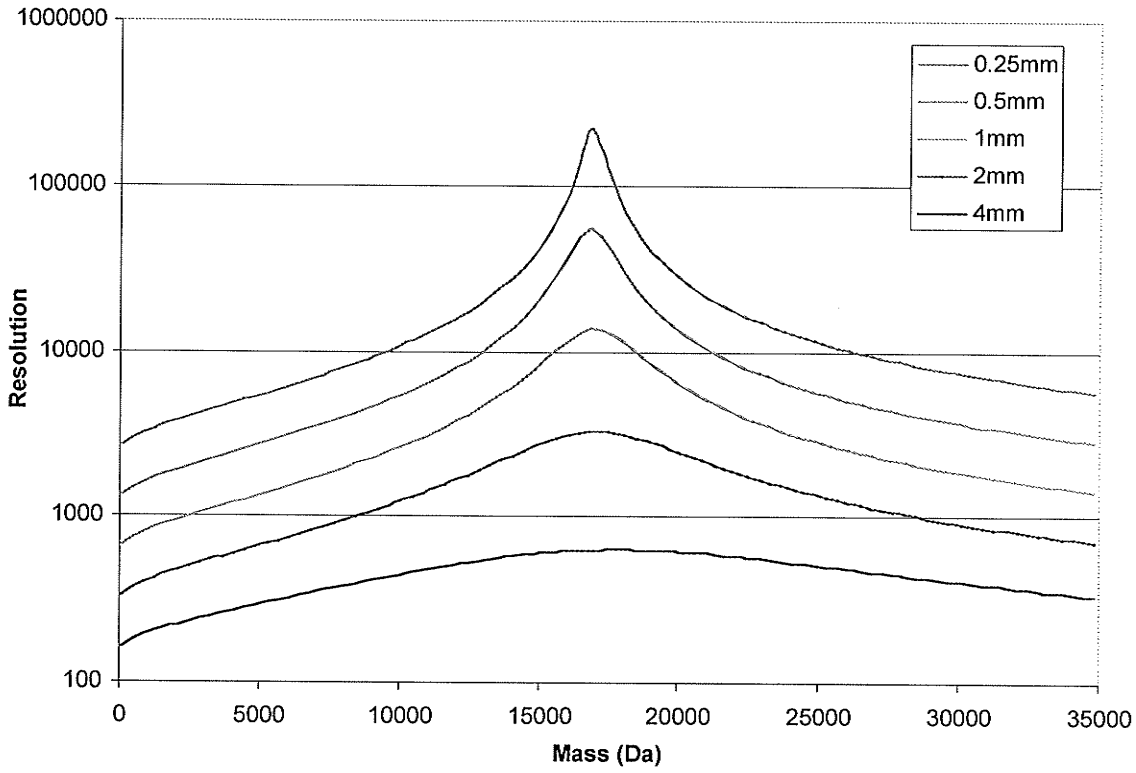

Figure 3-10 : Mass dependence of mass resolution for different slit widths.

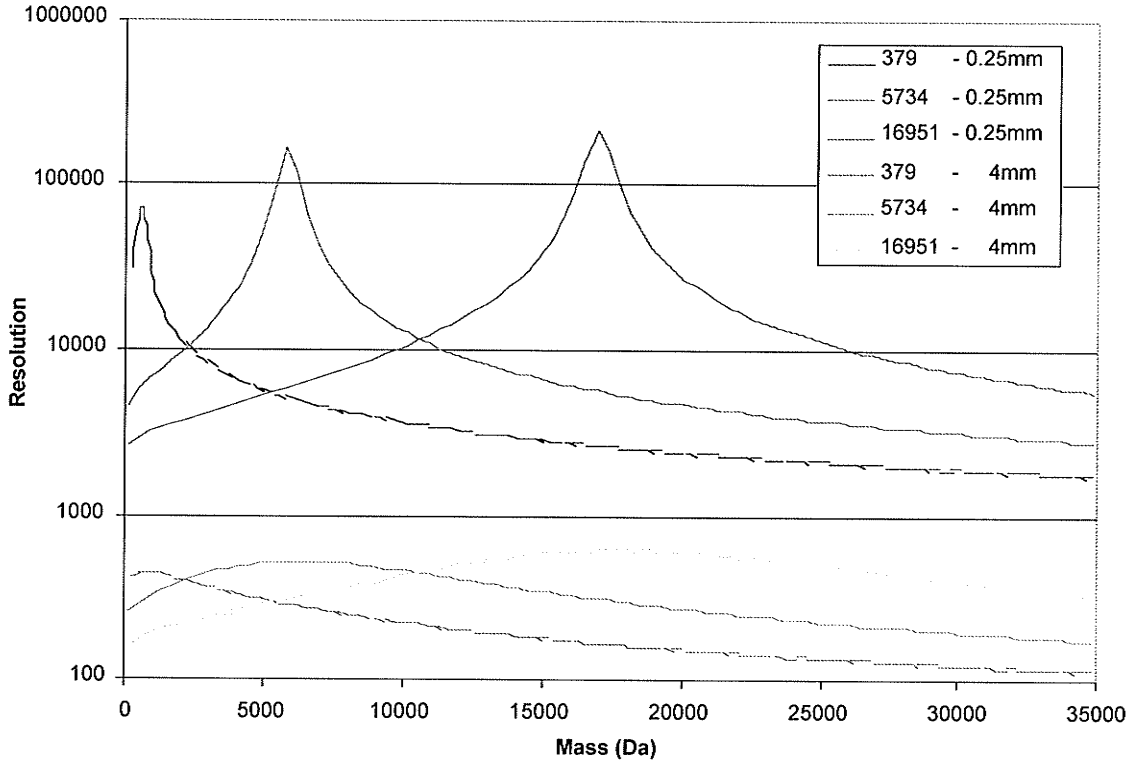

Figure 3-11 : The narrowest slit width results in acceptable resolution with 3 separate optimizations up to about m/z 20,000; for the widest slit width, the resolution is below 1000 over the entire mass range.

Figure 3-12 shows the effect of the accelerating voltage on the resolution vs. mass curve. For each potential, the extraction pulse is optimized for myoglobin, and a fixed aperture of 0.25 mm is used. The optimum V_{ext} values here are 1064, 2061 and 4025 V for the 7.5, 15 and 30 kV potentials, respectively. One interesting feature illustrated here is that the optimum resolution varies little with accelerating potential for a fixed drift length, but decreases slightly with increasing acceleration. However, the resolution is less mass-dependent for higher acceleration, so that for most of the mass range, resolution improves with increased acceleration potential. Accelerating voltages beyond about 30 kV are not practical because of the high pulse voltage required, in addition to the usual problems with arcing.

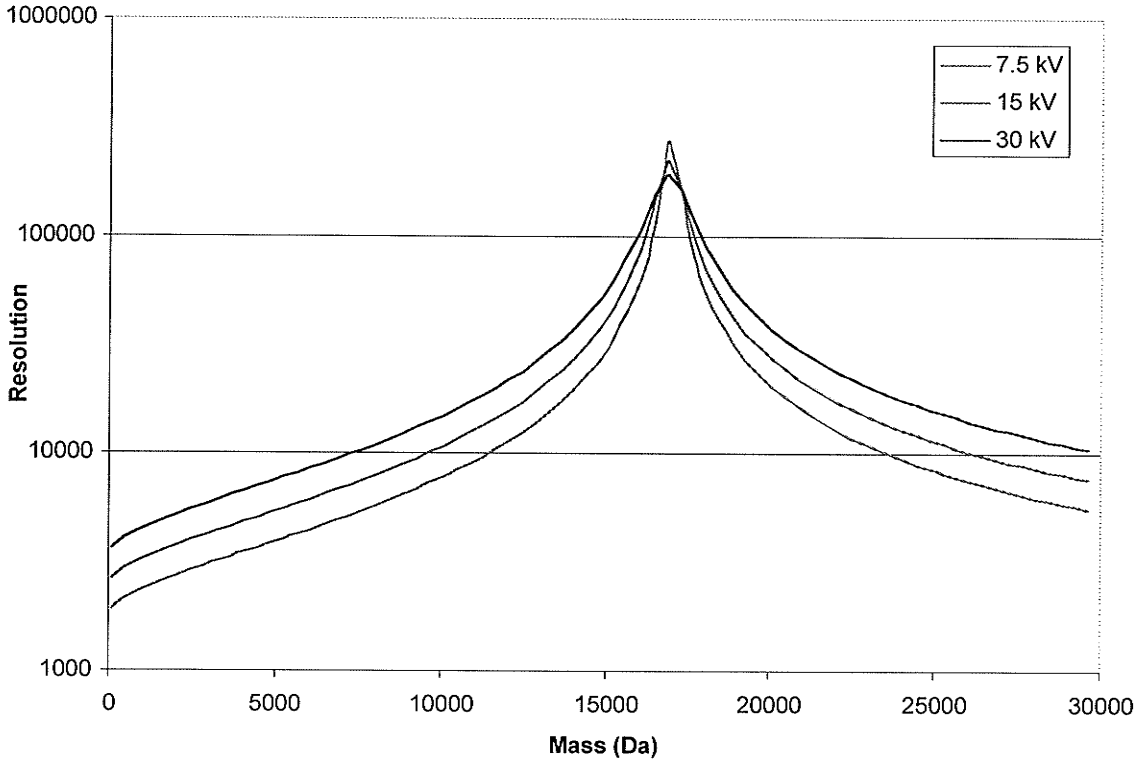

Figure 3-12 : R vs. mass with acceleration potentials at 7.5, 15 and 30 kV with a fixed aperture of 0.25 mm and Vext optimized for myoglobin for each potential.

3.4 Experimental Results

The TOF spectra from α-CHCA matrix, insulin and myoglobin are shown in Figure 3-13, and Table 3-1 summarizes the peak width (Δt) and resolution (equation 11) from the spectra shown and from the calculations used in the previous section. The experimental parameters were duplicated in the calculation. The matrix and insulin were acquired with a V_{ext} of 1.1 kV (optimized for insulin) and an acceleration potential of 10 kV. The myoglobin data were acquired with a V_{ext} of 1.6 kV and an acceleration potential of 20 kV. All species were acquired with a 4 mm aperture width. There is reasonably good agreement between the calculation and the experimental data. The agreement is weakest for the matrix ions, for which the extraction pulse is furthest from optimum.

Somewhat better resolution was observed with narrower slit widths, but the signal intensity even with the 4 mm slit was not competitive with axial MALDI.

As mentioned above, better resolution is expected with the use of a longer flight path and/or an electrostatic mirror. The observed resolution is consistent with the resolution of 3000 reported subsequently by Mlynski and Guilhaus using a similar source geometry, but with a 1.5 m flight path, a factor of 5 longer than the one used here [8].

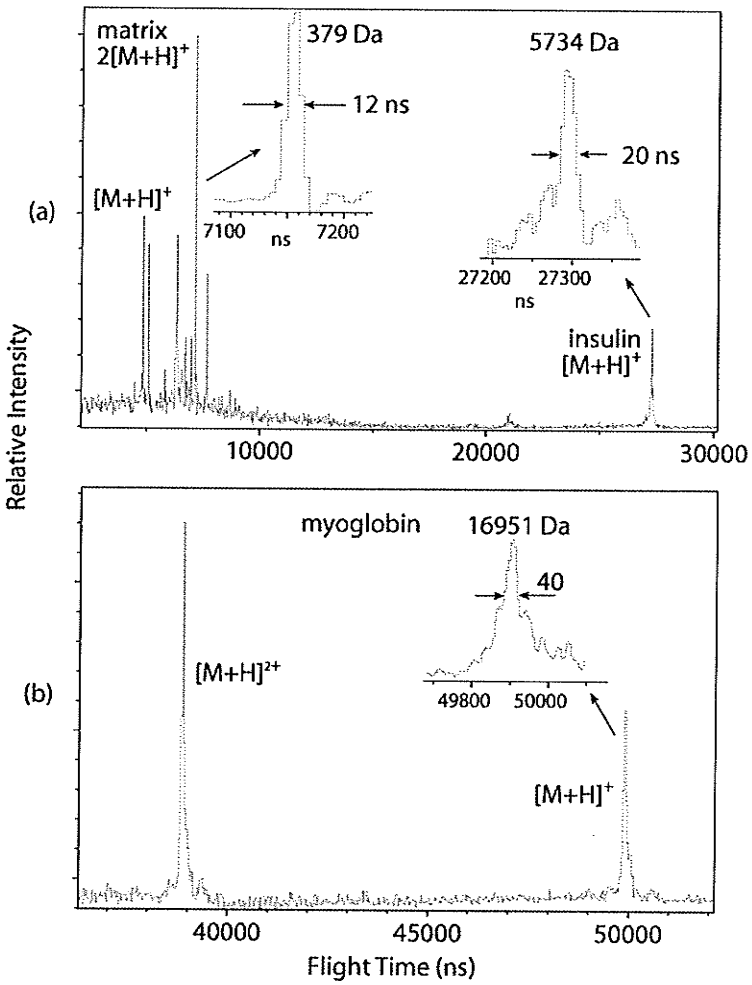

Figure 3-13 : TOF spectra and close-ups for α-CHCA matrix (379 Da), insulin (5734 Da) and myoglobin (16951 Da).

Table 3-1 : Experimental and modeled ΔTOF and resolution data for 3 species.

		ΔTOF (ns)		Resolution	
Species	Mass (Da)	Experiment	Model	Experiment	Model
	379	12	8	300	444
insulin	5734	20	21	680	676
myoglobin	16951	40	35	630	682

3.5 Discussion

OMALDI-MS without collisional cooling suffers from several fundamental problems that appear to make the configuration uncompetitive for measurements with both high resolution and high efficiency:

The radial velocity distribution, while much smaller than the axial velocity, is still large enough to cause substantial widening of the beam as it expands towards the axis of the TOF instrument. This beam divergence limits the resolution. The effect can of course be reduced by collimation as shown in the calculations above, but only at a significant sacrifice in sensitivity. The collimating slit must be placed at a considerable distance from the TOF axis to avoid distorting the extraction field, so the target must be placed far enough from the slit to produce a reasonably parallel beam.

As the width of the axial energy distribution, defined as the distribution of ion energies perpendicular to the target face, is comparable in magnitude with the energy $\frac{1}{2}mv^2$ itself, the beam has spread out along its axis by an amount comparable to the separation between the target and the TOF axis at the optimum time for acceleration into the flight path. The size of the aperture which admits ions from the extraction into the acceleration region spectrometer must

clearly be much smaller than this to maintain a uniform extraction field, particularly if an aperture is used in front of the target face as described earlier. This further reduces the sensitivity since the smaller the aperture, fewer and fewer ions will be accepted as discussed earlier.

The mass dependence of the trajectory angle mentioned earlier produces mass discrimination unless a time-dependent deflection is used. This is a result of the uniform velocity of the ions independent of mass. The same effect is observed when ESI ions are injected without collisional cooling [4,5,6]. In this experiment, time-dependent deflection was used to avoid mass discrimination, but this type of deflection introduces its own time dispersion which is not acceptable at high resolutions.

In contrast to orthogonal MALDI without cooling, acceptance is nearly complete in delayed extraction MALDI in the usual axial extraction geometry. Although the largest velocity spread in this case is along the TOF axis, the well defined target plane perpendicular to the TOF axis allows a combination of time lag focusing and electrostatic focusing in an ion mirror to produce resolution well above 10000 in some cases.

These considerations make it unlikely that competitive resolution and sensitivity can be obtained using the geometry of OMALDI-MS without collisional cooling. Moreover, some disadvantages of delayed extraction MALDI, such as the dependence of optimum extraction conditions on mass, and the more complex calibration required, are still present.

3.6 Conclusion

There are both advantages and disadvantages to an OMALDI-MS system. We have shown that in principle, very high resolution is achievable in this system with the use of an aperture to truncate the orthogonal extent of ions prior to their

extraction. Unfortunately, this is also the main limitation of this system since the use of such an aperture to gain resolution also severely limits the number of ions that can be extracted. The focusing condition and therefore resolution for this instrument is mass dependent, rendering its performance inferior to the delayed extraction – reflecting MALDI-TOF-MS system discussed in chapter 2. Since the success of using collisional cooling with an ESI-TOF-MS system as illustrated in Figure 3-1, the same idea was implemented later on an OMALDI-MS system by others in our laboratory [12]. Figure 3-14 shows a schematic of this system. With this system, the stream of ions from each laser shot is spread out axially and cooled such that its orthogonal velocity distribution is substantially reduced. The axial spreading results in a quasi-continuous ion beam into the extraction region and with a high rate of extraction pulsing, the system can realize the benefit of using a TDC for detection.

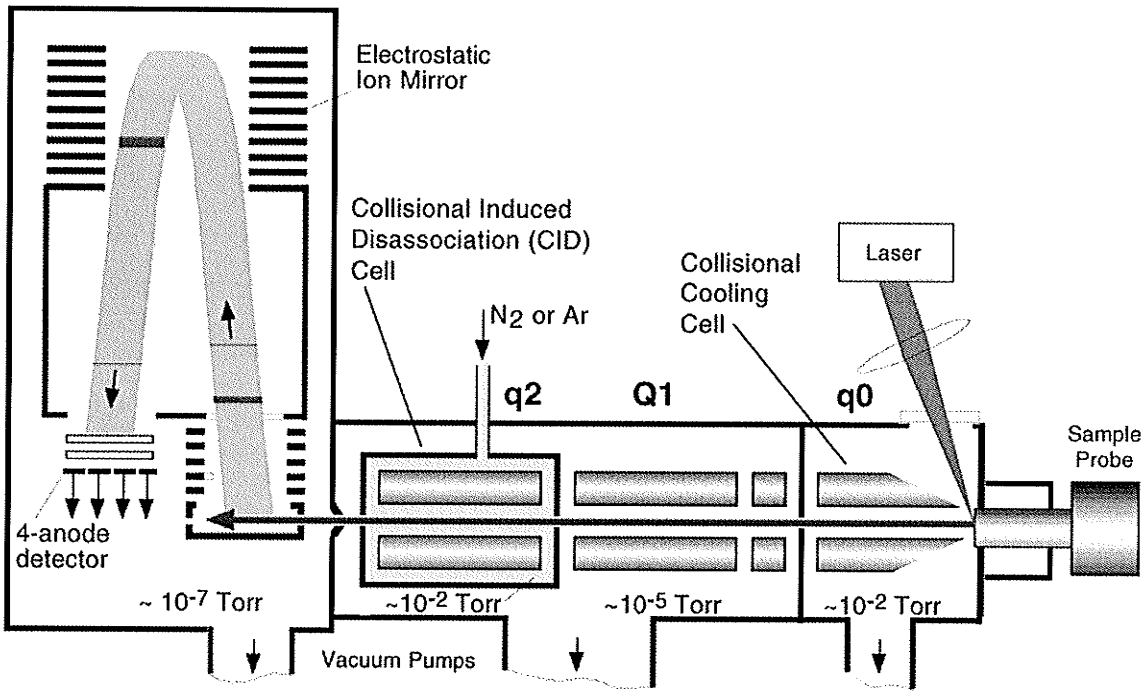

Figure 3-14 : The OMALDI-MS with collisional cooling.

3.7 References

1. B. Spengler and R. J. Cotter, *Anal. Chem.* **62** (1990) 793
2. A. F. Dodonov, I. V. Chernushevich and V. V. Laiko, in *Time-of-Flight Mass Spectrometry*, R. J. Cotter (Ed.), American Chemical Society: Washington, DC (1994), Symposium Series 549, p. 108.
3. A. N. Verentchikov, W. Ens and K. G. Standing, *Anal. Chem.* **66** (1994) 126
4. A. N. Krutchinsky, I. V. Chernushevich, V. Spicer, W. Ens and K. G. Standing, *Proceedings of the 43rd ASMS Conference on Mass Spectrometry and Allied Topics*, Atlanta, GA (1995)
5. I. V. Chernushevich, A. V. Tolmachev, A. N. Krutchinsky, V. Spicer, W. Ens and K. G. Standing, *Proceedings of the 44th ASMS Conference on Mass Spectrometry and Allied Topics*, Portland, OR (1996)
6. A. N. Krutchinsky, I. V. Chernushevich, V. Spicer, W. Ens and K. G. Standing, *J. Am. Soc. Mass Spectrom.* 9 (1998) 569
7. R. G. Dworschak, W. Ens, V. Spicer, K. G. Standing and A. V. Verentchikov, *Proceedings of the 43rd ASMS Conference on Mass Spectrometry and Allied Topics,* Atlanta, GA (1995)
8. V. Mlynski and M. Guilhaus, *Rapid Commun. Mass Spectrom.* **8** (1994) 865
9. X. Tang, R. C. Beavis, W. Ens, F. Lafortune, B. Schueler and K. G. Standing, *Int. J. Mass Spectrom. Ion Processes* **85** (1988) 43
10. B Spengler, D Kirsch, R Kaufmann, E Jaeger, *Rapid Commun. Mass Spectrom.* **6** (1992) 105.
11. R. C. Beavis, and B. T. Chait, *Chem. Phys. Lett.* **181** (1991) 479
12. A. N. Krutchinsky, A. V. Loboda, V. L. Spicer, R. Dworschak, W. Ens and K. G. Standing, *Rapid Commun. Mass Spectrom.* **12** (1998) 508

4 Initial Velocities of MALDI Ions: Measurements in an orthogonal MALDI instrument

4.1 Introduction

The discovery of MALDI led to a dramatic extension of mass range and sensitivity in the mass spectrometric analysis of proteins. The ejection dynamics of the ion production process have an important influence on the mass spectrum in TOF measurements. Measurements of initial time and velocity spreads contribute to the understanding of the ejection mechanism, and provide information relevant to the design and performance of linear TOF-MS instrumentation. By correcting for the time uncertainty due to the initial analyte ion velocity distribution, better mass accuracy of analyte molecules in linear TOF-MS measurements is possible. Several experimental measurements of initial velocity distributions in MALDI have been reported [1,2,3,4,5,6,7,8,9,10,11,12,13, 14,15,16,17].

The study by Beavis and Chait at Rockefeller University was the first to measure the velocity distributions of large ions in MALDI ejected into a field free region [4]. Previous measurements were dominated by effects of the strong extraction field normally used in time-of-flight measurements identified by Zhou et al. [11]. In the Rockefeller measurements, a two stage, gridded acceleration stage was used, and the flight time of a selected species was measured with and without a field in the first region. The difference in the two flight times of the selected ion corresponds to the drift time of the ion in the first field free region and indicates the initial velocity. The Rockefeller measurements showed that biomolecular ions above ~5 kDa have a similar initial velocity, with an average of about 750 m/s.

On the other hand, higher velocities were measured for smaller peptides, and for the sinapinic acid matrix ions of mass 224 Da that had a mean initial velocity of 1140 m/s.

Similar results were subsequently reported by other groups [7,12,13]. Measurements in this laboratory found somewhat lower velocities of ~500 m/s for molecular ions with mass higher than 5 kDa. In addition, the measurements also showed that the initial velocities of large proteins were independent of laser fluence [7].

As mentioned, in contrast to the high masses, velocities for smaller species are not uniform, but in general increase with lower mass and higher fluence [7]. In particular, Spengler found that with the laser focused to a spot diameter of 10 μm on a single crystal of DHB with 1 and 6 times the threshold irradiance, ions were desorbed with mean velocities as high as 2700 to 7400 m/s [12]. This behaviour was not observed for desorption of neutrals [18,19,20]. The different behaviour of light ions is not surprising since they are more sensitive to weak fields than heavier ions are, so the effects of space charge and of penetrating fields are more significant.

Juhasz demonstrated an alternative method to the field-free method to measure initial velocities using delayed extraction. In delayed extraction, a pulse is applied to the 1st acceleration region a delay time τ after the laser hits the sample. Juhasz showed that, to a good approximation, the flight time is linear with τ and the slope depends on the initial velocities. Measurements of the ion flight time as a function of τ therefore yields the initial velocity [1]. In contrast to the field-free method, in which the initial axial velocity *distribution* is extracted, the delayed-extraction method yields only the mean value of the axial velocity. The initial velocity values for bovine insulin with mass 5733 Da were measured by the delayed extraction method to be 300 – 350 m/s for a large variety of matrices such as α-CHCA, sinapinic acid, HABA and 2-thiohydantion. With some other

matrices such as sDHB and 3-HPA , velocities were in the range of 500 m/s. These results are substantially different from those obtained using the field-free method. For example, using the field-free method, measured velocities of insulin molecular ions desorbed from sinapinic acid matrix were in the range of 500 - 750 m/s, almost a factor of 2 higher than the velocity measured by Juhasz. Similarly, the matrix velocities were also found to be higher with the field-free method compared to the delayed extraction method.

There are several plausible explanations for the discrepancies between the field-free and delayed extraction methods. First, field penetration in the first stage is a problem in both methods, but the degree of the effect, and compensation for it may differ. The penetrating field can be largely eliminated by applying an offset voltage on the grid, as was done by Juhasz *et al.* [1], but it is difficult to determine the correct value [21].

Secondly, the different time scales involved in the two methods may be contribute to their differing results. Both experiments make the assumption that the ions leave the target with an axial component of velocity v_0 which is unchanged until the ion enters the next stage, or the extraction pulse is applied. However, the ions interact with the expanding gas plume and presumably the larger ions take an appreciable distance and time to be accelerated via collisions to their full velocity. Moreover, interactions with the plume may interfere with acceleration if the extraction pulse is applied before the plume has dissipated [11]. The time required for the plume to dissipate is not well-known, but it is reasonable to assume that after several hundred nanoseconds, the significance of plume interactions is small since very sharp peaks can be obtained with time delays of this order. However, recent delayed extraction measurements by Berkenkamp *et al.* suggest effects may last as long as 800 ns [21]. Plume interactions do not affect the field-free measurements significantly because the velocity is measured over approximately 10 μs. However, in the delayed

extraction measurements of Juhasz *et al.,* the velocity measurement is completed in 600 to 800 ns [1], so plume interactions may be significant.

Another effect on mean initial axial velocity, found by a group at Orsay, may be the incident angle of the laser [22]. The Orsay experiment suggested that ions were ejected back in the direction of the incident laser pulse that creates the MALDI plume. For glancing incidence angles, this would lead to a lower axial component of the ion velocity

Recently, since the measurements reported here were completed, Berkenkamp *et al.* [21] performed delayed extraction experiments similar to those of Juhasz *et al.* [1], but in a different geometry, using longer delay times, and with more attention paid to the compensation voltage, and compared the results directly with field-free measurements in the same instrument. In these experiments the results for the two methods are much close together. Indeed, in most cases, the error bars from the two measurements for a given analyte overlap, although the velocities obtained by the delayed extraction method still seem systematically lower by about 10 - 20%. Berkenkamp argues that collisions of (partially) accelerated ions with neutral plume constituents after application of the delayed extraction pulse likely account for the remaining discrepancy.

The present experiment was designed to remove or minimize the three complicating effects described above by taking advantage of the orthogonal-injection time-of-flight instrument described in the previous chapter to measure initial axial velocity *distributions*. In this method, the ions are allowed to drift several cm before acceleration, so the time and length scales of the plume are strictly negligible. Any penetrating fields in this geometry are perpendicular to the axial ejection velocity, so do not affect their values. Finally, the sample may be oriented to give various incidence angles of the laser (in particular, normal incidence). Both positive and negative ions were investigated to probe the effect of space charge on the velocities of smaller ions.

4.2 Experimental

4.2.1 Instrumental

Measurements were performed on the orthogonal-injection matrix-assisted laser desorption/ionization time of flight mass spectrometer (O-MALDI-MS) described in the previous chapter [9]. The overall system configuration is shown in Figure 4-1. As in the previous experiments, the ion plume is allowed to expand toward the time-of-flight axis, and is then pulsed into the spectrometer. The ions are detected with a microchannel plate detector and the spectrum is recorded with a transient recorder. Measurements were made using 15 kV acceleration voltage, and with the injection pulse height optimized for the mass range of interest, typically about 1.6 kV.

Detailed dimensions in the source region are shown in Figure 4-2. For these velocity measurements, a 4.5 mm slit was placed in the plane of the first grid, as shown, to select ions with a fairly narrow range of initial axial velocities for acceleration into the time-of-flight instrument. The selected axial velocity range is determined by the time delay between the laser pulse and the pulse that injects ions into the second acceleration region. Therefore, an axial velocity distribution can be obtained by scanning the time delay, and measuring the ion intensity. Because of the sensitivity problems described in Chapter 3, made worse with the slit at the first grid, the laser fluence was typically a few times the usual threshold fluence used in axial MALDI experiments to get useful signal.

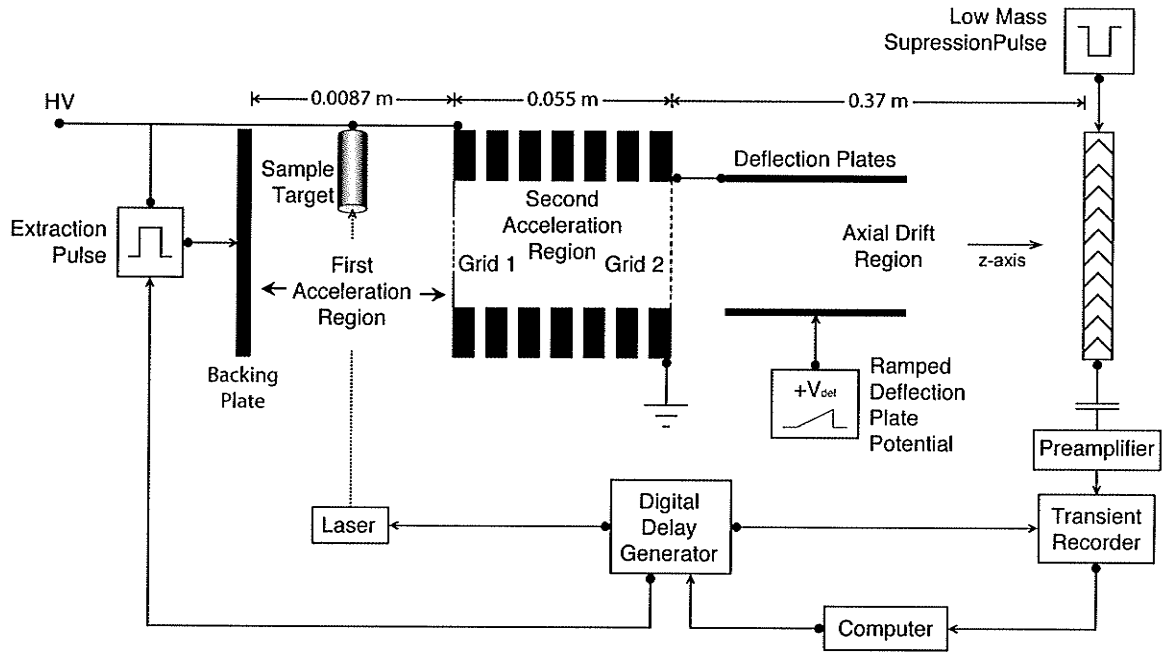

Figure 4-1 : Schematic diagram of the orthogonal TOF instrument used for initial velocity measurements.

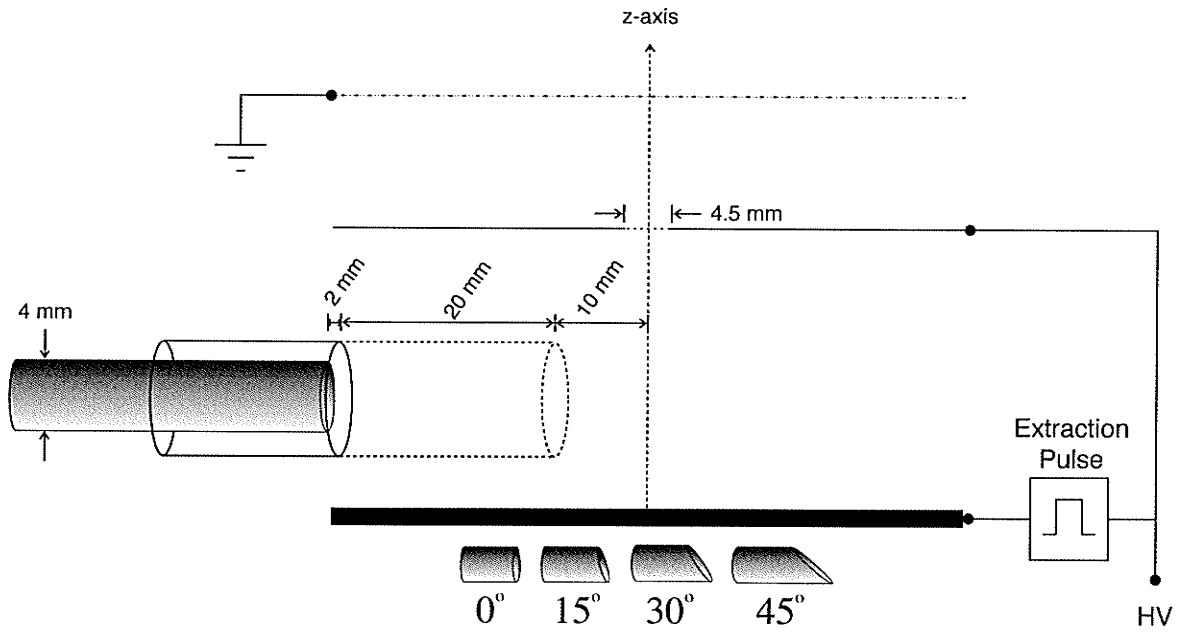

Figure 4-2 : Detail of orthogonal geometry source region, with schematic of 4 angled sample probe heads and relative orientation in the source. Two tube lengths are shown.

The trajectory of the ions entering the time-of-flight region depends on the ratio of the initial energy and the energy received during acceleration. Since the initial velocity of the selected ions depends on the delay time, the trajectory is correlated to the delay time, as well as being mass dependent. In order to keep the trajectory of the ions of interest centered on the detector, the voltage applied to the deflection plates shown in Figure 4-1 was therefore also correlated to the delay time.

The procedure for measuring velocity distributions is illustrated in Figure 4-3. In these measurements, time zero is coincident with the laser pulse, so the measured time includes the time for the ions to drift from the target to the admitting slit at the first grid – the delay time – and the flight time of the ions through the instrument. The initial velocity of the detected ions is the distance between the target and the slit (32 mm) divided by the delay time, and as the time delay is scanned to sample the velocity range, the measured detection time of a given ion species changes by the same amount. This allows the data for the complete distribution to be accumulated in a single histogram. Panel (a) of Figure 4-3 is a portion of the spectrum of the matrix DHB acquired with a delay time of 13 μs, showing the $(M+H-H_2O)^+$ peak at *m/z* 137. The initial velocity of the observed ions corresponds to 2460 m/s. Panel (b) represents the same *m/z* portion of the spectrum, but with a 18 μs delay, corresponding to an initial velocity 1520 m/s. At this velocity, the $(M+H)^+$ ion and the $(2M+H)^+$ are also observed. The spectrum in panel c was acquired with a 22.5 μs delay corresponding to 1250 m/s. Here only the $(2M+H)^+$ species is observed. The data for the complete velocity distributions of all 3 species observed within the selected *m/z* range are shown in the composite spectrum in panel d. The data were acquired by stepping the delay time from 10 μs to 30 μs in 500 ns steps, while at the same time stepping the low-time side of a 2-μs acquisition time window from 14.4 μs to 34.4 μs. The size of acquisition time window can be increased to include more ions in the analysis, but this increases the complexity

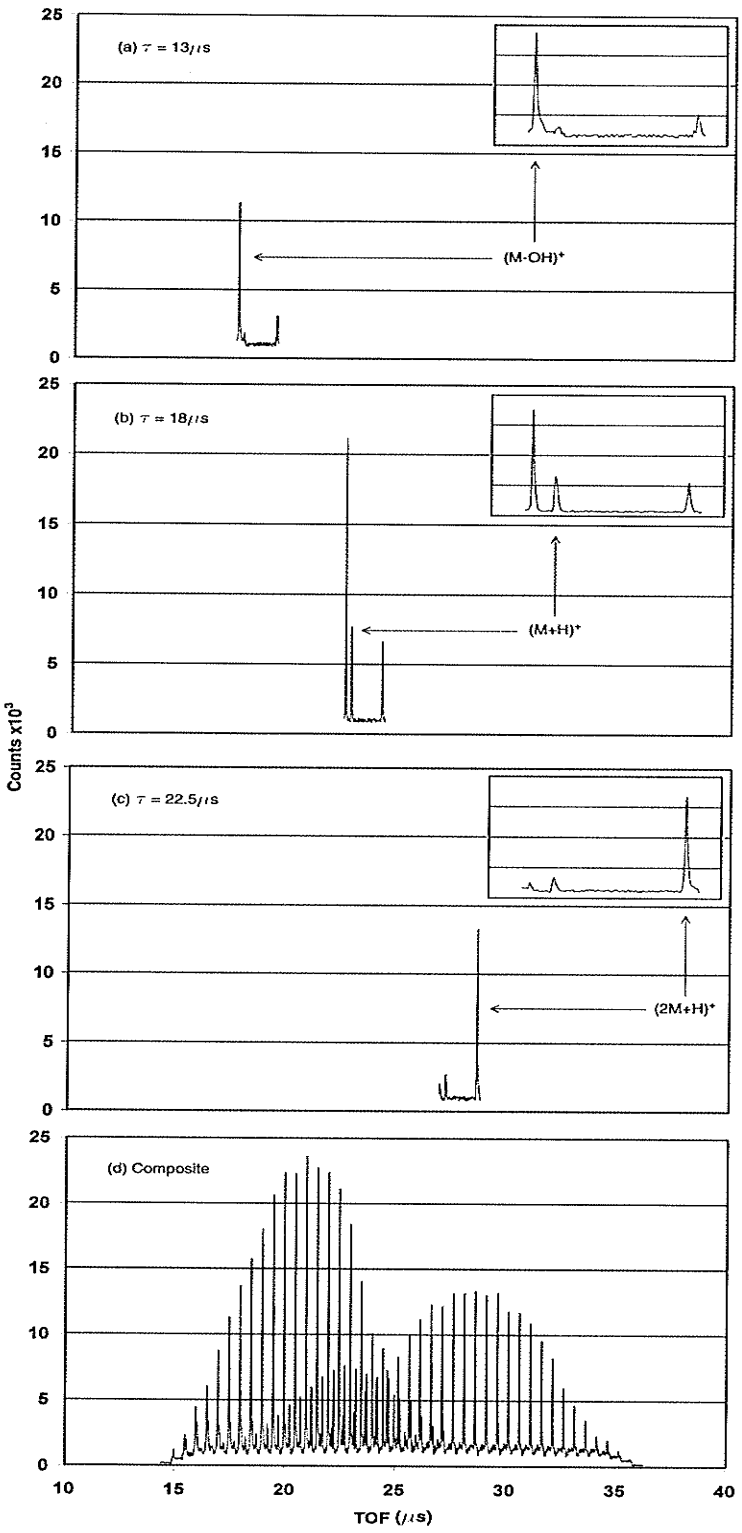

Figure 4-3 : Data acquisition in a single composite histogram (d) as the delay time and a selected time window in the spectrum are increased or decreased in 500 ns steps. The first three panels show the data acquired with delay of (a) 13 μs, (b) 18 μs, and (c) 22.5 μs.

of the analysis. To avoid systematic effects of sample degradation under laser bombardment, the time delay is stepped after each laser shot, and then scanned back and forth between the limits until sufficient statistics are accumulated. Typically, about 50 shots are used per delay time, corresponding to about 2000 shots total on the same sample spot.

Three quite different distributions can be seen clearly in the raw composite spectrum in Figure 4-3d. Figure 4-4 shows the result of converting the time distributions to velocity distributions. Since the three distributions were acquired simultaneously, one can exclude most systematic effects and be confident that the ions have different distributions; in this case it may simply be an effect of the molecular mass of the ions.

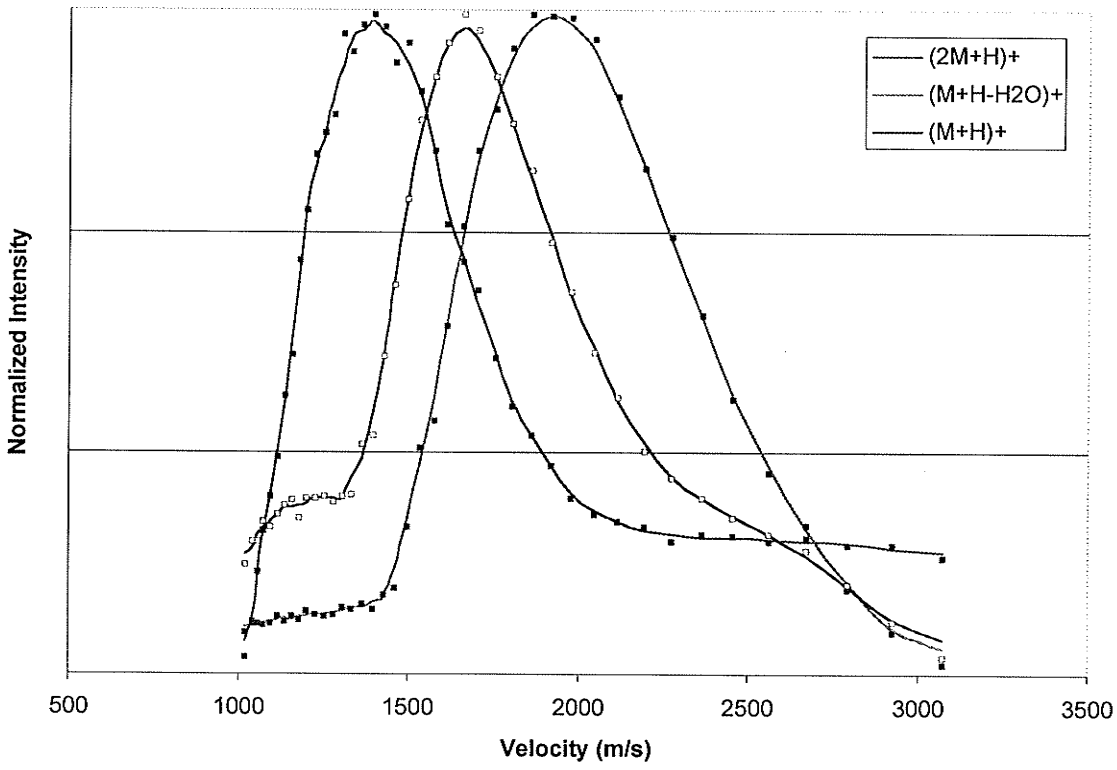

Figure 4-4 : Velocity distributions of 3 DHB species, extracted from the data of Figure 4-3.

An important advantage of the orthogonal geometry is that it avoids problems of penetrating fields that can affect measurements in an axial geometry. This is partly because the dc accelerating stage is considerably longer than is normally used in an axial TOF instrument, so the field strength is much weaker for the same accelerating potential. More importantly, the main effect of a penetrating field, if present, acts at right angles to the direction along which the initial velocity is measured, so the effect should be small. To verify that field penetration was not significant, velocity distributions of matrix ions, such as the those in Figure 4-4, were measured using acceleration potentials of 4 kV and 16 kV. The signal intensity was much lower using 4 kV acceleration, but no difference in the velocity distribution was observed.

Figure 4-2 shows a conducting tube around the sample probe extending either 2 mm or 22 mm beyond the end of the sample surface. The longer tube was used to mount a collimating slit in the experiments of Chapter 3. A collimating slit was not used in these experiments, and most of the data shown was acquired with the short tube in place. However, a few experiments were done with the longer tube to test the effect of spatial confinement of the plume on the velocity distribution.

Some experiments were also performed with sample probes with oblique tips as shown in Figure 4-2. These were designed to test the effect of the incident laser angle on the velocity distribution.

Finally, a few measurements in the negative mode were made by keeping the source region at -10kV during ionization and then pulsing the grid just prior to the acceleration region to a smaller negative voltage to extract the negative ions.

4.2.2 Sample Preparation

All matrices were dissolved in a 1:1 solution of acetonitrile and aqueous 0.1% trifluoroacetic acid. The α-cyano-4-hydroxycinnamic acid (α-CHCA), 3,5-dimethoxy-4-hydroxycinnamic acid (sinapinic acid), and 3-hydroxy-2-pyridinecarboxylic acid (3-HPA) matrices were dissolved to saturation. The samples were prepared by first drying several μL of matrix on the sample probe and then crushing with the smooth bottom edge of a clean glass beaker [23]. For the matrix only samples, several more μL of matrix were added to the probe, and this was allowed to dry completely prior to analysis. For the samples with analyte, several μL of a 10:1 matrix:analyte mixture were added to the sample probe and allowed to completely dry prior to analysis. The sDHB matrix is a 9:1 mixture of 2,5-dihydroxybenzoic acid (DHB):5-methoxysalicylic acid (MSA). The ssDHB matrix is a 50% DHB and 50% sucrose mixture. The DHB, sDHB, and ssDHB matrices were dissolved to a concentration of approximately 20 g/L. These samples were prepared as described for the previous matrices except with no prior crushing step, both for the matrix alone and matrix/analyte samples.

4.2.3 Crystal Preparation

The crystal DHB samples were grown within a solution initially at 20 g/L. The crystals were allowed to grow at room temperature for 3 days before being removed from the solution, washed and sorted. A suitable crystal of approximately 3 x 1 mm was then lightly glued with polystyrene in toluene to a sample holder prior to analysis.

4.2.4 Scanning Electron Microscopy

Some of the crystals were irradiated to various levels of damage by the laser. To determine if the level of damage could influence the emission direction, and therefore the axial velocity, the damaged samples were then coated with a

metallic film, preparing them for SEM. The micrographs were taken at 25kV and up to a few thousand magnification showing the damage very clearly.

4.3 Results and Discussion

4.3.1 Initial velocities of analyte ions

Mass dependence. Velocity distributions were obtained for leucine-enkephalin (555 Da), substance P (1348 Da), bovine insulin (5733 Da), cytochrome C (12360 Da), and myoglobin (16951 Da). The data are shown in Figure 4-5. As has already been established, the average velocities of the larger ions were found to be very similar; these measurements give an average of approximately 720 m/s. Only the lowest mass analyte, leucine enkephalin, had a higher average velocity at about 910 m/s. Although the average velocities are roughly mass independent above about 1000 Da, the width of the velocity distribution clearly increases with increasing analyte mass.

Matrix dependence. Velocity distributions were measured of the molecular ion of bovine insulin (5734 Da) desorbed from 6 different matrices. The velocity distributions are shown in Figure 4-6, and the average values are shown in Table 4-1, along with the average velocities measured by Gluckmann and Karas using the delayed-extraction method [3]. Although the values are quite different (see below), the trend is the same.

Table 4-1: Measured average velocities of ions of insulin ejected from various matrices.

	Average velocity (m/s)		
Matrix	*This work*	*Ref. 3*	**Ratio**
Sinapinic acid	820	332	2.5
α-CHCA	700	291	2.4
3-HPA	900	444	2.0
DHB	940	543	1.7
sDHB	946	565	1.7
ssDHB	790	522	1.5

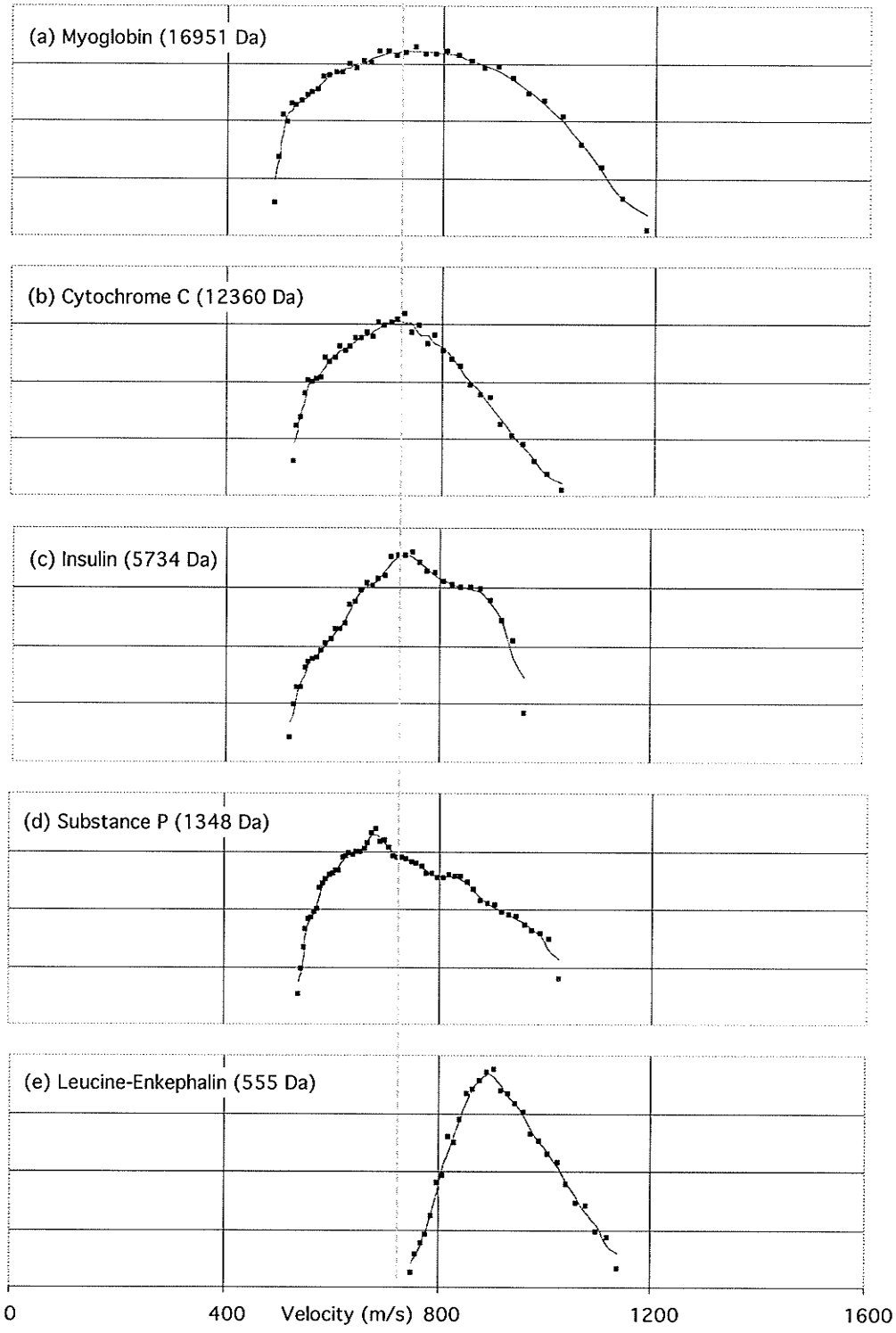

Figure 4-5 : Initial velocity distributions for various analytes desorbed from sinapinic acid.

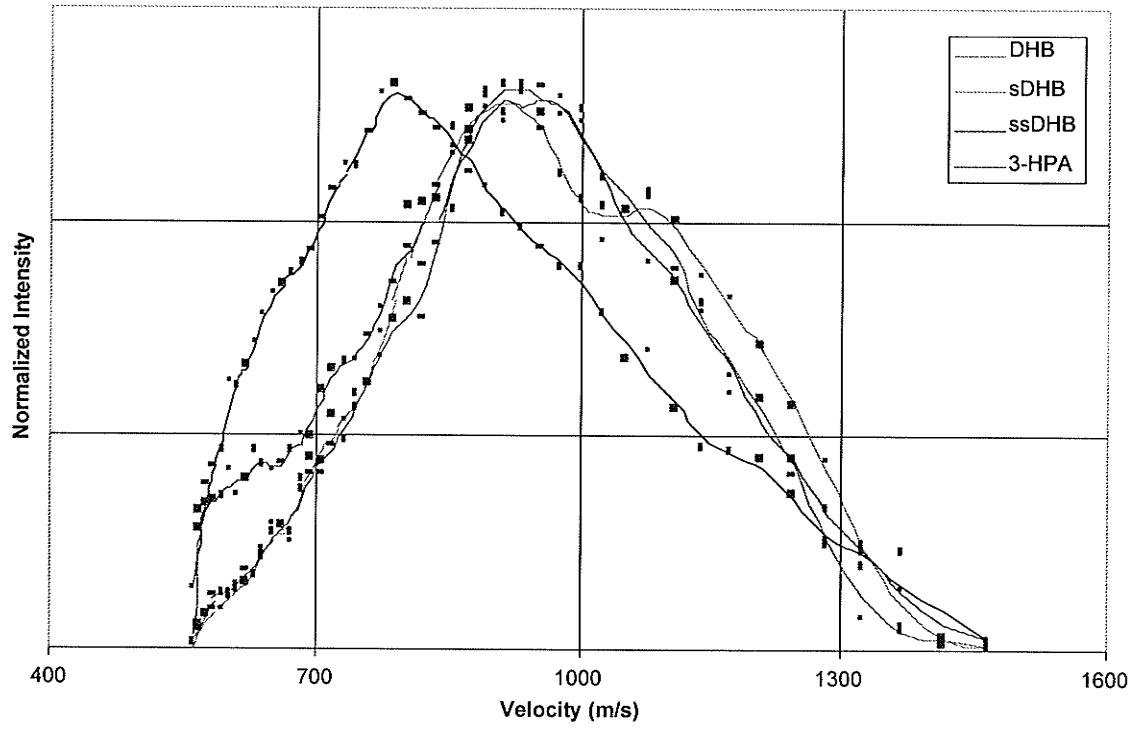

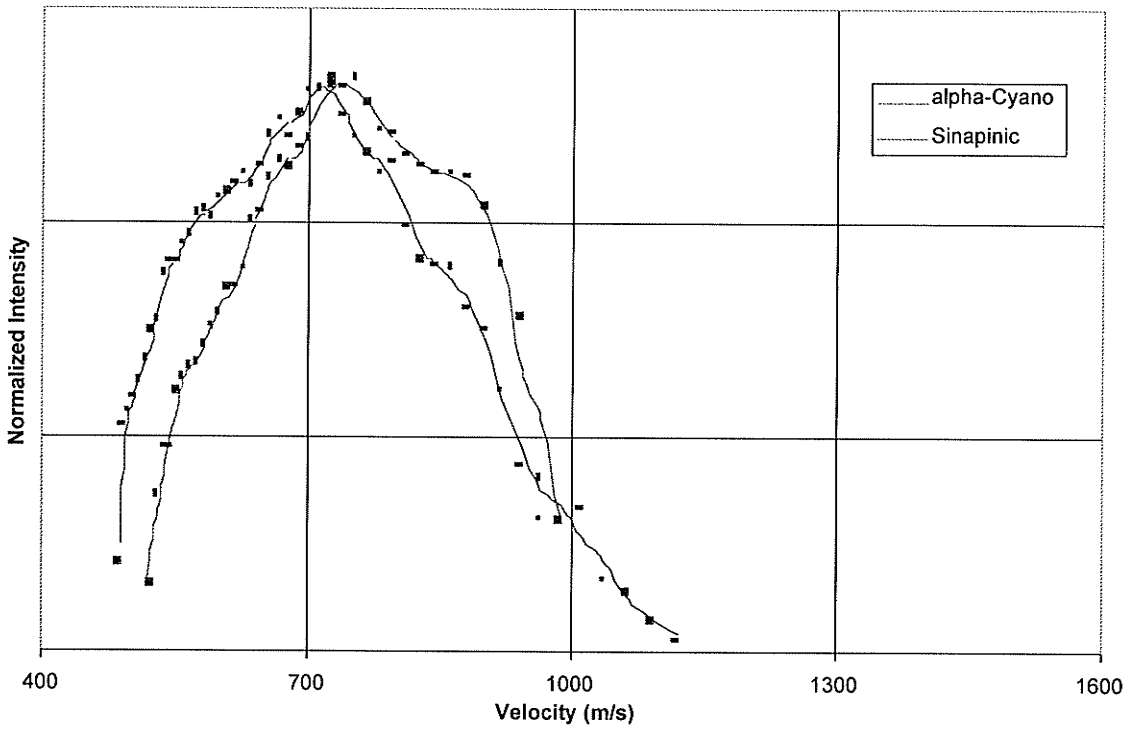

Figure 4-6 : Initial velocity distributions for bovine insulin desorbed from various matrices

The velocities measured above for analytes above about 1000 Da are consistent with most of the measurements made with the delayed extraction method, particularly the Rockefeller measurements [4], but as can be seen in Table 4-1, they are about a factor of two higher than the early measurements made using the delayed extraction method [1, 3]. However, the recent delayed extraction experiments by Berkenkamp [21], performed after our measurements were reported [9], are also consistent with our results, suggesting systematic errors in the early delayed extraction experiments. The present measurements are arguably the most definitive for the higher mass range (at least for normal laser incidence) because the problems of time-scale and penetrating fields are most easily dismissed, and the interpretation is straightforward. The high fluence in our experiment represents a difference from the usual axial MALDI experiment, but Verentchikov has shown that initial velocities of large analytes are independent of fluence [7]; this appears to be the case for IR MALDI with solid matrices as well [21].

4.3.2 Initial velocities of matrix ions

Figure 4-7 shows the velocity distributions of the $(M+H-H_2O)^+$ species of 6 matrices. The benzoic acid derivatives have a similar velocity average of ca. 2000 m/s, while the cinnamic acid derivatives are somewhat slower at 1340 m/s and 1710 m/s. This correlates somewhat to the situation for analytes desorbed from these matrices: analytes desorbed from the benzoic acid derivatives have higher initial velocities (see Table 1). To some extent the matrix velocities seem to rank according the molecular weights: from fastest to slowest: DHB (154 Da), MSA (137 Da), α-CHCA (189 Da), 3-HPA (139 Da), sinapinic acid (224 Da). The biggest exception to the trend is the picolinic acid matrix (3-HPA), close to the lightest matrix, with close to the slowest velocity at 1400 m/s.

As mentioned in the experimental section, the orthogonal-injection method allows several velocity distributions to be measured simultaneously. This avoids

systematic effects like laser fluence or surface characteristics. Figure 4-8 shows the distributions for the DHB and MSA molecular ions: $(M+H-H_2O)^+$ and the DHB dimer: $(2M+H)^+$ and for the complex ion $(M_{DHB} + M_{MSA}+H)^+$ measured in one experiment. The matrices have very similar mass, and again, this seems to govern the velocity distribution.

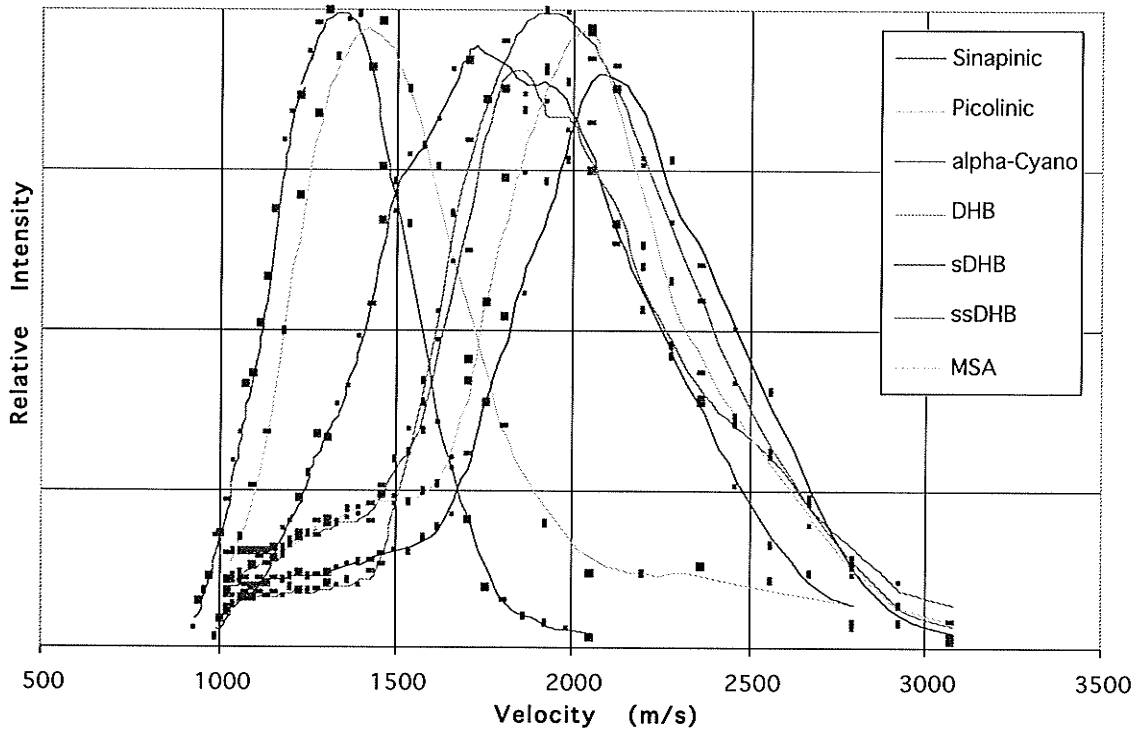

Figure 4-7 : Initial velocity distributions of $(M+H-H_2O)^+$ ion from various matrices.

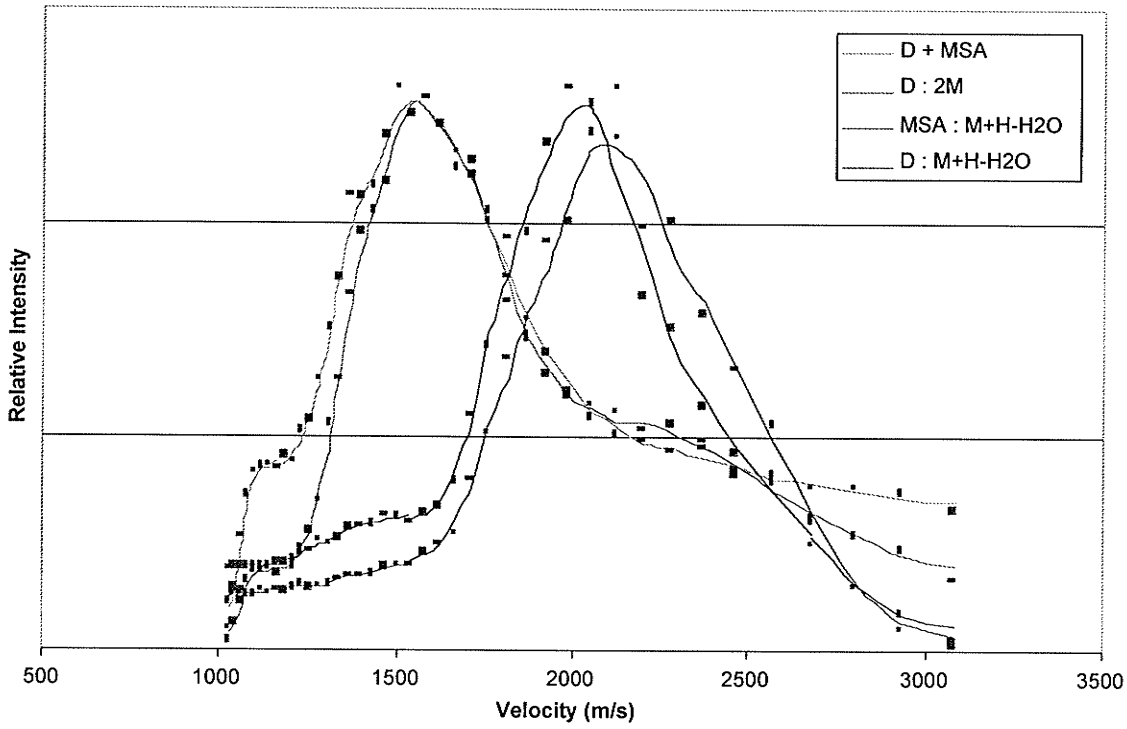

Figure 4-8 : Initial velocity distributions for the species desorbed from the sDHB matrix measured simultaneously.

In contrast to the situation for large analytes, our measured velocities for matrix ions are much higher than most other experiments. This almost certainly reflects the higher fluence in our experiment, and not a discrepancy in the measurement. Verentchikov reported that light ions are sensitive to fluence [7]. The simplest explanation is that the higher velocities are produced by space charge in the plume. The sample starts out neutral of course, but If the laser pulse produces electrons in high abundance, they will escape the sample much more rapidly than ions, leaving a net positive charge in the plume. This effect, would be likely to increases with laser fluence. The strong correlation of initial velocity with mass is also consistent with a space-charge effect, since lighter ions are more sensitive to electric fields.

4.3.3 Confined plume dynamics

The difference in the velocity distributions of small matrix ions and larger analyte ions suggests they are accelerated by different mechanisms. For example, as suggested above, the light ions could accelerated by a weak electric field such as might be produced by space charge, whereas the heavy ions are likely accelerated by collisions with the expanding gas plume. This appears to be consistent with the velocity distributions measured with a 22 mm tube placed over the sample probe (see Figure 4-2). Such a tube confines the plume and should therefore increase the density and the probability of collisions. As shown in Figure 4-9, the velocity of the matrix ions increases substantially in this configuration, and the velocity of the insulin ions decreases slightly. It seems that increased collisions in the higher pressure plume slow the matrix ions down and speed large ions up, as would be the case in the example scenario given above.

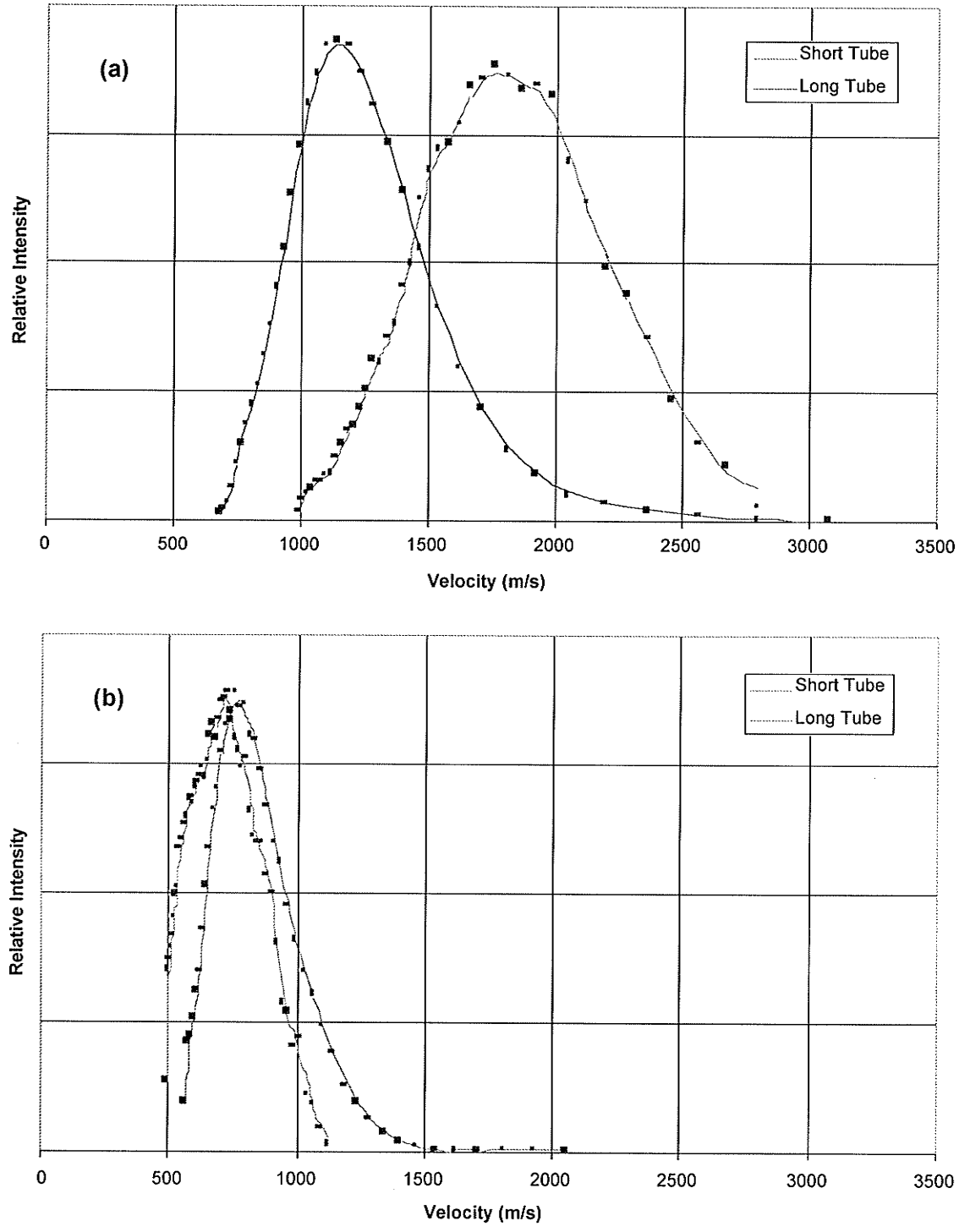

Figure 4-9 : Velocity distributions measured with a 2mm and 22 mm tube covering the sample probe. (a) $(M+H-H_2O)^+$ ion from α-CHCA; (b) insulin ions desorbed from α–CHCA matrix.

4.3.4 Space Charge

As described above in sections 4.3.2 and 4.3.3, the higher velocity of light positive ions seems to suggest that they are accelerated by a weak electric field, such as might be produced by positive space charge. A positive space charge could be produced if electrons are rapidly liberated by the laser pulse. If the explanation for the higher velocity of light positive matrix ions related to the presence of a weak electric field (from any source), then one should expect that light negative ions would be slowed down by the same electric field. The data of Figure 4-10, which compares the velocity distributions for positive and negative light ions therefore seem to exclude the presence of an electric field as an explanation. Thus, the reason for the higher velocities of light ions, their greater sensitivity to fluence, and their different response to the confined plume, remains unknown.

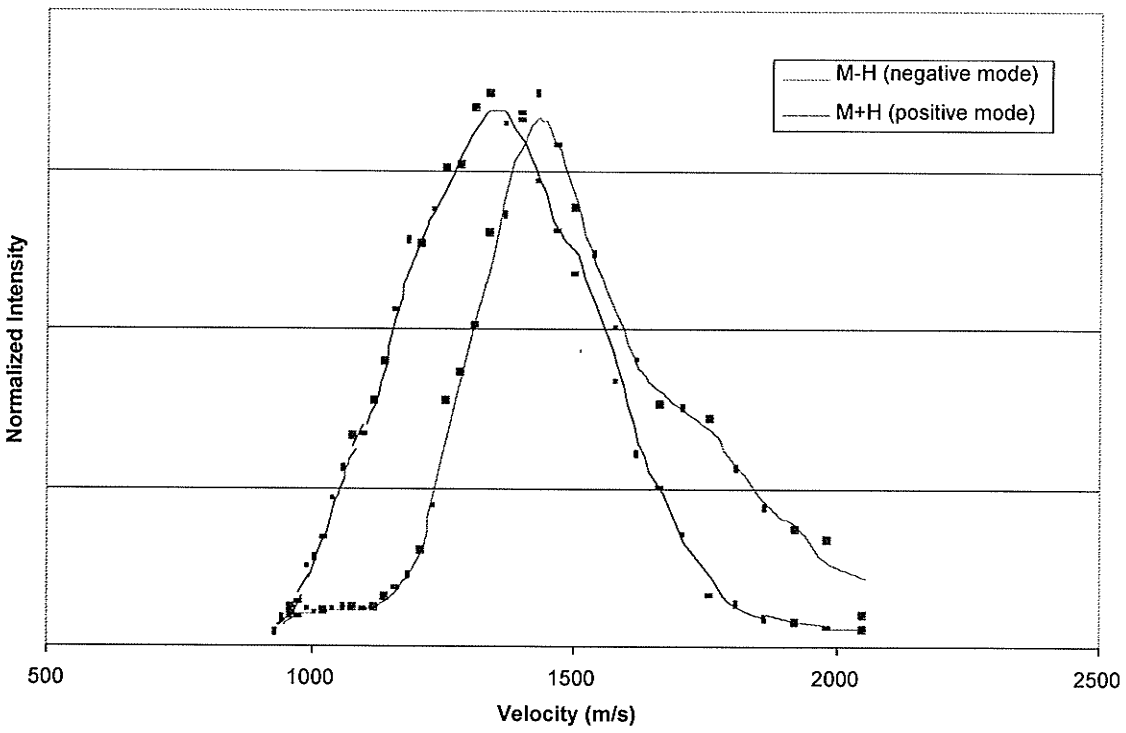

Figure 4-10 : Initial velocity distributions of $(M+H)^+$ and $(M-H)^-$ of sinapinic acid.

4.3.5 Laser incidence angle

One factor that may contribute to different initial velocities measured in different instruments is the incident angle of the laser. Experiments at Orsay suggest that the MALDI plume may be directed back in the direction of the laser rather than normal to the target surface [22]. To test this idea, sample probes with different orientations of the sample surface (Figure 4-2) were used to measure velocity distributions. If the plume is directed back toward the laser, no effect of the angle should be observed. At the other extreme, if the plume is directed normal to the surface, the decrease in observed velocity for a 45° angle would be at most $1/\sqrt{2}$ for a strongly forward directed plume. A more isotropic distribution would show less dependence of the velocity on the angle. Figure 4-11 shows the velocity distributions for the $(M+H-H_2O)^+$ ion from a polycrystalline sample of sinapinic acid for 4 different probe-face angles ranging from 0 to 45°. As the angle increases, the mean velocity decreases gradually by about 20%, a little less than the maximum 30% for this angle. One possible explanation for the Orsay observations is that the crystal faces normal to the incident laser will see a higher fluence and therefore the most intense plumes will be directed normal to this surface. We therefore performed a similar experiment using an analyte substance P in a single crystal of DHB. The distributions obtained for 0° and 45° are shown in Figure 4-12. Again the velocity decreases by about 20%, suggesting the orientation of the surface is the main determiner of the plume direction.

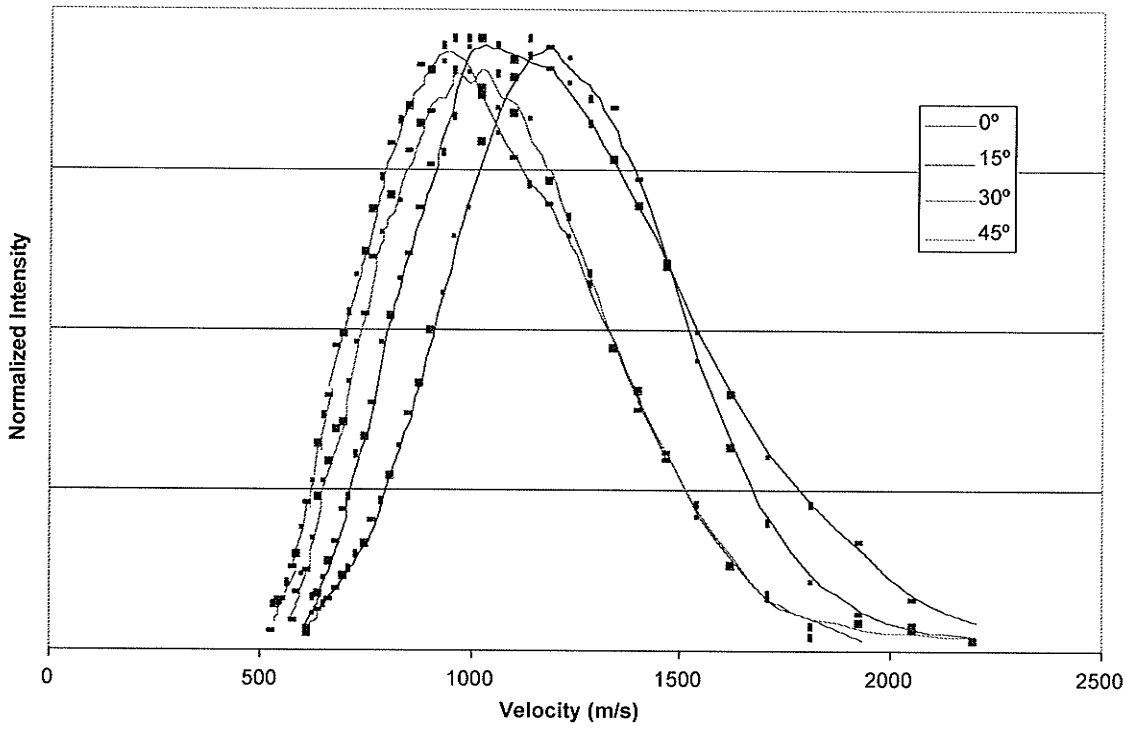

Figure 4-11 : Velocity distributions for the $(M+H-H_2O)^+$ ion from sinapinic acid using four different sample probe angles (see Figure 4-2).

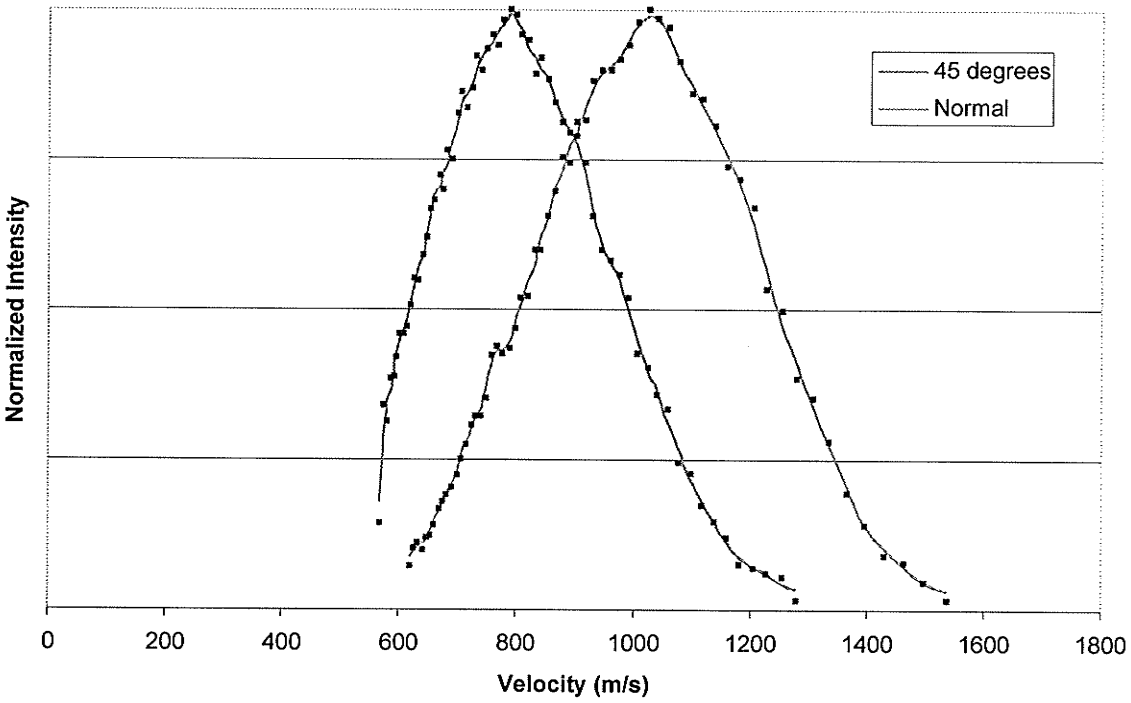

Figure 4-12 : Velocity distributions for substance P in a single crystal of DHB at normal and 45° laser incidence.

4.3.6 Laser damage on single crystals

It is well-known that the laser produces damage in crystals in MALDI experiments. Significant damage may affect both emission angle and velocity distributions, judging from the confined plume experiments described above. We therefore examined DHB crystals by SEM after variable number of laser shots at both zero and 45° incident angles.

Figure 4-13 shows a DHB crystal after normal irradiation with 100, 200, 400, 800, 1600, and 3200 laser shots. Clearly, after 3200 shots, the damage is severe enough to be essentially independent of the original orientation of the crystal, and therefore the emission angle would be determined mainly by the laser direction. This is also consistent with the damage shown in Figure 4-14, where a crystal was irradiated with 3200 shots at zero and 45° incident angles. The depth of the cavity may also be deep enough to influence the plume expansion, and therefore the velocity distributions. Based on these images, in all the measurements reported above, the laser focus was moved to a new spot after 200 shots or less.

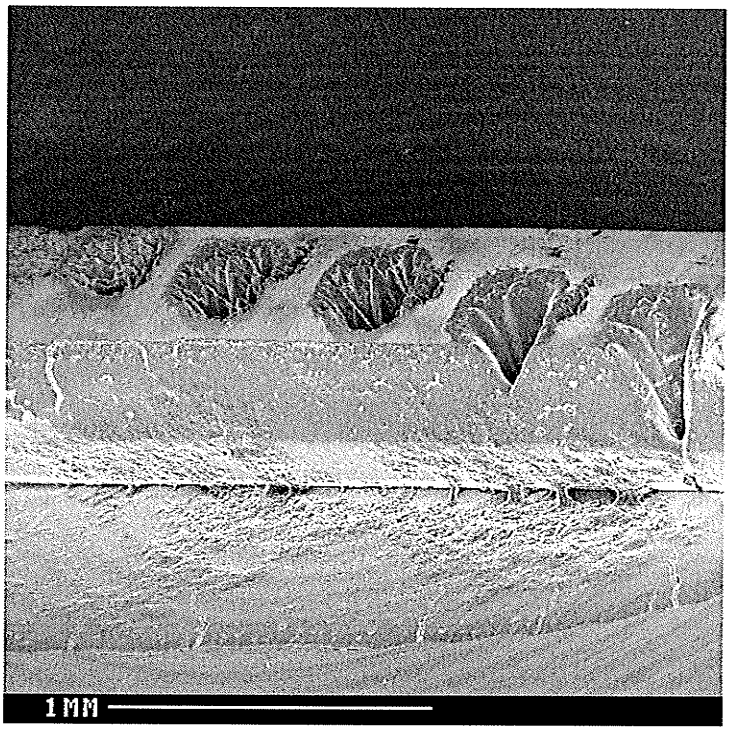

Figure 4-13 : DHB crystal irradiated at normal incidence with 100, 200, 400, 800, 1600, and 3200 laser shots.

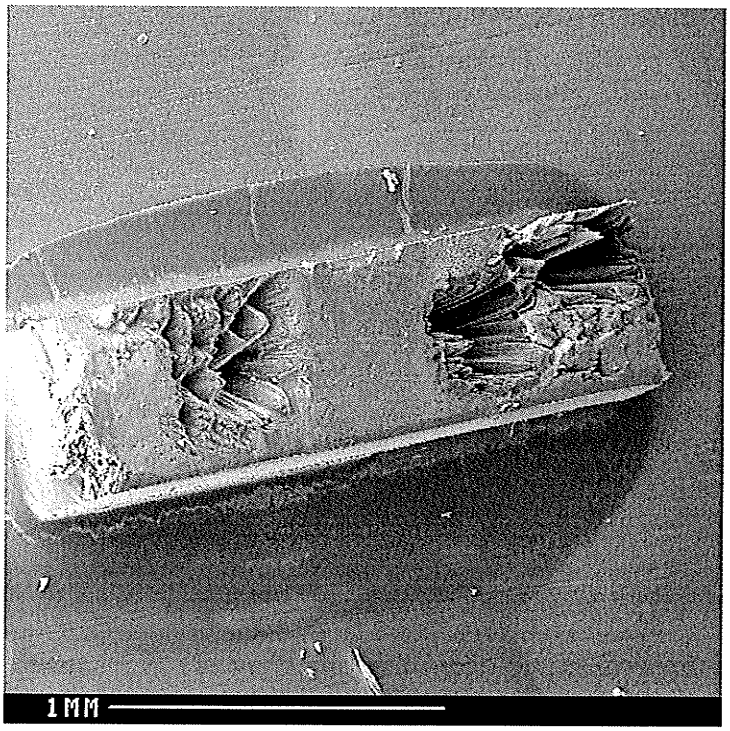

Figure 4-14 : DHB crystal after irradiation with 3200 laser shots at normal and 45° incident angles.

4.4 Conclusions

The average initial axial velocities of analytes in MALDI are roughly mass independent above about 1000 Da, with velocities approximately 800 m/s, according to measurements made in an orthogonal TOF geometry. The *width* of the velocity distribution, on the other hand, clearly increases with increasing analyte mass, from about 300 m/s at mass ~ 1000 Da to about 500 m/s at mass ~ 17 kDa. There is about 15% variability in the velocities of a specific analyte desorbed from various matrices. For the high fluence used in this experiment, the measured initial velocities of the matrix ions are much higher, between 1200 m/s and 2000 m/s, with the benzoic acid derivatives generally faster than the cinnamic acid derivatives. Velocities measured using various angles of the sample surface with respect to the fixed incidence angle suggest that the surface orientation is the main determiner of the plume direction, provided the laser damage is not signifiicant.

4.5 References

1. P. Juhasz, M. L. Vestal and S. A. Martin, *J. Am. Soc. Mass Spectrom.* **8** (1997) 209
2. M. Schurenberg, T. Schulz, K. Dreisewerd and F. Hillenkamp, *Rapid Commun. Mass Spectrom.* **10** (1996) 1873
3. M. Gluckmann and M. Karas, *J. Mass Spectrom.* **34** (1999) 467
4. R. C. Beavis, and B. T. Chait, *Chem. Phys. Lett.* **181** (1991) 479
5. W. Zhang and B. T. Chait, *Int J. Mass Spectrom. Ion Processes* **160** (1997) 259
6. Y. Pan and R. J. Cotter, *Org. Mass Spectrom.* **27** (1992) 3
7. A. Verentchikov, W. Ens, J. Martens and K. G. Standing, *Proceedings of the 40st ASMS Conference on Mass Spectrometry and Allied Topics*, Washington, DC (1992) 360
8. G. Kinsel and D. H. Russell, *Proceedings of the 40th ASMS Conference on Mass Spectrometry and Allied Topics*, Washington, DC (1992) 1928

9. R. G. Dworschak, V. Spicer, W. Ens and K. G. Standing, *Proceedings of the 46th ASMS Conference on Mass Spectrometry and Allied Topics*, Orlando, FL (1998) 932
10. T. Huth-Fehre and C. H. Becker, *Rapid Commun. Mass Spectrom.* **5** (1991) 378
11. J. Zhou, W. Ens, K. G. Standing and A. Verentchikov, *Rapid Commun. Mass Spectrom.* **6** (1992) 671
12. B. Spengler and V. Bokelmann, *Nucl. Instr. Meth.* **B82** (1993) 379
13. V. Bokelmann, B. Spengler and R. Kaufmann, *Eur. Mass Spectrom.* **1** (1995) 81-93
14. W. Zhang and B. T. Chait, *Int J. Mass Spectrom. Ion Processes* **160** (1997) 259
15. G. R. Kinsel, R. D. Edmondson and D. H. Russell, *J. Mass Spectrom.* **32** (1997) 714
16. A. A. Puretzky, D. B. Geohegan and G. B. Hurst, *Phys. Rev. Lett.* **83** (1999) 444
17. G. R. Kinsel, M. E. Gimon-Kinsel, K. J. Gillig and D. H. Russell, *J. Mass Spectrom.* **34** (1999) 684
18. B. Spengler, U. Bahr, M. Karas and F. Hillenkamp, *Anal. Instrum.* **17** (1988) 173
19. B. Spengler, U. Bahr and F. Hillenkamp, in: *Resonance Ionization Spectroscopy* (1988), eds.
20. T. B. Lucatorto and J. E. Parks, *The Institute of Physics Conf. Ser.* **94** (1988) 137
21. S. Berkenkamp, C. Menzel, F. Hillenkamp, K. Dreisewerd, J Am Soc Mass Spectrom 13 {2002) 2009
22. F. Aksouh, P. Chaurand, C. Deprun, S. Della-Negra, J. Hoyes, Y. Le Beyec and R. R. Pinho, Rapid *Commun. Mass Spectrom.* **9** (1995) 515
23. F. Xiang and R. C. Beavis, *Rapid Commun. Mass Spectrom.* **8** (1994) 199

5 Initial Velocities of MALDI Ions: Preliminary Observations in an axial Time-of-Flight Instrument

5.1 Introduction

In this chapter, ion velocities measured using the field-free technique originally described by Beavis [1] are presented. With this configuration, samples consisting of DHB matrix only and insulin with DHB matrix are analysed both in polycrystal and monolithic crystalline form at two different angles of laser incidence. The main goals of these preliminary measurements are to provide a direct comparison with the measurements in the previous chapter for a representative light ion and heavy ion, and to extend the investigation of the effect of the incident angle of the laser beam. In the orthogonal configuration, ion velocity is always measured back along the direction of the incident laser, but the target plane can be varied. Here the velocity is always measured normal to the target surface. The effect of the emission direction is related to the orientation of the crystal surfaces, and so both crystal and polycrystalline samples were used to explore possible differences In the polycrystalline form, the micro-crystal facets are randomly distributed and the monolithic sample crystal face is oriented normal to the instrument axis.

This chapter will begin with a brief section on sample preparation followed by a detailed look at how the field-free type measurements are acquired and finally preliminary data is presented of the various sample and instrument configurations.

5.2 Experimental

5.2.1 Sample Preparation

For the polycrystalline samples, the sample preparation technique is as described in section 2.2.2. The analysis of the matrix and insulin and matrix only samples actually occurred with physically the same sample as the presence of the insulin did not affect the analysis of the matrix alone.

The monolithic crystal samples were prepared by first making a saturated solution of DHB in acetonitrile. The samples were contained in vials with a small puncture made in the lids. These vials were then refrigerated to allow the liquid to evaporate slowly so that larger crystals could form. If the DHB had been solubilized in acetone, and allowed to dry, the crystals formed would have been too small to be of any practical use. After the fluid has evaporated the clump of crystals is removed from the vial and individual crystals are removed by tweezers under a microscope to look for one of sufficient size. Typically, the useful crystals were on the order of 3mm long by 1mm wide and 0.5mm thick. After a crystal was selected, a solution of styrene and toluene was used to adhere the crystal to the stainless steel target plate of the mass spectrometer. For crystals of DHB with insulin, a molar ratio excess of matrix to analyte on the order of 10^5:1 was mixed in solution and then allowed to dry as mentioned earlier. Visually the two types of crystals were indistinguishable. Other researchers have found that the protein is homogeneously distributed throughout the crystal. In the work of Strupat et al., x-ray crystallography of DHB crystals with cytochrome c at approximately the same concentration as the insulin in this work, showed no apparent disturbance of the crystal structure [2].

5.2.2 DC Extraction Technique

The field-free method is a way of measuring initial MALDI ion velocity distributions with a linear MALDI-MS. Figure 5-1 shows a schematic diagram of the Manitoba TOFII MALDI-MS with the high field and field-free configurations shown. This mass spectrometer was first described in an early paper from this lab [3]. Also, the two laser angles are shown: the low angle of incidence at 11° from the instrument axis or the sample surface normal, and the high angle of incidence at 85°. To measure a velocity distribution, a spectrum is acquired of the ion in high-field mode which is the conventional DC extraction mode described in Chapter 2. Here, the target is at the accelerating HV potential and grid 2 is at ground so that the ions are desorbed into the high field and are promptly accelerated. Past grid 2 they are simply drifting to the detector. The next step is to change the HV connections to the spectrometer so that the target and grid 2 are at the same potential. In this case the ions are desorbed into a field-free region at the floated HV potential and drift to grid 2 with their initial velocities. On passing grid 2, they are accelerated through to ground potential at grid 1 past which they drift to the detector. The TOF of the ions measured in the field-free configuration will naturally be longer than that measured in the high field. To calculate the mean initial velocity V_0, the high field TOF value is subtracted from the field-free TOF value and divided into x_1, the distance between the target plate and grid 2 (Figure 5-1):

$$V_0 = \frac{x_1}{TOF_{field-free} - TOF_{high-field}} \qquad (1)$$

Electrostatic grid screening can cause an unwanted field in a region that is bounded by a fine mesh metal grid as in the region between grid 2 and the target as shown in Figure 5-1 [4]. The correction potential V_{scr} that may be applied to grid 2 to minimize this effect is linear with accelerating potential and is on the order of 10V. To verify this was the appropriate magnitude, Na^+ and K^+ ions were

analysed and V_{scr} adjusted to allow just the appearance of the alkali ions under the field-free condition. Then the matrix ions were measured with different acceleration voltages and the independence of the matrix ΔTOF to the acceleration voltage was confirmed; therefore verifying the field-free condition within the measurement capabilities of the experimental equipment.

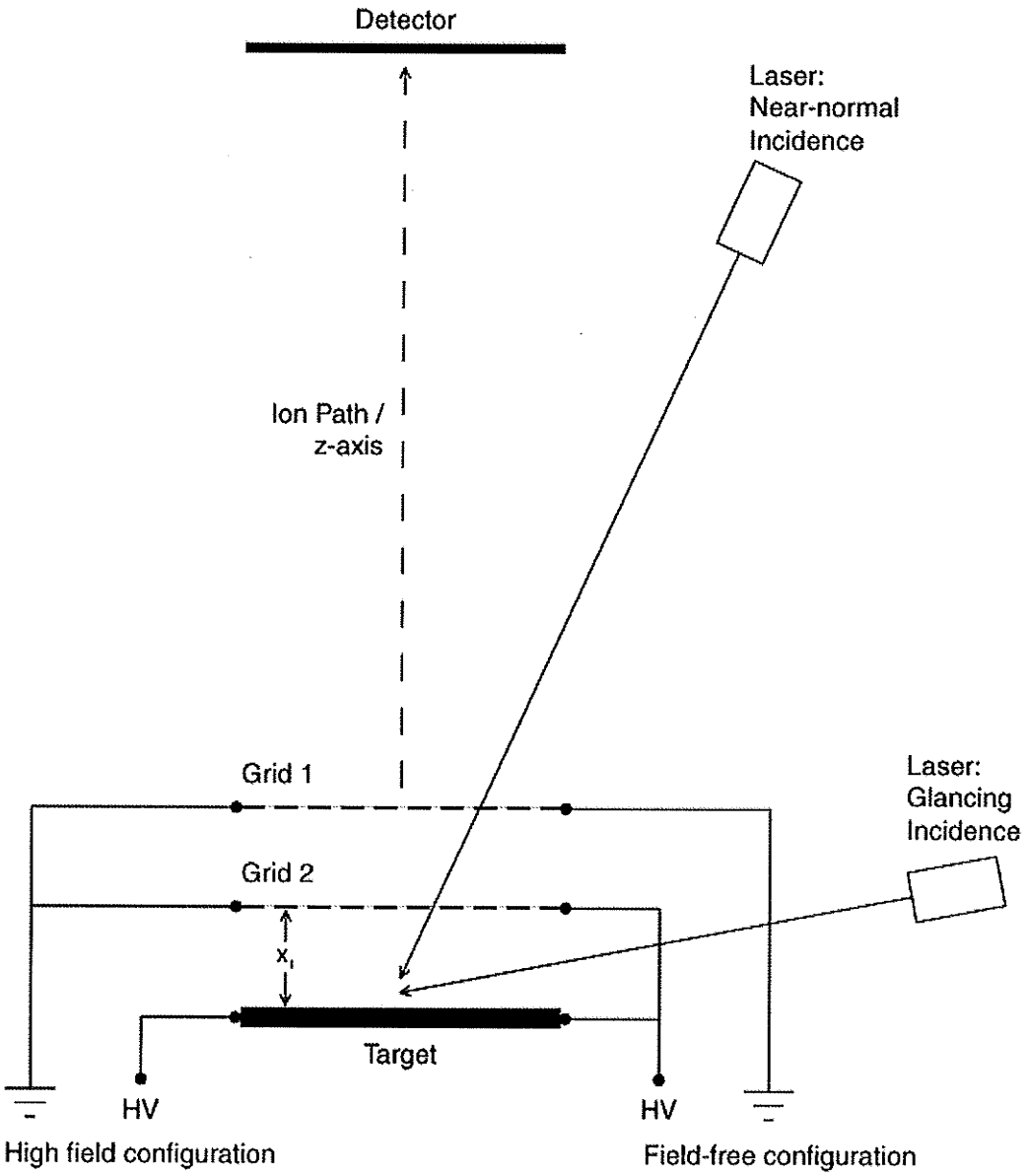

Figure 5-1 : Manitoba TOFII MALDI-MS showing the high-field and field-free configuration for the field-free type velocity measurement technique.

Figure 5-2 illustrates the data acquisition hardware for Manitoba TOFII required for operation in either high-field or field-free operation. The sequence begins with a trigger pulse (TP) from the computer to CFD 1 which converts the TP into a positive TTL pulse which is immediately relayed to GDG 1. The laser receives a TP from GDG 1 which causes it to fire at the target. At the same time GDG 2 receives a TP from GDG 1 and relays it to the converter plate pulser. This effectively shuts off the converter plate for a predetermined time to prevent low mass ions from being detected and possibly saturating the detector. The laser pulse is guided through a partial reflector on the way to the target and a portion of the beam is reflected into a photodetector (PD). The PD sends a pulse to CFD 2 which outputs a clean TP to the digital oscilloscope to trigger the start of data acquisition during which time the scope "listens" to the detector and records a TOF spectrum. The data is then transferred to the computer which sums and records the spectra.

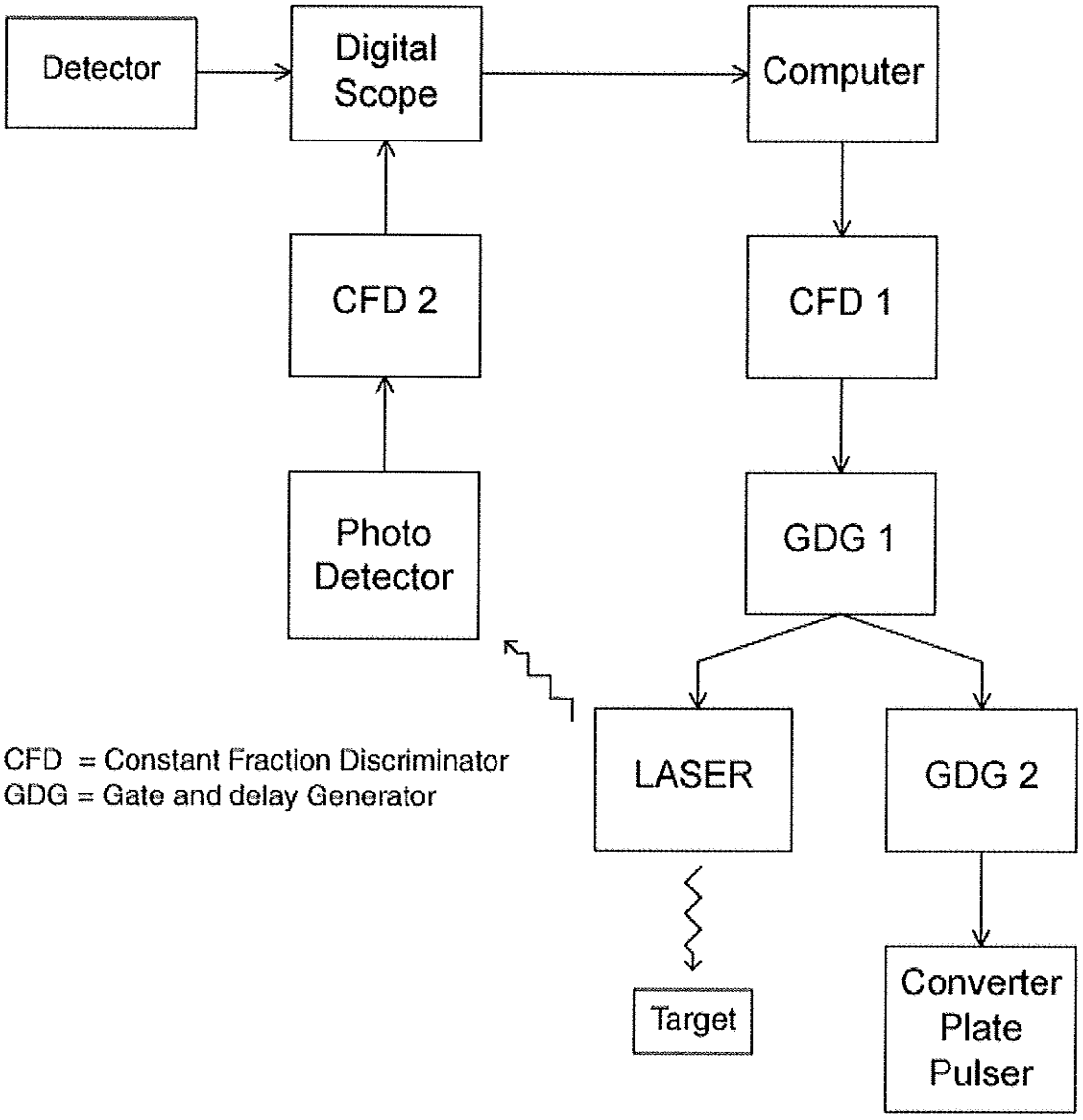

Figure 5-2 : Data acquisition hardware schematic for Manitoba TOFII.

An example of the data recorded for such a measurement is shown in Figure 5-3. The data was acquired for insulin in a polycrystalline DHB matrix with the laser incidence at the low angle of incidence configuration. With x_1 = 6.233mm and the difference in the TOF values shown in Figure 5-3, the mean initial velocity is calculated to be 800 m/s. This technique gives both the mean velocity as well as the velocity distribution determined by calculating the velocities at all TOF values in the low-field spectrum. This sample velocity distribution is shown in Figure 5-4, calculated from the low-field spectrum in Figure 5-3.

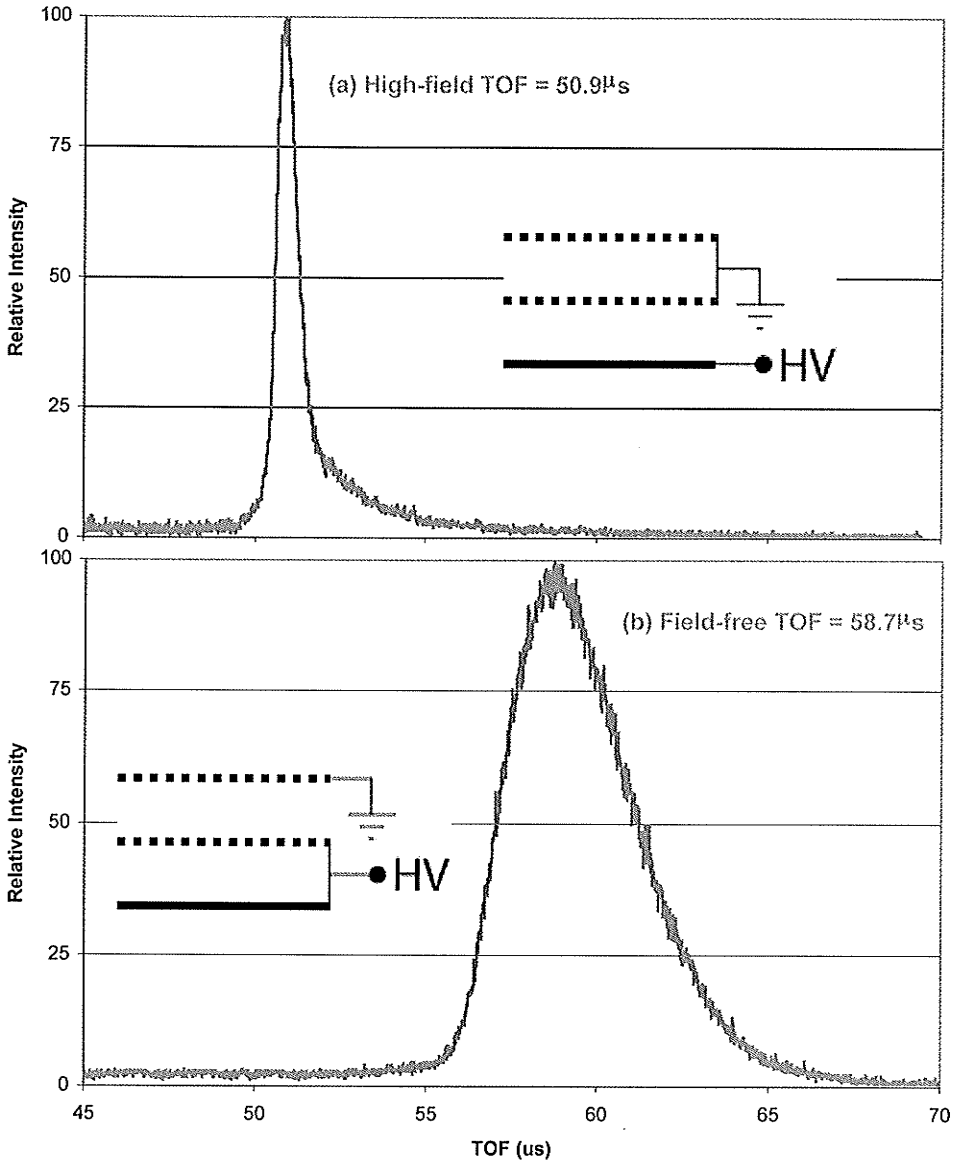

Figure 5-3 : TOF spectra showing the (a) high-field and (b) field-free data from insulin in DHB matrix with the average time-of-flight indicated for each.

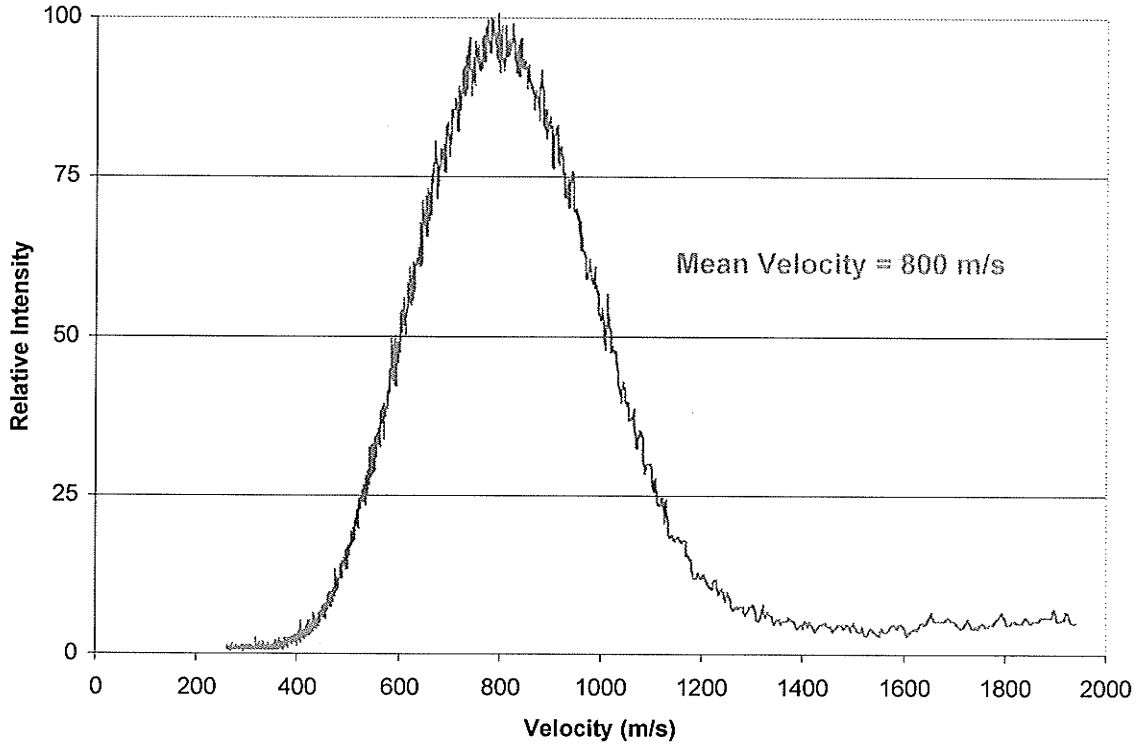

Figure 5-4 : Velocity distribution of insulin calculated from the TOF spectrum in Figure 5-3.

5.3 Results and Discussion

Figure 5-5 shows the experimental configurations and sample types for the field-free velocity measurements presented here. Figure 5-1 shows the angles of incidence used in these measurements. Figure 5-6 shows a summary plot of the data obtained. The velocity for insulin desorbed from polycrystalline DHB with the more normal incident angle was about 600 m/s, considerably lower than the 940 m/s observed in the OMALDI experiment. This is also considerably lower than results from most other field-free experiments and may represent a systematic error in these preliminary experiments; more measurements are needed for a detailed comparison. Nevertheless, the relative values between the measurements are meaningful.

As in the OMALDI experiment, the initial velocities of the matrix ions are substantially higher than that of the analyte ions, but again this experiment gave lower values than observed in the OMALDI experiment (1300 m/s compared to 1900 m/s for polycrystalline DHB). As mentioned in the previous chapter, part of this difference is probably due to the increased laser fluence used in the OMALDI experiment.

Higher velocities were observed with the more normal incidence angles for both Insulin and DHB matrix ions, and velocities from the single crystals are generally higher than from the polycrystalline samples. These two observations from this preliminary set of data suggest that the orientation of the crystal face of the sample to direction of the incident laser irradiation plays a role in the desorption process, consistent with the observations of the Orsay group [5].

In the case of the polycrystalline sample, the laser is incident on many microscopic crystal facets of random orientation. If initially the ions are desorbed in a direction normal to the local crystal surface, even in the microcrystalline case, then the polycrystalline surface will yield on average a lower velocity in the direction normal to the sample surface compared to the crystal, consistent with our observation..

Higher velocity for more normal laser incidence on polycrystalline samples may be a result of ions being preferentially desorbed from crystal facets normal to the incident laser. The same trend from single crystals is more difficult to explain, but may be related to crystal damage illustrated in the previous chapter. More experiments with careful control of laser fluence are needed to understand these results.

The difference between the observed velocities from single- and poly- crystalline targets is much more pronounced for the matrix ions compared to the analyte ions. Since the velocity of matrix ions are known to be more sensitive to the laser

fluence, this may reflect a higher average fluence for single crystals parallel to the target compared to randomly oriented crystals.

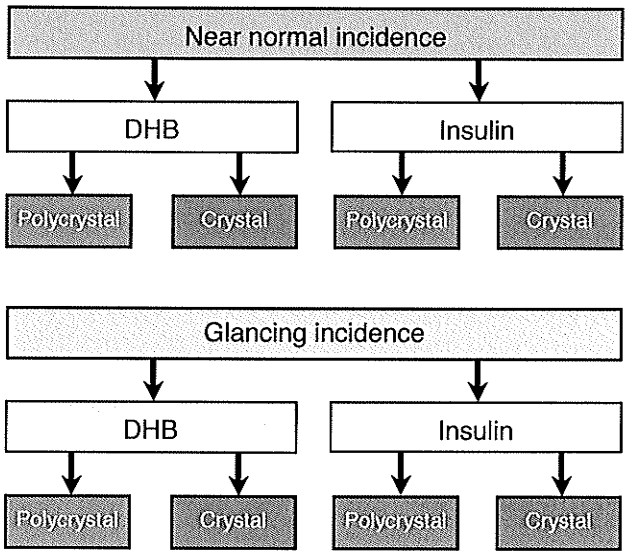

Figure 5-5 : Experimental configurations and sample types for the field-free velocity measurements carried out.

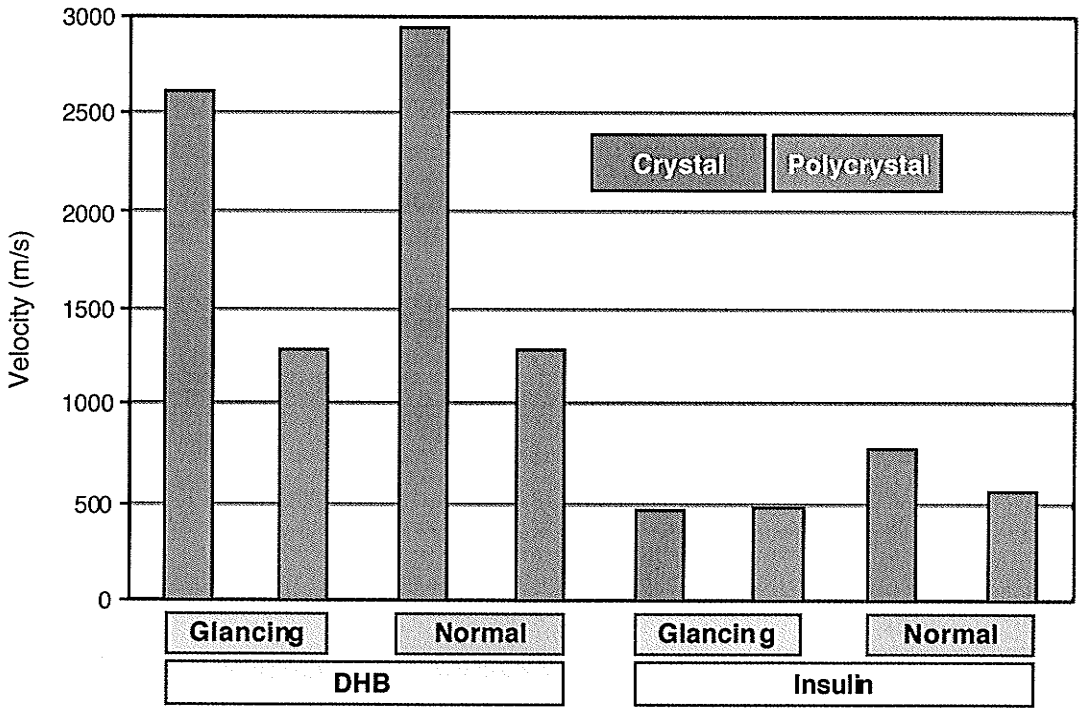

Figure 5-6 : Summary of velocities acquired with the configurations shown in Figure 5-5.

5.4 Conclusions

Initial ion velocities were measured using the axial field-free technique. With this configuration, samples consisting of DHB matrix only and insulin with DHB matrix are analysed both in polycrystal and monolithic crystalline form at two different angles of laser incidence. Higher velocities are observed with the more normal incidence angles for both Insulin and DHB matrix ions, and velocities from the single crystals are generally higher than those from polycrystalline targets. These observations from this preliminary set of data suggest that the orientation of the crystal face of the sample to direction of the incident laser irradiation plays a role in the desorption process.

5.5 References

1. R. C. Beavis, and B. T. Chait, *Chem. Phys. Lett.* **181** (1991) 479
2. K. Strupat, M. Karas and F. Hillenkamp, *Int. J. Mass Spectrom. Ion Processes* **111** (1991) 89
3. X. Tang, R. C. Beavis, W. Ens, F. Lafortune, B. Schueler and K. G. Standing, *Int. J. Mass Spectrom. Ion Processes* **85** (1988) 43
4. J. Grosser and H. Schultz, *J. Phys. D: Appl. Phys.* **22** (1989) 723
5. F. Aksouh, P. Chaurand, C. Deprun, S. Della-Negra, J. Hoyes, Y. Le Beyec and R. R. Pinho, Rapid *Commun. Mass Spectrom.* **9** (1995) 515

6. Analysis of Wheat Gluten Proteins by Matrix-Assisted Laser Desorption/Ionization Mass Spectrometry

In addition to the fundamental and instrumental studies of MALDI presented in the previous chapters, we have also been involved in applications of the method. This contents of this chapter have been published in a paper on applications to characterizing wheat proteins. [R. G. Dworschak, W. Ens, K. G. Standing, K. R. Preston, B. A. Marchylo, M. J. Nightingale, S. G. Stevenson and D. W. Hatcher, Analysis of Wheat Gluten Proteins by Matrix-Assisted Laser Desorption/Ionization Mass Spectrometry, *J. Mass Spectrom.* **33** (1998) 429].

6.1 Abstract

Matrix-assisted laser desorption/ionization mass spectrometry (MALDI/MS) was used to analyse the protein composition in several common and durum wheat varieties. Mass spectra were obtained directly from crude and partially purified wheat gliadin and reduced glutenin subunit fractions. Mass spectra of the gliadins and the low molecular weight (LMW) glutenin subunits show a complex pattern of proteins in the 30 - 40 kDa range. The observed gliadin patterns may be suitable for differentiation between wheat varieties, but the complexity of the mass spectra precludes the use of MALDI/MS as a stand-alone technique for the identification of most individual gliadin components. The mass spectra of the high molecular weight (HMW) glutenin subunits are much simpler and the complete HMW subunit profile can be determined directly from a single mass spectrum. This may prove particularly useful in wheat breeding programs for rapid

identification of lines containing subunits associated with superior quality. The correspondence between previously identified HMW subunits and the mass spectral peaks was established with MALDI measurements of HPLC separated subunits. Delayed extraction proved effective in improving the mass resolution for the monomeric gliadins and LMW glutenin subunit fractions, with masses less than 40 kDa. However, it gave little improvement for the HMW glutenin subunits which have masses of ~ 80 kDa.

6.2 Introduction

The physical dough properties and processing characteristics of wheat flours are determined primarily by the quantitative and qualitative properties of the gluten protein complex. Both major protein groups in this complex, the monomeric gliadins and the polymeric inter-chain disulphide-bonded glutenins, are associated with quality differences among wheat varieties [1,2,3,4]. The gliadins are a heterogeneous group consisting of more than 100 proteins [5] divided into four subgroups (α, β, γ, ω) based upon electrophoretic mobility [6]. Most have molecular masses in the 30 to 40 kDa range, although some ω-gliadins have a molecular mass near 80 kDa [7]. The polymeric glutenin proteins, with molecular masses ranging from less than 300 kDa into the millions [4,7,8,9,10], are composed of two groups of subunits. The low molecular weight (LMW) glutenin subunits are similar in size and structure to the γ-gliadins (30 – 40 kDa). The high molecular weight (HMW) glutenin subunits range in molecular mass from ~ 65-90 kDa [7]. There is a substantially larger variety of LMW subunits compared with the HMW subunits and they account for most of the mass of the glutenin proteins [4,7].

At present, characterization of the protein composition in wheat and other grains is done almost exclusively by a combination of gel electrophoresis and reversed-

phase high-performance liquid chromatography (RP-HPLC). These techniques have been used to establish strong positive relationships between dough strength and/or baking quality and the size distribution of the glutenin polymers [11]. This size distribution appears to be determined by the genetically controlled composition of both LMW and HMW subunits [4,8,9,12,13], although the relative amount of the larger polymers appears to correlate most strongly with the distribution of HMW subunits [8,9]. Sodium dodecyl sulphate polyacrylamide gel electrophoresis (SDS-PAGE) and HPLC methods are used routinely in many breeding programs for the selection of specific HMW subunits associated with superior quality [4]. Varietal quality can also be assessed by similar analysis of the gliadins [14,15] but this method is not currently widespread in breeding programs. On the other hand the wide diversity in the gliadin patterns is very useful for varietal identification [16,17]. In Canada and other exporting countries, these procedures are used extensively to confirm the classification of commercial samples [18].

Mass spectrometry has recently emerged as an alternative method to characterize high molecular mass molecules and molecular composition with the development of new ionization methods. In particular, matrix-assisted laser desorption/ionization (MALDI) in combination with time-of-flight mass spectrometry (TOF-MS) has made it possible to study complex mixtures of large, thermally labile, non-volatile biopolymers such as peptides, proteins and oligonucleotides with molecular masses up to several hundred kilodaltons [19,20,21]. The technique typically requires less than 1 pmol of sample and is relatively tolerant of impurities compared with other MS techniques, allowing analysis of crude or partially purified protein or peptide mixtures [21,22]. Compared with the separation methods described above, MALDI is much more accurate and much faster, requiring only a few minutes per sample to perform the measurement. The high throughput is particularly attractive for the possibility of rapid varietal identification in the field.

MALDI has recently been used to assess the molecular mass of purified wheat α-gliadins [23] and HMW glutenin subunits after separation by HPLC [24] and for the direct analysis of unfractionated prolamins from various grains, including the gliadins from wheat [25]. This latter study showed that the observed pattern of the prolamins is characteristic of the grain.

Here we report the use of MALDI for assessing the composition and mass distribution of crude and partially purified wheat gliadin and reduced HMW and LMW glutenin subunit fractions from common and durum wheat varieties [26]. MALDI was also used to determine the molecular masses of several HPLC-purified HMW glutenin subunits to establish a correspondence between proteins observed in the mass spectra of the crude mixtures and proteins already identified and coded by HPLC and electrophoresis. The results are discussed in relation to potential applications involving wheat gluten protein component identification for quality assessment in breeding programs, for molecular mass characterization, and for varietal identification.

6.3 Experimental

Pure samples of the following wheat varieties were obtained from stocks maintained at the Grain Research Laboratory in Winnipeg: Katepwa, Teal, Columbus and Pasqua varieties from the Canada Western Red Spring common (hexaploid) commercial class; Kyle, Plenty and Arcola varieties from the Canada Western Amber Durum (tetraploid) commercial class; Biggar and AC Tober varieties from the Canada Prairie Spring commercial class; and Glenlea and Wildcat varieties from the Extra Strong Red Spring commercial class. Each sample was confirmed for varietal purity by electrophoresis [27]. All chemicals were of reagent grade unless stated otherwise. HPLC-grade acetonitrile,

dithiothreitol (DTT) and ethanol were obtained from Fisher Scientific (Fair Lawn, NJ, USA) and trifluoroacetic acid (TFA) from Sigma (St. Louis, MO, USA). HPLC-grade deionized water, prepared with a Milli-Q plus-TOC water purification system (Millipore, Bedford, MA, USA), was employed to prepare all solutions.

6.3.1 Protein Extraction

Wheat samples (25 g) were ground in a sample mill equipped with a 1 mm sieve. Gliadins were extracted from ground grain (1.0 g) into 70% (v/v) ethanol (6 ml) at room temperature for 60 min. Extracts were then centrifuged at 20000g for 10 min. Glutenins were extracted sequentially from ground grain (1.0 g) into 50% (v/v) propan-1-ol containing 1% (w/v) DTT as described previously [28] with some modification (albumins and globulins were not pre-extracted with 0.5% (w/v) salt). HMW glutenins were purified by precipitation as described previously [28] and the remaining LMW glutenin supernatant fraction was retained. All fractions were filtered through Gelman 0.45 μm syringe filters prior to HPLC analysis and aliquots of each extract (150 μl) were dried using a Juoan Vacuum Concentrator prior to MALDI analysis.

6.3.2 HPLC

A Waters (Milford, MA, USA) HPLC system with Waters Millenium 2010 software was used to fractionate HMW glutenin subunits for some measurements. Analyses were performed with a Zorbax 300SB-C8 column (300 Å pore size, 5 μm particle size, 15 cm x 4.6 mm i.d.; Chromatographic Specialties, Brockville, ON, Canada). The column temperature was 50° C and the eluent was monitored at 210 nm. Three aliquots (3x5 μl) were injected onto the column and the proteins were resolved with an aqueous (0.1% TFA) linear gradient extending from 24-

48% acetonitrile at a flow rate of 1 ml/min for 120 min [29]. Individual HMW glutenin subunits were collected and dried as above.

6.3.3 MALDI

The dried gliadin samples were reconstituted in 300 μl of 0.1% trifluoroacetic acid in water. The dried LMW and HMW glutenin samples were reconstituted in 150 μl of acetonitrile mixed with 150 μl of 0.1% trifluoroacetic acid in water. All reconstituted stock protein solutions were then kept in a water-bath at 60° C for 30 min with intermittent vortexing to dissolve the protein completely. The resulting stock solutions had concentrations varying from 30-600 μmol/l. A saturated solution of the matrix 3,5-dimethoxy-4-hydroxycinnamic acid (sinapinic acid) in aqueous 0.1% TFA-acetonitrile (2:1, v/v) was first applied to the sample probe, dried and then crushed [30]. The stock solution was then mixed (1:10, v/v) with the matrix solution and a few microlitres were applied to the crushed spot on the sample probe. When a visible film began to form on the probe surface (about 10 s), the spot was rinsed with cold deionized water for 10 s and then allowed to dry thoroughly prior to analysis [30].

The above washing procedure significantly improved the signal-to-noise ratio in the mass spectra, particularly for the LMW and HMW glutenin subunit fractions. This may be a result of the removal of DTT, which was used as a reducing agent during the preparation of the subunits. Spectra of alkylated (with vinyl pyridine) and non-alkylated reduced glutenin subunits were comparable, which confirmed that alkylation was not required to prevent re-oxidation (results not shown).

Positive ion mass spectra were obtained on a MALDI/TOF mass spectrometer built in-house (Manitoba TOFII) [31] and run in the linear mode. A nitrogen laser

(VSL 337 ND, Laser Science, Cambridge, MA, USA) was used to illuminate the target with a pulse frequency of 2-3 Hz. For some of the gliadin and LMW glutenin subunits, a 2-grid delayed extraction system [32] was employed using a 25 kV d.c. accelerating potential on the probe and first grid with a pulse of 3 kV applied to the probe 1.2 μs after the laser pulse. The 3 kV pulse was supplied by a high-voltage switch (Behlke, Frankfurt, Germany). For the HMW glutenin subunits, d.c. extraction was employed with target and first grid potentials of 30 and 18 kV, respectively. Following desorption and acceleration, ions drift through a field-free region of 1.2 m in which the nominal pressure was 3 x 10-7 Torr (1 Torr = 133.3 Pa) measured with an ion gauge. The ions were detected with microchannel plates and the signal was recorded with a transient recorder (LeCroy TR8828D) from which the spectra were summed by an Atari (TT030) computer. There were ~150-200 shots accumulated per spectrum. The gliadin and LMW glutenin subunit spectra were calibrated externally with carbonic anhydrase (29 021 Da) while the HMW glutenin subunit spectra were calibrated externally with human transferrin (79549 Da) 33. Better mass accuracy would be possible with internal calibration but the emphasis here is more on the overall pattern and the feasibility of the technique for rapid and routine analysis.

6.4 Results and Discussion

6.4.1 Delayed Extraction

The use of delayed extraction in MALDI/TOF-MS to give improved resolution has mainly been emphasized for peptides and small proteins up to about 10 kDa [32,34,35], although some examples up to 30 kDa have been presented [34,36]. Above ~20 kDa, the improvement compared with d.c. extraction drops rapidly and above 30 kDa little or no improvement has been reported. Recently, Bahr et al. reported that with judicious choice of matrix and pulsing conditions to minimize metastable fragmentation, delayed extraction can give enhanced

resolution up to about 60 kDa [37]. In our measurements, using sinapinic acid as the matrix, we observed a significant improvement in the mass resolution using delayed extraction compared with d.c. extraction for proteins up to ~40 kDa. The enhanced resolution is particularly beneficial for the complex mixtures of gliadins (compare Figure 6-1 and Figure 6-2) and reduced LMW glutenin subunit fractions. No significant improvement for the HMW glutenin subunits was observed.

6.4.2 Gliadins

Mass spectra were obtained for gliadin fractions from ten different wheat varieties in four commercial classes, using DC MALDI. Each sample was run several times to determine the reproducibility. Although the absolute signal strength is variable from sample to sample and from shot to shot, the measured masses and the observed intensity patterns were consistent for different samples of the same fraction. Four representative spectra are shown in Figure 6-1, one from each of the four commercial classes. Although the spectra consist of many unresolved peaks, the different wheat varieties showed distinct mass spectral fingerprints indicating the potential of automated MALDI for rapid varietal identification. At present, electrophoretic and HPLC patterns of gliadin proteins are used extensively in variety identification of commercial samples [16,17,18] but this is much more time consuming than MALDI. Further experiments are in progress to evaluate a larger sample set and to use delayed extraction to improve discrimination.

Delayed extraction mass spectra were obtained for two of the gliadin fractions, Katepwa and Kyle. The increased number of resolved peaks in the spectra shown in Figure 6-2 illustrates the advantage of delayed extraction. Even so, only about 20 protein masses can be determined from the spectra, compared with more than 100 gliadin proteins indicated by two-dimensional electrophoresis [5].

The many different gliadin proteins have not been characterized in detail so their molecular masses are not accurately known, but the broad width and irregular shape of the observed gliadin peaks (compared with spectra of mass standards in this range) strongly suggest that most of the components are simply unresolved. The majority of components for the wheat variety Katepwa exhibit masses ranging from about 29.5-32.5 kDa whereas a smaller number of components fall in a second region between 33.5 and 35.7 kDa. The spectrum of

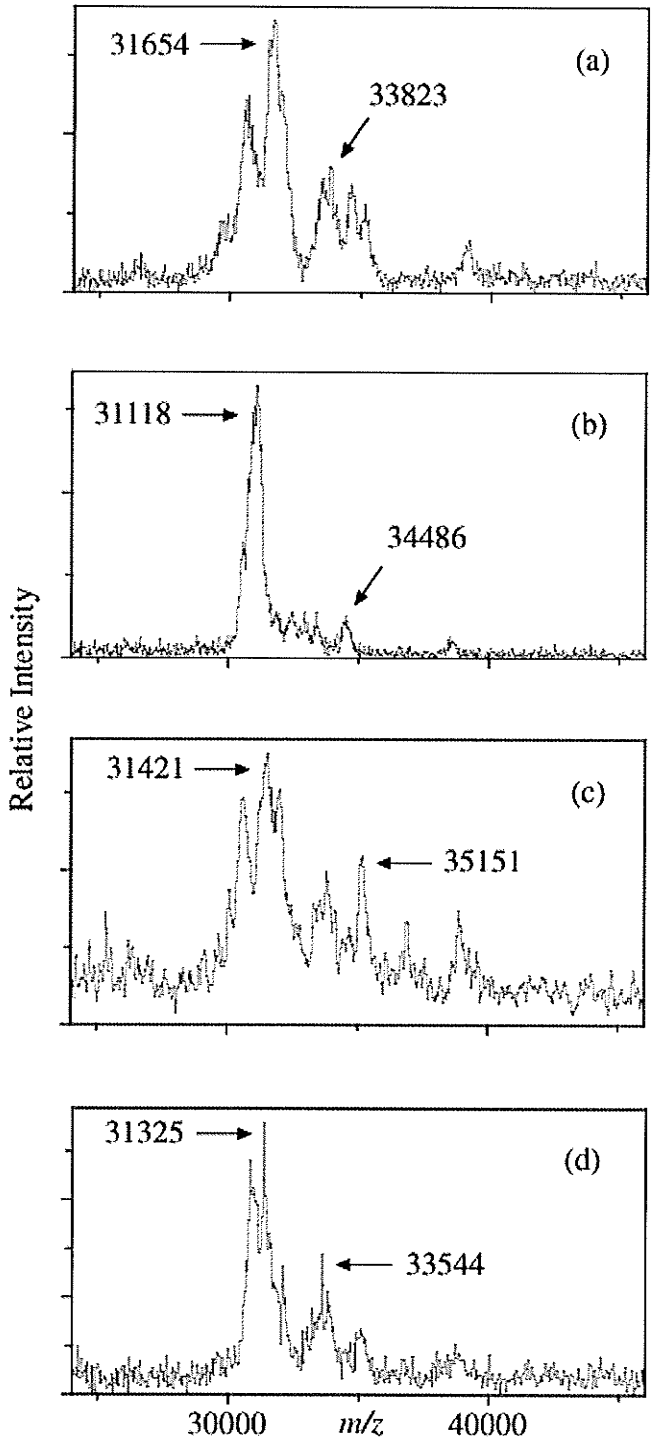

Figure 6-1 : DC-extraction MALDI mass spectra of gliadin fractions from four commercial wheat classes: (a) Katepwa variety from the Hard Red Spring class; (b) Kyle variety from the Amber Durum class; (c) Biggar variety from the Canada Prairie Spring class; (d) Glenlea variety from the Extra Strong Red Spring class. Selected peaks are labeled in daltons.

the durum wheat variety Kyle shows less complexity than Katepwa. Presumably the tetraploid durum wheat, which is missing the D chromosome, has a smaller number of gliadin proteins than the hexaploid common wheat. Even so, the distribution of durum wheat components is similar to that of common wheat components with most of the masses ranging from about 30.5-32.2 kDa and a smaller number being present between 32.5 and 35 kDa. No major peaks are visible for either variety above 39 kDa indicating that most, if not all, of the gliadins are within the normal mass range normally attributed to the majority of gliadin proteins [7].

Although the observed patterns show some potential to differentiate between \varieties, the complexity of the gliadin mass spectra precludes the use of MALDI/MS, even with delayed extraction, as a stand-alone technique for identification of most individual gliadin components unless much higher mass resolution can be obtained. Characteristically, other common one-dimensional fractionation techniques such as electrophoresis [38] and HPLC [39] also are unable to resolve all gliadin components. Currently, two-dimensional electrophoresis offers the best indication of the gliadin composition [5]. Similar separation may be possible with MALDI used in combination with this technique or another technique such as HPLC or capillary electrophoresis (CE). Such a combination might also provide a means of obtaining more accurate molecular masses [24,40].

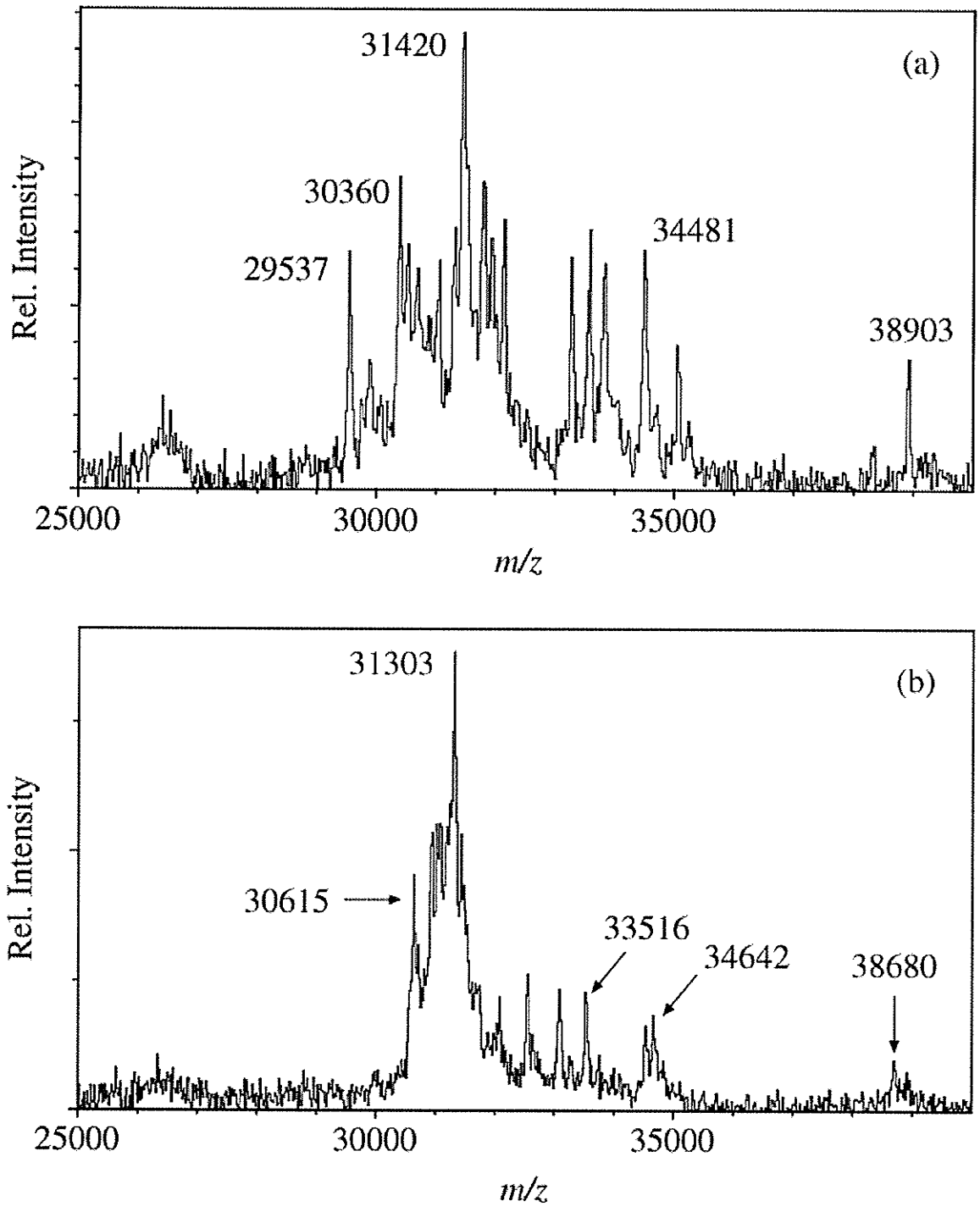

Figure 6-2 : Delayed-extraction MALDI mass spectra of gliadins from the (a) Katepwa and (b) Kyle wheat varieties with selected peaks labeled in daltons.

6.4.3 Low Molecular Mass Glutenin Subunits

The LMW glutenin subunits of Katepwa and Kyle were analysed by delayed-extraction MALDI. Like the spectra of the gliadins, the spectra of the LMW subunits, shown in Figure 6-3, reflect a complex mass spectral pattern, consistent with a large number of subunits [4,5]. Three major regions with masses from ~30.5-33, 37.5-39 and 42-43 kDa are present, with no peaks evident above 43 kDa. The first region is similar in mass to the major gliadin range. This is probably a reflection of their similar evolutionary relationship [4]. The other LMW glutenin subunit regions appear to be distinct from those obtained for the gliadins. These results are consistent with SDS-PAGE, which shows extensive overlap between gliadins and LMW glutenin subunits in addition to lower mobility LMW glutenin subunit regions distinct from the gliadins [28,38]. In view of the increasing interest in LMW glutenin subunits associated with their potential important relationship to wheat protein quality, [41,42] a two-dimensional approach using HPLC followed by MALDI may prove useful for the further characterization of individual components.

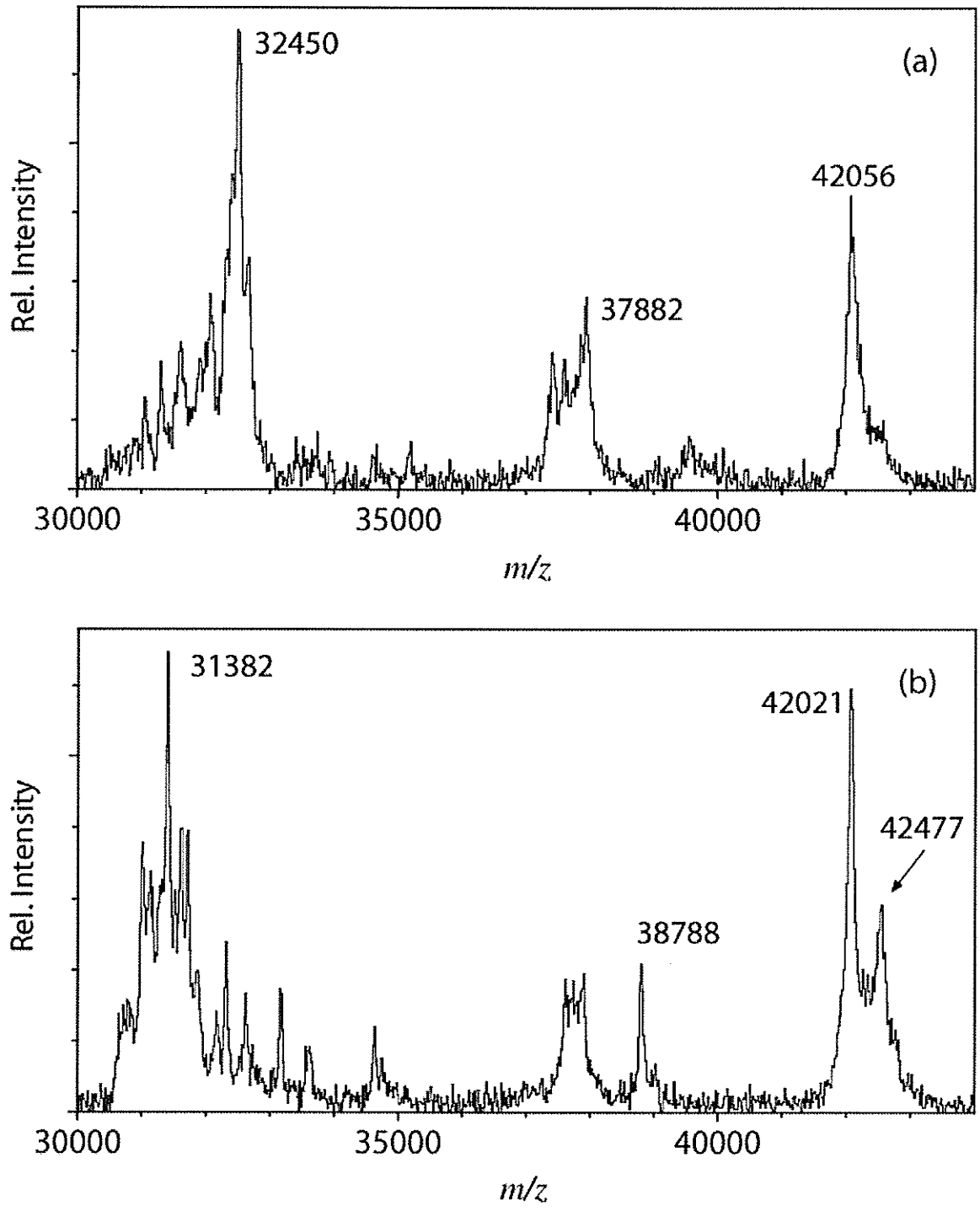

Figure 6-3 : Delayed-extraction MALDI mass spectra of low molecular weight glutenins from the (a) Katepwa and (b) Kyle wheat varieties with selected peaks labeled in daltons.

6.4.4 High Molecular Mass Glutenin Subunits

Mass spectra of the HMW glutenin subunits for Katepwa and Kyle are shown in Figure 6-4. In contrast to the mass spectra of gliadins and LMW subunits, the mass spectra of HMW subunits are fairly simple. Five distinct, well separated peaks are observed in the spectrum for Katepwa and four distinct peaks are evident in the spectrum for Kyle. The relatively simple spectra are consistent with the small number of these subunits previously identified in both wheat varieties [12,38]. The results indicate the feasibility of using MALDI to obtain a rapid and complete profile of HMW glutenin subunits without prior separation by HPLC. Automated sample analysis using this technique may prove particularly useful in wheat breeding programs where rapid isolation of lines containing subunits associated with superior quality is a major objective [4]. Hickman et al. [24] reported difficulty in obtaining molecular ion signals of the unseparated HMW subunits and the peaks obtained from the separated proteins were broader than those in Figure 6-4, but they did not use a washing procedure prior to MALDI analysis and they used a different matrix (α-cyano-4-hydroxycinnamic acid).

Most HMW glutenin subunits have been identified by both SDS-PAGE and HPLC and have been classified based upon electrophoretic mobility, but a size-fractionation technique such as SDS-PAGE does not provide accurate mass values [43]. To establish a correspondence between the classified subunits and the observed molecular ion peaks in the mass spectra, HPLC was used to separate the glutenin subunit fraction into constituent components (described previously [40]) before analysis by MALDI. This step would not be necessary to obtain the HMW profile of a wheat sample once the known subunits have been characterized individually by mass spectrometry; measurements are in progress to determine the molecular mass of the known HMW subunits in Canadian wheat varieties [44].

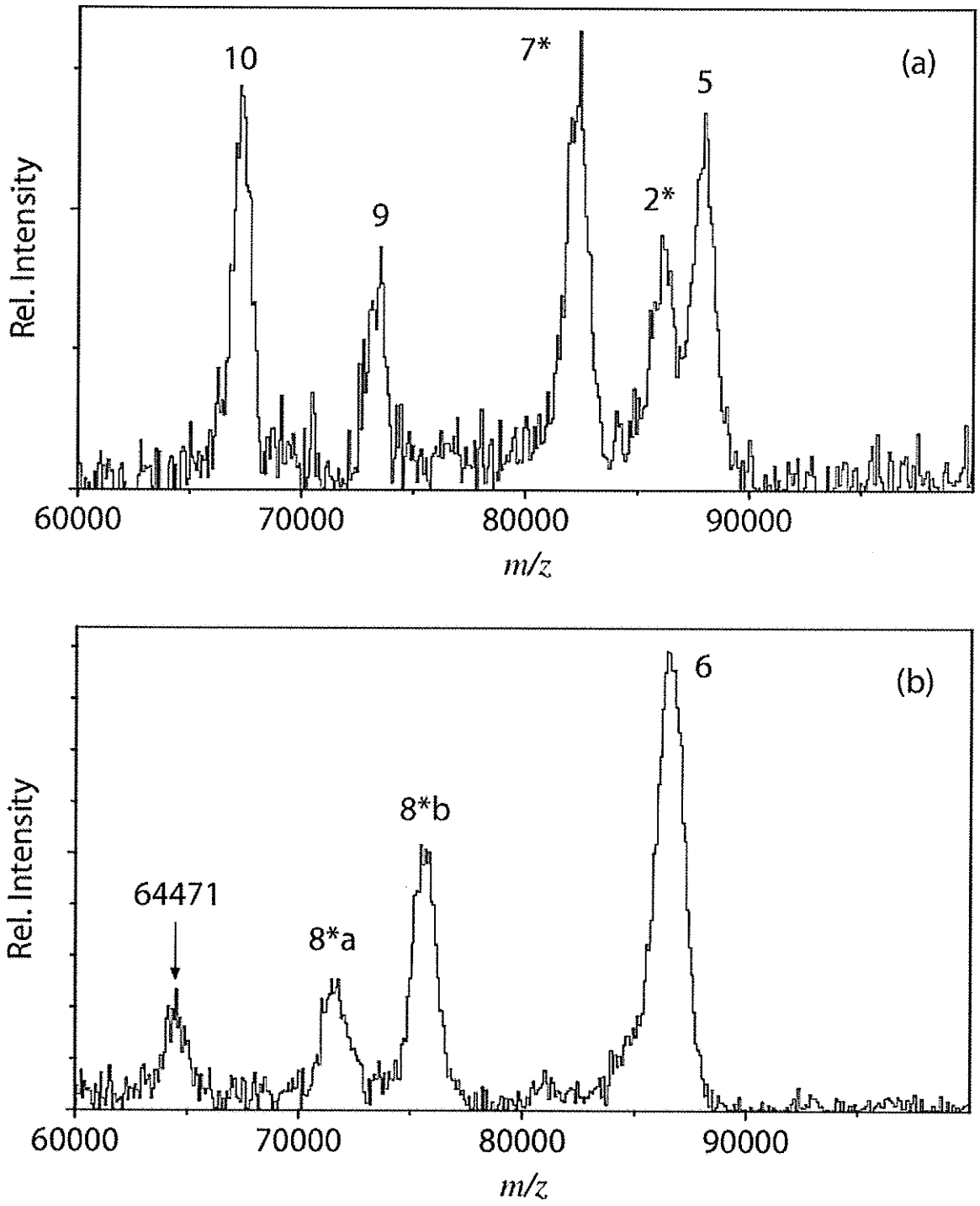

Figure 6-4 : MALDI mass spectra of high molecular weight glutenins from the (a) Katepwa and (b) Kyle wheat varieties. The peaks are labeled with the subunit number; corresponding masses are given in Table 6-1.

Five subunits have previously been identified in Katepwa with the designations 2*, 5, 7*, 9 and 10 [45], and there is a one-to-one correspondence between them and the mass spectral peaks; each HPLC component gave a single mass peak. The measured masses are listed in Table 6-1 along with predicted masses, if available, from the corresponding gene sequences [46]. The difference between the prediction and the measured mass is about 200 Da or less in all cases, which is consistent with an estimated measurement accuracy of a few tenths of a percent for broad peaks in this mass range. The correspondence is remarkably good and it is tempting to attribute some significance to the systematic mass deficit in the measurements and assume a precision better than 0.1%, but it should be mentioned that there are discrepancies in the literature of 500-1000 Da for the predicted masses from gene sequences of subunits 5 [47], 9 [48] and 10 [47], and that previous MALDI results for these three subunits differ from the present results by 1000 Da or more [24]. Measurements of the mass spectra of enzymatic digests of the proteins may help to resolve the differences.

Table 6-1: Measured masses of high molecular weight protein subunits from the Katepwa and Kyle wheat varieties and predicted molecular masses from available gene sequences [46].

	MALDI		Gene Sequence		
Subunit	Cultivar	Mass (Da)	Cultivar	Mass (Da)	Difference
2*	Katepwa	86202	Cheyenne	86309	-107
5	Katepwa	87936	Cheyenne	88137	-207
6	Kyle	86539			
7*	Katepwa	82279			
8a*	Kyle	71520			
8b*	Kyle	75624			
9	Katepwa	73308	Cheyenne	73518	-210
10	Katepwa	67280	Cheyenne	67495	-215

The situation is less straightforward for the Kyle sample. Four mass spectral peaks were detected in the HMW glutenin fraction of Kyle [Figure 6-4(b)]

whereas only two main peaks were resolved by HPLC, as shown in Figure 6-5(a). As established by SDS-PAGE [38,45], the HPLC peaks correspond in position to those of subunits 6 and 8*. To determine the identity of the mass spectral peaks, the two HPLC peaks were collected and then analyzed separately by MALDI. Comparison of the mass spectra showed that the highest molecular mass peak at 86 539 Da corresponds to the HMW glutenin subunit 6 (Table 6-1). The other HPLC fraction, corresponding in elution time to subunit 8*, gave the two mass spectral peaks with masses of 71 520 and 75 624 Da (Table 6-1). This result is consistent with recent studies by Marchylo and Nightingale (unpublished), which show that the HPLC 8* peak in Kyle can be resolved into two closely spaced peaks when a modified higher resolution HPLC procedure is employed. The HPLC spectrum is shown in Figure 6-5(b); the two peaks and the corresponding mass peaks in Figure 6-4(b), are designated 8a* and 8b*. The remaining lower mass peak at 64 471 Da [Figure 6-4(b)] was not present in any HPLC fractions eluting in the HMW glutenin subunit region. This peak may represent an ω-gliadin contaminant present in the HMW glutenin extract since these proteins are difficult to extract completely into the gliadin fraction [28].

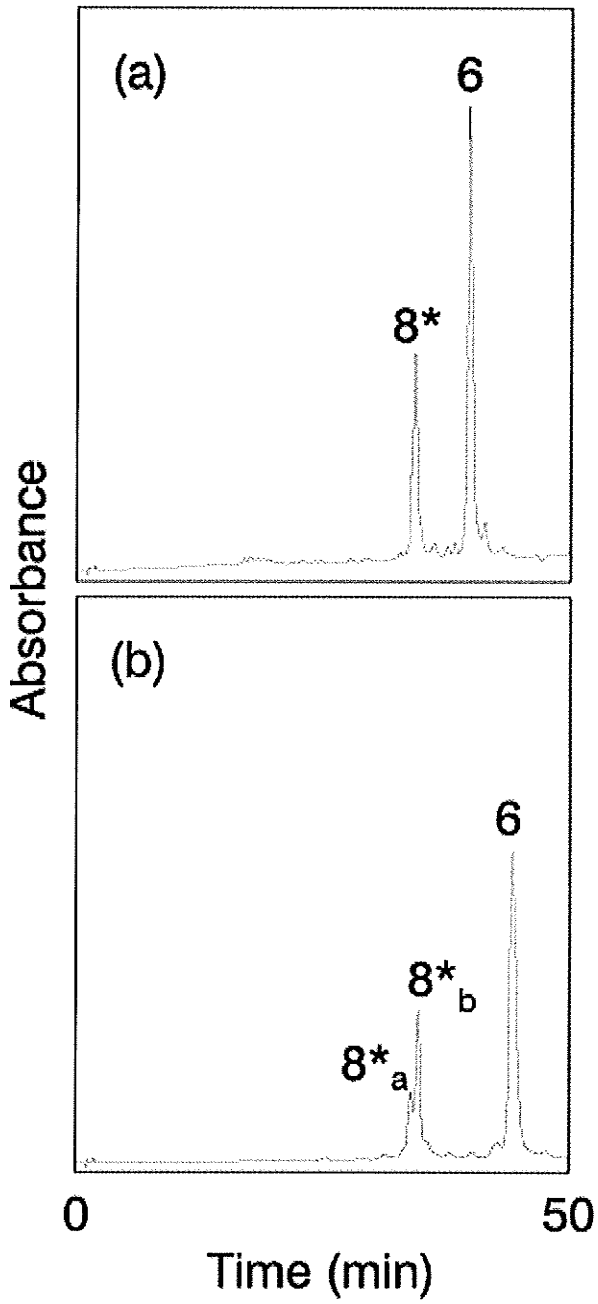

Figure 6-5 : HPLC traces of high molecular mass glutenins from the Kyle wheat variety, showing subunits (a) 6 and 8* and (b) 6, 8*a and 8*b.

6.5 Conclusions

MALDI mass spectra can be obtained directly from crude and partially purified wheat gliadin and reduced glutenin subunit fractions from common and durum wheat varieties without prior separation by HPLC. The spectra of the gliadins and the LMW glutenin subunits show some promise for variety identification but reliable identification of individual components will probably require a second spectroscopic dimension such as HPLC or CE. The spectra of the HMW glutenin subunits are much simpler and the complete HMW subunit profile can be determined directly from a single mass spectrum. This may prove particularly useful in wheat breeding programs for rapid identification of lines containing subunits associated with superior quality.

6.6 References

1. K. F. Finney, *Cereal Foods World* **30** (1985) 794
2. F. MacRitchie, *J. Cereal Sci.* **6** (1987) 259
3. R. A. Orth and W. Bushuk, *Cereal Chem.* **49** (1972) 268
4. P. I. Payne, *Ann. Rev. Plant Physiol.* **38** (1987) 141
5. R. Tkachuk and V. J. Mellish, In *Proc. 3rd International Workshop on Gluten Proteins,* Budapest, Hungary; edited by R. Lásztity and F. Békés, p. 111. World Scientific (1987)
6. J. S. Wall, In *Recent Advances in the Biochemistry of Cereals,* p. 275, Academic Press, London/New York (1979)
7. P. R. Shewry and A. S. Tatham, *Biochem. J.* **267** (1990) 1
8. R. Huebner and J. S. Wall, *Cereal Chem.* **53** (1976) 258
9. J. M. Field, P. R. Shewry and B. J. Miflin, *J. Sci. Food Agric.* **34** (1983) 370
10. S. G. Stevenson and K. R. Preston, *J. Cereal Sci.* **23** (1996) 121
11. F. MacRitchie, *Advances in Food and Nutrition Research* **36** (1992) 1
12. P. I. Payne, K. G. Corfield and J. A. Blackman, *Theoretical and Applied Genetics* **55** (1979) 153
13. E. J. Lew, D. D. Kuzmicky and D. D. Kasarda, *Cereal Chem.* **69** (1992) 508
14. G. Branlard and M. Rousset, *Ann. Amerlior. Plant.* **30** (1980) 133
15. F. R. Huebner and J. A. Bietz, *J. Cereal Sci.* **4** (1986) 379

16. L. Lookhart and C. W. Wrigley, In *Identification of Food Grain Varieties, American Association of Cereal Chemists*, Minneapolis, MN, edited by C. W. Wrigley, p. 55 (1995)
17. A. Bietz and F. R. Huebner, In *Identification of Food Grain Varieties, American Association of Cereal Chemists*, Minneapolis, MN, edited by C. W. Wrigley, p. 73 (1995)
18. L. Lookhart, B. A. Marchylo, V. J. Mellish, K. Khan, D. B. Lowe and L. Seguin, In *Identification of Food Grain Varieties, American Association of Cereal Chemists*, Minneapolis, MN, edited by C. W. Wrigley, p. 201 (1995)
19. M. Karas, U. Bahr and F. Hillenkamp, *Int. J. Mass Spectrom. Ion Processes* **92** (1989) 231
20. F. Hillenkamp, M. Karas, R. C. Beavis and B. T. Chait, *Anal. Chem.* **63** (1991) 1193A
21. R. C. Beavis and B. T. Chait, *Proc. Natl. Acad. Sci. USA* **87** (1990) 6873
22. D. N. Nguyen, G. W. Becker and R. M. Riggin, *J. Chromotography A* **21** (1995) 705
23. J. B. Turner, D. B. Gordon, G. A. Lord and C. A. Smith, *Biochem. Soc. Trans.* **22** (1994) 403S
24. D. R. Hickman, P. Roepstorff, P. R. Shewry and A. S. Tatham, *J. Cereal Sci.* **22** (1995) 99
25. E. Méndez, E. Camafeita, J. San Sebastián, L. Valle, J. Solís, F. J. Mayer-Posner, D. Suckau, C. Marfisi and F. Soriano, *J. Mass Spectrom. and Rapid Commun. Mass Spectrom.* S123 (1995)
26. R. G. Dworschak, W. Ens and K. G. Standing, In *Proc. 44th ASMS Conference on Mass Spectrometry and Allied Topics,* Portland, OR, 1996, p. 993
27. R. Tkachuk and V. J. Mellish, *Ann. Technol. Agric.* **29** (1980) 207
28. B. A. Marchylo, J. E. Kruger and D. Hatcher, *J. Cereal Sci.* **9** (1989) 113
29. B. A. Marchylo and J. E. Kruger, *Cereal Chem.* **65** (1988) 192
30. F. Xiang and R. C. Beavis, *Rapid Commun. Mass Spectrom.* **8** (1994) 199
31. X. Tang, R. C. Beavis, W. Ens, F. Lafortune, B. Schueler and K. G. Standing, *Int. J. Mass Spectrom. Ion Processes* **85** (1988) 43
32. R. S. Brown and J. Lennon, *Anal. Chem.* **67** (1995) 1998
33. The calibration masses were determined in-house using ESI-TOF and are consistent to reasonable accuracy with published masses in R. D. Smith, J. A. Loo, R. R. Ogorzalek Loo, M. Busman and H. R. Udseth, *Mass Spectrom. Rev.* **10** (1991) 359
34. M. L. Vestal, P. Juhasz and S. A. Martin, *Rapid Commun. Mass Spectrom.* **9** (1995) 1044
35. R. M. Whittal and L. Li, *Anal. Chem.* **67** (1995) 1950
36. W. Ens, R. G. Dworschak, V. Spicer and K. G. Standing, In *Proc. 43rd ASMS Conference on Mass Spectrometry and Allied Topics,* Atlanta, GA, 1995, p. 684

37. U. Bahr, E. Gleitsmann, J. Stahl-Zeng and M. Karas, In *Proc. 45th ASMS Conference on Mass Spectrometry and Allied Topics,* Palm Springs, CA, 1997
38. B. A. Marchylo, K. A. Handel and V. J. Mellish, *Cereal Chem.* **66** (1989) 186
39. B. A. Marchylo, D. W. Hatcher, J. E. Kruger and J. J. Kirkland, *Cereal Chem.* **69** (1992) 371
40. B. A. Marchylo, M. J. Nightingale and J. J. Kirkland, In *Gluten'96 - Proc. 6th International Gluten Workshop*, Sydney, Australia, September 1996, Ed. C. W. Wrigley, Cereal Chemistry Division of the Royal Australian Chemical Institute, p 387
41. R. B. Gupta and F. MacRitchie, *J. Cereal Sci.* **14** (1991) 105
42. R. B. Gupta, J. G. Paul, G. B. Cornish, G. A. Palmer, F. Békés and A. J. Rathjen, *J. Cereal Sci.* **19** (1994) 9
43. N. A. C. Bunce, R. P White and P. R. Shewry, *J. Cereal Sci.* **3** (1985)131
44. R. G. Dworschak, W. Ens, K. G. Standing, K. R. Preston, B. A. Marchylo and M. J. Nightingale, In *Proc. 45th ASMS Conference on Mass Spectrometry and Allied Topics,* Palm Springs, CA, 1997
45. B. A. Marchylo, O. M. Lukow and J. E. Kruger, *J. Cereal Sci.* **15** (1992) 29
46. P. R. Shewry, N. G. Halford and A. S. Tatham, *J. Cereal Sci.* **15** (1992) 105, A. C. Bunce, R. P White and P. R. Shewry, *J. Cereal Sci.* **3** (1985) 131
47. O. D. Anderson, F. C. Greene, R. E. Yip, N. G. Halford, P. R. Shewry and J. M. Malpica, *Nucleic Acids Res.* **17** (1989) 461
48. N. G. Halford, J. Forde, O. D. Anderson, F. C. Greene and P. R. Shewry, *Theor. Appl. Genet.* **75** (1987) 117